DYNAMIC PNEUMATIC MUSCLE ACTUATOR

CONTROL SYSTEM FOR AN AUGMENTED ORTHOSIS

A dissertation submitted in partial fulfillment of the
requirements for the degree of
Doctor of Philosophy

By

MARIA J. GERSCHUTZ
M.S., Wright State University, 2004
B.S., Wright State University, 2003

2008
Wright State University

WRIGHT STATE UNIVERSITY

SCHOOL OF GRADUATE STUDIES

April 28, 2008

I HEREBY RECOMMEND THAT THE DISSERTATION PREPARED UNDER MY SUPERVISION BY Maria Jane Gerschutz ENTITLED Dynamic Pneumatic Muscle Actuator Control System for an Augmented Orthosis BE ACCEPTED IN PARTIAL FULFILLMENT OF THE REQUIREMENTS FOR THE DEGREE OF Doctor of Philosophy.

_____

Chandler A. Phillips, M.D., P.E.
Dissertation Director

_____

Ramana V. Grandhi, Ph. D.
Director, Ph.D. in Engineering Program

_____

Joseph F. Thomas, Jr., Ph.D.
Dean, School of Graduate Studies

Committee on Final Examination:

_____

Chandler A. Phillips, M.D., P.E.

_____

David B. Reynolds, Ph.D.

_____

Raymond Hill, Ph.D.

_____

Stanley R. Mohler, M.D.

_____

Dana Rogers, Ph.D.

ABSTRACT

Gerschutz, Maria Jane. Ph.D., Department of Biomedical, Industrial, and Human Factors Engineering, Wright State University, 2008. Dynamic Pneumatic Muscle Actuator Control System for an Augmented Orthosis.

This dissertation develops, implements and analyzes a dynamic control system for a pneumatic muscle actuator (PMA) utilizing an augmented orthosis application. The application of PMAs are limited due to poor control capabilities resulting from dynamic nonlinearities. An adequate control system applying an appropriate dynamic pneumatic muscle actuator model increases the potential utility of PMAs in high-force applications including augmented orthotic applications.

The research conducts an initial analysis evaluating the feasibility of PMAs in high-force applications (force assistance with minimal displacement). A computational simulated control system (CSCS) is developed to analyze three different control schemes. The three PMA control schemes (position feedback, moment/force feedback and adaptive control) are theoretically developed and compared using MATLAB software code. The biomimetic/biomechanical phenomenological model is utilized in the CSCS to characterize the pneumatic muscle actuator. The augmented orthotic application of the physical therapy knee extension task represents the human operator within the CSCS. By implementing the PMA model variations and human operator perturbations, the CSCS is evaluated for each control scheme. The moment/force feedback control outperformed the other schemes by providing accuracy less than ±0.5 degrees.

Finally, the dissertation implements the moment/force feedback control scheme on a physical dynamic test system. The dynamic test system contains a commercially available pneumatic muscle actuator. A comparison between open loop control utilizing strictly the phenomenological PMA model and the closed loop control implementing the moment/force feedback is conducted. Statistical analysis concludes that the closed loop method better controls the PMA dynamic nonlinearities associated with displacement. The closed loop method provides significantly lower root mean square error values for all cases analyzed.

This research develops and implements a PMA control system utilizing the phenomenological model. It provides an adequate control scheme that responds and compensates for PMA nonlinearities. Additionally, this research provides a unique high-force augmented orthotic application compared to conventional low-force applications. It introduces the use of a commercially available PMA allowing the results to be reproduced and compared. Finally, the research implements a dynamic test system providing time-dependent responses. The PMA dynamic control system presented in this research enhances the potential of PMA applications especially in the rehabilitation, assistive, and aerospace fields.

TABLE OF CONTENTS

TABLE OF CONTENTS (CONTINUED)

TABLE OF CONTENTS (CONTINUED)

TABLE OF CONTENTS (CONTINUED)

TABLE OF CONTENTS (CONTINUED)

LIST OF FIGURES

LIST OF FIGURES (CONTINUED)

LIST OF TABLES

LIST OF TABLES (CONTINUED)

SYMBOLS, ABBREVIATIONS, AND ACRONYMS

CSCS	Computational Simulated Control System
CM	Center of Mass
HOP	Human operator perturbation
LVDT	Linear Variable Differential Transducer
MSE	Mean Square Error
PID	Proportional-Integral-Derivative
PMA	Pneumatic Muscle Actuator
PT	Physical Therapy
PPR	Proportional Pressure Regulator
SCS	Simulated Control System
SD	Standard Deviation
RMSE	Root Mean Square Error
a, b, c	F_{CE} piecewise parameters
a', b'	F_B piecewise parameters
a", b"	F_K piecewise parameters
a_2, b_2, c_2	Standard deviation altered F_{CE} piecewise parameters
a_2', b_2'	Standard deviation altered F_B piecewise parameters
a_2", b_2"	Standard deviation altered F_K piecewise parameters
b, B	Viscosity Constant, Dashpot Coefficients
dt	Sampling time rate

SYMBOLS, ABBREVIATIONS, AND ACRONYMS (CONTINUED)

e	Position error
F	Force
F_A	Force exerted by the PMA
F_B	Dashpot Element Force
F_{CE}	Contractile Force Element
F_{ext}	External Force
F_K	Spring Element Force
F_i	Inertial load force
g	Gravity
g_1, g_2	Arbitrary positive scalar gain
H	Height
k, K	Spring Constant, Spring Coefficients
K_C	Updated parameter block
$\dot{K}_{C1}$, $\dot{K}_{C2}$	Minimized updated parameter
L	Length
L_1	Length of the Thigh
L_2	Length from the Hip to Center of Mass (CM)
L’	Horizontal length from Center of Mass (CM) to knee
ΔL	PMA length change
L_{LL}	Lower leg length
m	Mass of a Load/Human

SYMBOLS, ABBREVIATIONS, AND ACRONYMS (CONTINUED)

m_L	Mass of additional load
M_A	Moment Generated by the PMA
ΔM_A	Difference between consecutive PMA moments
M_A’	Updated time dependent PMA moment
M_{AR}	Required PMA moment
M_{AM}	Generated PMA moment
M_{ANEW}	Updated PMA moment
M_f	Updating Moment Component
M_K	Moment about the Knee
$\overline{M}_K$	Required Moment about the Knee to Stand
$\hat{M}_K$	Total Moment Generated by the Human
$\overline{M}_K^{'}$	Moment not accounted for by the human to complete the task
$\hat{M}_{K,T}$	Total human operator moment
$\hat{M}_{K,F}$	Human operator function
$\hat{M}_{K,P}$	Human operator perturbation
M_m	Moment Generated by the Human Muscle
M_p	Moment Generated by the Human Arm Push
M_{tot}	Total Moment Generated
ΔM	Required Moment ($\overline{M}_K$) Minus Total Moment (M_{tot})

SYMBOLS, ABBREVIATIONS, AND ACRONYMS (CONTINUED)

n	Number of sample points
P	Pressure
P_P	Predicted Pressure
r	Radius
R_{yA}	Ankle reaction force in the y-direction
t	Time
t_i	Initial Time
t_f	Final time
t_p	Time when the Push-Force is Eliminated
V	Voltage
W	Weight
x	Open loop/Closed Loop LVDT data
y	Displacement, position
$\dot{y}$	Velocity
$\ddot{y}$	Acceleration
y_i	Ideal LVDT output
α	Dynamic implementation of τ (time constant)
β	Angle Between Torso and Thigh
β_0	Intercept parameter
β_1	Slope parameter
ε	Moment error

SYMBOLS, ABBREVIATIONS, AND ACRONYMS (CONTINUED)

θ	Angle Between Thigh and Horizontal Seated Position
$\dot{\theta}$	Angular velocity
$\ddot{\theta}$	Angular acceleration
θ_f	Final Angle (CM is Directly over the Knee)
θ_p	Angle when the Push-Force is Eliminated
θ_r	Required angular position
$\dot{\theta}_r$	Required angular velocity
θ_{NEW}	Updated position
θ_0	Output angular position
τ	Visco-elastic time constant

ACKNOWLEDGEMENTS

Sincere acknowledgements is hereby granted to recognize and honor ***Dr. Chandler A. Phillips, Dr. David B. Reynolds, Dr. Raymond Hill, Dr. Stanley Mohler, and Dr. Dana Rogers*** for their devotion, guidance, assistance and support in helping me achieve this important milestone. Without their personal sacrifice, my graduation and this dissertation work would not have been possible.

Sincere appreciation and admiration are hereby expressed to: ***Jennifer Serres, Rachel Kinsler, Dave Kender, Daisy Stieger, Dr. S. Narayanan, Dr. Ramana Grandhi, Dr. Bor Jang, the Dayton Area Graduate Studies Institute, Wright State University College of Engineering and Computer Science*** and especially my family ***(David, David & Jane, Lisa & Tom, Aaron & Julie, Steven & Katie, Jennifer, Christopher, John & Catherine, Ann)*** for their support, advice and understanding through this achievement.

DEDICATION

This work is dedicated to my husband
David L. Gerschutz
without whose love, support, understanding, and patience
this degree would not have been possible

and

in gratitude to my parents
David J. and Jane A. Kahle
whom instilled in me principles of hard work and family.

1.0 INTRODUCTION AND BACKGROUND

1.1 Overview of the Research Problem

High-force pneumatic muscle actuators (PMAs) are used for force assistance with minimal displacement applications. However, poor control due to dynamic nonlinearities has limited PMA applications. With the use of an appropriate model, a control system can be designed to control the nonlinear effects. An adequate control system increases the applications of high-force PMAs. This research focuses on two augmented orthotic applications: elderly sit-to-stand task and knee extension physical therapy task. The elderly sit-to-stand task is used in a feasibility study analyzing the application of the PMA as an augmented orthosis. The knee extension physical therapy task is implemented in a simulated control system analyzing different control methods. Additionally, the knee extension task is used in a PMA dynamic test system to evaluate the preferred control method.

The PMA dynamic test system utilizes a commercially available Festo PMA. One advantage of implementing a commercially PMA is that it allows the experiment and results to be reproduced. This standardization permits the comparison of other experiments and control schemes on similar PMAs. Since the research explores high-force PMA for augmented orthoses, it is beneficial to use a commercially available PMA rated for high forces applications.

This dissertation is directed towards the analysis, development, implementation and validation of a dynamic high-force PMA control system for an augmented orthosis. PMA control is limited due to nonlinear responses and poor modeling. Implementation of an accurate model and development of feasible dynamic control scheme can enhance the potential of PMA applications. Ultimately, this research may lead to implementation of PMAs in rehabilitation and assistive applications.

1.2 Background and Review of the Literature

1.2.1 Pneumatic Muscle Actuators

Actuators have the main purpose of transferring energy into mechanical energy in particular mechanical force. Traditional pneumatic muscle actuators (PMAs) contain an internal air bladder usually constructed of rubber. It is surrounded by an outer nylon protective material. Both ends are tightly fixed with metal fastens. One end contains an air inlet and the other is completely closed. The outer protective material is constructed in a braided mesh design that allows flexibility in the radial direction and high longitudinal stiffness in the axial direction. As air pressure increases, the internal air bladder and outer material expands in the radial direction causing it to shorten in the axial direction. This action results in an axial direction exertion of force when fixed to a load; thus, it produces tension in the system. The outcome is external work at a rapid rate. Therefore, PMAs demonstrate a power/weight ratio of 1 W/g and a power/volume ratio of 1 W/cm^3 [1]. The PMA operation can be found in Figure 1. The structure and compressibility of the outer protective material causes the PMA to respond with variable

spring-like stiffness and nonlinear passive elasticity [2, 3]. The design also provides light weight and flexibility.

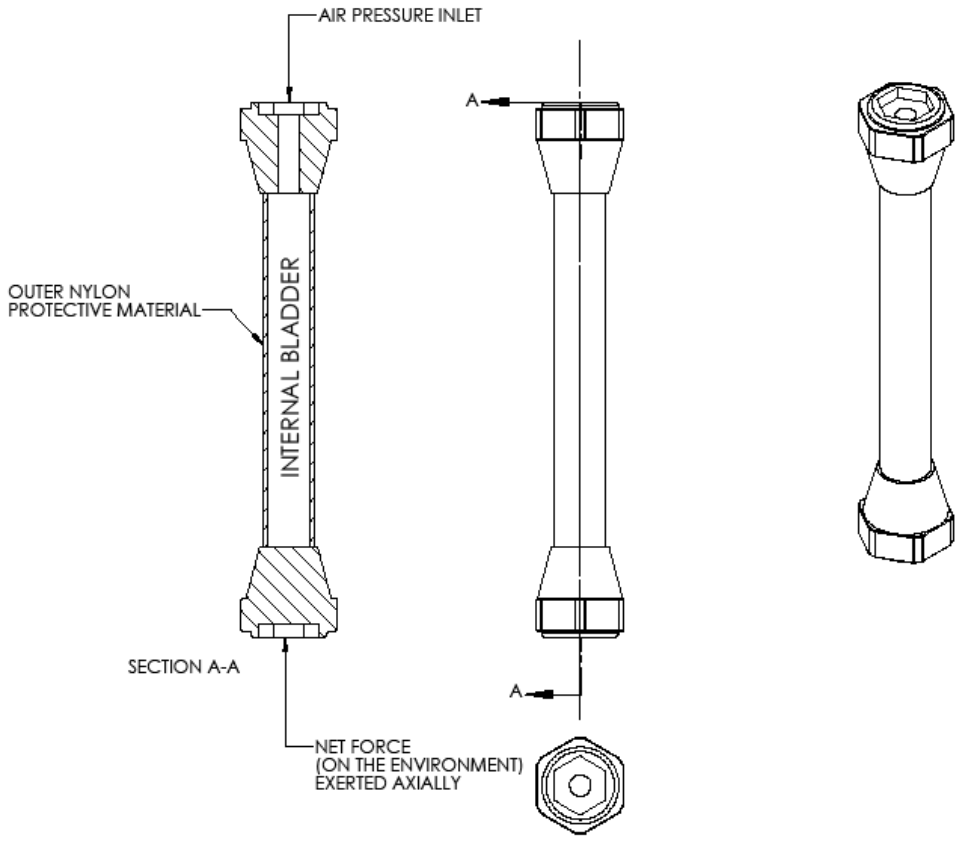

Figure 1: Operational configuration of the pneumatic muscle actuator. As the air pressure increases, the internal bladder and protective outer material expands in the radial direction generating a force in the axial direction.

1.2.1.1 Advantages and Disadvantages of Pneumatic Muscle Actuators

Three main types of actuators for robotic applications include: electrical actuators, hydraulic actuators, and pneumatic actuators. A list of actuator advantages and disadvantages are in Table 1 [4, 5, 6, 7]. Electrical actuators, which are most common, are easy to control, have low noise, and are relatively cheap. Their major disadvantages are low power and torque to weight ratios. Electrical actuators also have the possibility of sparking. Hydraulic actuators, which utilize pressurized oil, have a high power to weight ratio and low backlash. However, they are difficult to maintain, noisy, less reliable and expensive. PMAs, utilizing compressed air, contain a high power to weight ratio, power to volume ratio and a quick response time. They are also low in cost, compact, safe and available in a wide range of sizes. On the other hand, PMAs are difficult to control and can be noisy. Overall, PMAs contain numerous desirable characteristics compared to other actuators especially regarding human orthosis.

The major problem with PMAs is the control difficulties due to the non-linearity associated with the compressibility of air. The bladder expands proportionally to the square of the diameter [7]. In order to accurately control the pneumatic muscle, an adequate model is required.

TABLE 1: Advantages and Disadvantages of Actuators [4, 5, 6, 7].

	Advantages	Disadvantages
Electrical	• Easy to control • Low noise • Relatively Cheap	• Lower power and torque to weight ratio • Possible sparking
Hydraulic	• High power to weight ratio • Low backlash	• Difficult to maintain (oil leaks) • Noisy • Less reliable • Expensive • Complex servo-control
Pneumatic	• High power to weight ratio • High power to volume ratio • Low cost • Quick response time • Compactness • Inherent Safety	• Lack of accurate control • Fluid compressibility noise

1.2.1.2 Research Development of Pneumatic Muscle Actuators

Research associated with the pneumatic muscle actuators started with limb orthoses. The McKibben pneumatic muscle was developed by Joseph L. McKibben in the 1950's and early1960's and published by Baldwin [8, 9]. However, it was abandoned for electric prosthesis due to the requirement of a large gas supply. It was not until the 1980's that it was recreated by (the Japanese company) Bridgestone [9]. In 1987, the pneumatic (artificial) muscle was explored and renamed the "Rubbertuators" by Inoue [6, 9]. Throughout the years different models of pneumatic (artificial) muscle have been created and renamed with different titles. The most current is 'pneumatic muscle' coined by Caldwell in 1995 [9, 10].

The PMA sparked renewed interest due to similarities to biological muscle. Biological muscle is based on three components: pure force generator, elastic component and damping component [9]. PMAs reflect biological muscle with their high power to weight ratio, high power to volume ratio [5], and contraction mechanism. Biological muscle exhibits good position and force control. However, pneumatic muscle has shown slow advancements with control due to nonlinearities.

Another limitation of PMAs includes a small contraction percentage of approximately twenty percent. However, this is comparable to skeletal muscle's contraction ability. The PMA is not ideal for high precision task [6]. Therefore, it is important to address the task and task rate designated for the application of the PMA.

1.2.2 Pneumatic Muscle Actuator Modeling

Three distinct modeling approaches have been explored in order to characterize the PMA. They include a physical geometric model, biomimetics model, and a phenomenological model.

1.2.2.1 Physical Geometric Model

One of the first to analyze the relationship between pressure and force of the PMA was Schulte [11]. Complex theoretical equations were created relating the geometric structure and the contractile force [5, 12]. The generated equations were functions of the input pressure, initial length and diameter of the PMA, braid thread angle, thread length, and the number of thread turns.

$$F = \frac{\pi D_0^2 P'}{4}(3\cos^2 \theta - 1) \quad (1)$$

Where θ is the angle between threads, P' is the relative pressure, and $D_0 = \frac{b}{n\pi}$ is the diameter when θ = 90 degrees (b is the thread length and n is the number of turns of a thread) [12].

Static length-tension testing were performed by Chou and Hannaford [3, 12]. The results were compared to human skeletal muscle to determine feasibility in a robotic arm. Tondu and Lopez [9] altered the physical geometric model (which previously contained only braid dimension parameters) by incorporating a muscle contraction ratio. They also compared the physical model to human skeletal muscle. Klute and Hannaford [13] conducted nonlinear modeling using Mooney-Rivil mathematical description. Bladder material properties were inserted into the physical geometric model. The improved results still displayed a discrepancy in predicting actuator force.

Additional PMA structure modifications have been studied to help improve the accuracy of the physical geometric model. The air flow was analyzed to help increase the bandwidth, system stiffness and reduce the air consumption [14].

The physical geometric model research strictly analyzes PMA behavior in a quasi-static state and incorporated no hysteresis (time) information. The physical geometric models are not beneficial for real time control application because the geometric structure is difficult to obtain during experimentation, in other words, these variables are in accessible.

1.2.2.2 Biomimetics Perspective Model

Biomimetics explores natural occurring phenomena for an insight in device design. It provides reliability and robustness [15]. The biomimetic approach models the PMA by revising the Hill muscle model to include energetic and viscoelastic parameters. The energetic parameter refers to the chemo-mechanical energy conversion and viscoelastic refers to the internal-element stiffness variation [16]. The research models the excitation and contraction of isometric skeletal muscle. The biomimetic controller is a biophysical, biochemical, and biomechanical model of the excitations-contractions coupling during skeletal muscle isometric contraction [17].

In the case of the PMA, the behavior is analogous to biological muscle [15]. Both biological muscle and PMA generate force only by the means of contraction. As pressure builds in the PMA, it expands radially causing a force contraction in the axial direction mimicking biological muscle.

1.2.2.3 Phenomenological Model

From the biomimetic principle discussed above, a phenomenological biomimetic/biomechanical model is proposed by Reynolds et al. [7]. Similar to biological muscle, PMA experiences viscoelastic resistance as it expands which can be modeled as a dashpot and spring respectively. The mechanical Voight Model (Eq. (2)) best explains this viscoelastic resistance. It combines the dashpot and spring in parallel with a viscosity constant b, and spring constant k respectively. Knowing the displacement y and velocity $\dot{y}$, the total force can be determined by the following equation:

$$F = b\dot{y} + ky \tag{2}$$

Using biomimetic principles, Eq. (2) can be applied to the PMA. However, the PMA requires an additional element to describe the internal force. The contractile force element, F_{ce}, explains the internal active contraction force source of the PMA [18]. The Voight Model is altered to contain the F_{ce} in parallel with the dashpot and spring. The elements configuration is displayed in Figure 2. The contraction force opposes the action of the dashpot and spring. The new equation to describe the force in the PMA can be found in Eq. (3).

$$F_A = F_{ce} + b\dot{y} + ky \tag{3}$$

An in-house PMA is constructed at Wright Patterson Air Force Base [7]. The research focuses on characterizing the phenomenological PMA model with respect to dynamic motion. The following equation is formulated to explain the dynamic motion of the vertical test system:

$$m\ddot{y} + B\dot{y} + Ky = F_{ce} + F_{ext} \tag{4}$$

where the B, K and F_{ce} are the dashpot, spring, and contractile element coefficients, respectively. F_{ext} is the external force applied and m is the mass of the load. In Reynolds et al. [7] article, F_{ext} is the load weight (load mass times gravity). Finally, the

displacement is symbolized by y. The velocity and acceleration are $\dot{y}$ and $\ddot{y}$, respectively.

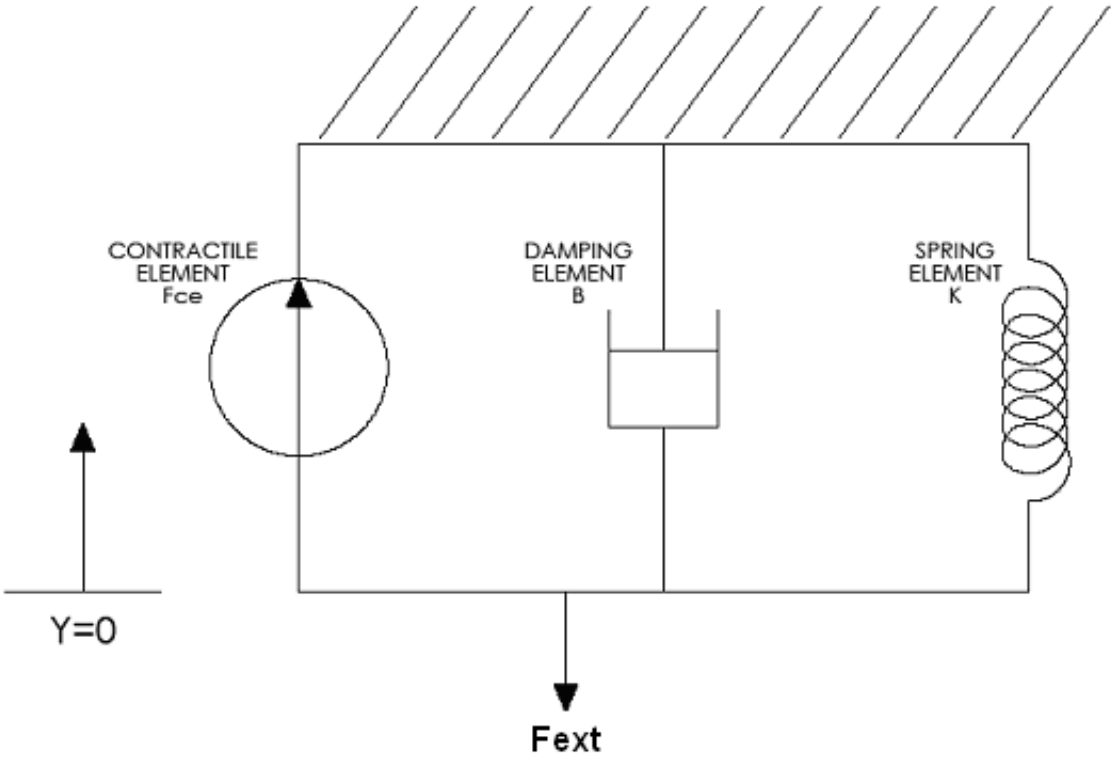

Figure 2: Phenomenological PMA model: Parallel configuration of the contractile element, damping element, and spring element.

To characterize the elements as functions of pressure, a "bell ringer" study was conducted to parameterize the dashpot (B) and spring (K) responses [7]. After the "bell ringer" study, the contractile force element (F_{ce}) was determined at several pressures and loads by analyzing total contraction curves, using the solution to Eq. (4). The following in-house PMA parameter characterization was determined for pressure up to 600 kPa [7]:

$$K(P) = 5.71 - 0.0307P \quad (5)$$

$$B(P) = 1.01 - 0.00691P \text{ for PMA contraction} \quad (6)$$

$$B(P) = 0.60 - 0.000803P \text{ for PMA relaxation} \quad (7)$$

$$F_{CE}(P) = 2.29P \text{ for } 0 \leq P > 200 \text{ kPa} \quad (8)$$

$$F_{CE}(P) = 179.2 - 1.39P \text{ for } P \geq 200 \text{ kPa} \quad (9)$$

It is determined that the F_{ce} is approximately independent of the applied load (F_{ext}). The characterized dashpot, spring, and contractile force parameters are entered into Eq. 4 to express the length change of the PMA. The validation concludes that the phenomenological model accurately predicts the length change of the PMA.

1.2.3 Pneumatic Muscle Actuator Control

1.2.3.1 Complexity Theory

Complexity theory emerged in the 90's as concepts used to simplify a complex system [19]. Since systems are generally so complex, there is no one simplifying

technique. However, there are many possible approaches. In general, complexity theory models a system by characterizing system elements in a non-reduced form [19].

Complexity theory entertains new concepts that the general system theory lacks. First, it considers the nonlinear relationship between dynamic elements of the system while system theory analyzes static linear relationships. Second, complexity theory incorporates the quality and quantity components compared to only the quantity component. Finally, general system theory assumes time-invariant parameters. Therefore, it is not necessary to study the interaction between system elements. However, complexity theory studies dynamic (time information) element interaction characteristics [19].

Categories are formulated to help understand the concepts behind complexity theory. There are three main categories: algorithmic complexity, deterministic complexity, and aggregate complexity [19]. Algorithmic complexity utilizes mathematical complexity and information theory. This method is normally implemented when the characteristics of the system are hard to describe. It also helps in determining the best solution approach to a system [19]. The goal is to formulate the simplest model that can accurately predict the system behavior. Deterministic complexity is directly related to the chaos theory (nonlinear dynamics) and catastrophe theory. The complex system is modeled largely with a few elements to create a stable system susceptible to discontinuities [19]. Deterministic complexity contains four predominate characteristics: deterministic mathematics/mathematical attractors (asymptote over time), feedback notion, initial condition sensitivity/bifurcation (sudden change in attractors), and deterministic chaos [19]. Finally, aggregate complexity studies the relationship between

individual elements and their behavior in a complex system. The technique or combinations of techniques are dependent on the characteristics of the complex system.

1.2.3.2 Nonlinear Dynamics and Control

Nonlinear dynamics occurs when a small change in an element does not necessarily cause a proportional (linear) relationship with other elements in the system. On the other hand, linear dynamics refers to the proportional relationship between two states. Nonlinear dynamic systems require the use of new techniques including complex theory. The term dynamics refers to the study of time responses.

Modern nonlinear control techniques are mathematically complex and computationally difficult. They are usually not feasible with large scale systems [20]. A detailed dynamic model within a predictive controller is commonly used in systems with strong nonlinear characteristics [20]. Therefore, an adequate model is required for accurate control. The process of system identification is used to design a control model for linear systems [21]. This is only useful if the dynamic behavior for the operating region is linear. Linear systems are commonly used because there is a lack in understanding nonlinear systems. There are nonlinear system identification techniques that can be useful in modeling nonlinear systems. They include Poincaré maps, Lyapunov exponents, and dimension techniques [21]. The type of nonlinear behavior exhibited by the system is classified by Poincaré maps. Lyapunov exponents explain the steady-state nonlinear behavior. Finally, dimension techniques identify the number of first-order differential equations required for the mode [21]. These identification

techniques aid in the construction of a nonlinear model. Modeling usually incorporates model variables and time characteristics of the dynamic system.

In classical control literature, many control techniques require exact knowledge of the system which is impossible with nonlinear systems. Some control methods include LQ control strategy (linear optimal control with quadratic cost function) and active controllers: frequency domain, neural networks and fuzzy control [22]. The active control strategies can be used for nonlinear control. The neural networks and fuzzy control are unique because they do not necessarily require mathematical modeling for control [22]. Fuzzy control provides mathematical structure for resolving "fuzzy" or uncertain information.

Nonlinear systems have also been controlled using the control engineering approaches of feedback linearization, adaptive control and variable-structure control. Feedback linearization helps reduce uncertainty and stabilizes an unstable system [20]. This method is similar to PID (proportional-integral-derivative) control. PID is usually the first approach of control attempt. Adaptive control is used in practical engineering environments where there is limited knowledge of parameters [23]. In particular, a technique called minimal control synthesis utilizes adaptive controls with reference linear models to account for nonlinearities [23]. Wagg [23] concludes that nonlinear dynamic behavior could be predicted using the minimal control synthesis model when nonlinearity changes were minimal. Additionally, the technique is only sufficient when nonlinearities associated with the reference model and the system is similar [23]. Another method of control is variable-structure control used in controlling robotic manipulators, power converters and chemical processes. A central feature requirement is a sliding mode

where the system state crosses subspaces [24]. Knowledge about the nonlinear system's characteristics is an asset to nonlinear control.

1.2.3.3 Research Development in Pneumatic Muscle Control

Pneumatic muscle actuators contain many beneficial characteristics for robotics and rehabilitation applications. However, application is hindered by control difficulties. Another limitation directly relates to PMA control is modeling errors [14]. Model errors are associated with its complex structure. Therefore in order to control the PMA, an adequate model is required. PMA models are previously discussed in section 1.2.2.

Multiple control strategies have been developed in an attempt to control PMAs. One of the first control attempts developed an adaptive pole-placement controller for a robotic elbow by Caldwell et al. in 1994 and 1995 [4, 10]. The controller utilizes the physical geometric model and an online identification. A correction factor is also implemented because the force estimation from the theoretical physical geometric model was approximately 40-50% efficient. The control system assumes a linear control process and implemented a step reference input. There is an improvement on position regulation. The reported results indicate a trajectory accuracy of ±1 degree for constant steady-state points at pressures under 200 kPa.

Another control method proposed by Repperger et al. in 1998 [18] is a variable structure controller. The large scale antagonistic PMA controller utilizes the first generation of the phenomenological model. The first generation phenomenological model is composed of an elastic (spring) and viscous (dashpot) elements in parallel (Voight Model). The theoretical development addresses issues of robustness, passivity,

and stability regarding different dynamics (inflation and deflation characteristics). Position and velocity feedback information is subjected to bandwidth limitations and a complex structure.

An additional control method developed by Repperger et al. in 1999 [1] is a nonlinear feedback controller using gain scheduling for position tracking. Gain scheduling look-up tables are constructed for the first generation phenomenological model elastic and viscous elements. This controller provides a simpler implementation structure than the variable structure controller. Simple sawtooth testing using the gain scheduling look-up tables is performed. The controller is able to reproduce reasonable dynamics for the given parameters. However, no statistical analysis is conducted. Additionally, time delay problems and missing nonlinear effects are still present with this control system and PMA model.

Another method, sliding mode control using Lyapunov stability theory, is tested on simulated data by Cai et al. [25]. Only simulated results are presented. Fuzzy logic control with a nonlinear feed forward controller is also investigated by Balasubramanian et al. [26]. Two methods, weight average and least square error, are implemented in the simulation. The least square errors produce better results compared to the weighted averages. Overall, the fuzzy logic controller is difficult to implement in practice.

A nonlinear proportional-integral-derivative (PID) control with neural networks is proposed by Thanh et al. [27]. Instead of step reference inputs, sinusoidal waveforms are utilized. A comparison between conventional PID and the new proposed PID with neural networks is analyzed. It is concluded that the proposed PID with neural networks

performed better than conventional PID control. The conclusions are not supported with statistical analysis.

Most recently, a controller proposed by Repperger et al. in 2006 [15], conducts an empirical and theoretical study. A force feedback control for an agonist-antagonist system utilizes the biomimicry model. Reasonable dynamic results are produced.

Most attempted control systems assume linear analysis and step reference inputs. The results are commonly simulated and contain no statistical analysis. The methods that addressed the PMA nonlinear dynamics lack actual physical application. Additionally, the models used in these control methods insufficiently characterize the nonlinear dynamics of the PMA. It is vital that an accurate model that incorporates the PMA's dynamics formulates the foundation of the controller.

1.3 RESEARCH GOAL AND OBJECTIVES

PMAs respond with nonlinear dynamics with regards to pressure changes. It is important to understand the reason for nonlinearity. Assuming that pressure is a linear function of time, the volume expansion that occurs in the PMA tubing is a nonlinear function of the input pressure. This is explained by the mechanics of the PMA system. Since the force (equal to the pressure times the area of the PMA tubing) and the area are directly related to the volume, the external contractile force generated is also nonlinear. Therefore, the output force is a nonlinear function of the input pressure.

The goal of this research is to advance control of the PMA. By exploring the control system's dynamics, greater knowledge associated with control characteristics can

be obtained. Greater understanding of the system allows for more accurate control. This goal will be achieved by addressing three objectives.

1.3.1 Objective 1

The first objective implements the phenomenological model within a PMA controller. From this model, a simulated control system (SCS) is developed. Even though the outer control loop includes position information, the feedback is preformed on the internal force information. The SCS model also contains time constant information which is incorporated in the internal force feedback loop.

1.3.2 Objective 2

The second objective is to develop a computational simulated control system (CSCS). The CSCS incorporates the knee extension physical therapy task, load cell (force) information, and an external position feedback loop. It compares a moment/force feedback controller, position feedback controller, combined moment/force and position feedback controller and an adaptive controller with predictor-corrector properties.

1.3.3 Objective 3

The third objective is to implement the CSCS in a PMA dynamic test system. The dynamic test system is constructed with a commercial FESTO PMA, DC servo motor and sensors. Experimental testing evaluates the preferred control method determined in the second objective. It compares the control method with the open loop phenomenological model.

2.0 METHODS: COMPUTATIONAL SIMULATED CONTROL SYSTEM DEVELOPMENT AND IMPLEMENTATION

2.1 A computational simulated control system for a high-force pneumatic muscle actuator: System definition and application as an augmented orthosis

A simulated control system (SCS) is developed utilizing the physical sit-to-stand task. The SCS implements the characterized phenomenological PMA model from Reynolds et al. (2003) in-house PMA and time constant information. It computationally evaluates the feasibility of the PMA as an augmented orthosis.

2.1.1 Introduction and Background

Orthoses as devices that assist an impaired bodily function have been utilized even before recorded history. The walking stick carried by ancient people was not only a defensive weapon, but an early form of crutch-cane to offload weight on an arthritic hip. Orthoses can be categorized as either passive (conventional brace orthoses [28, 29]) or active (additional power source added to the passive conventional orthoses [28, 29, 30]).

Technological developments allow for the design of augmented orthoses. Augmented orthoses are active orthoses with intelligent control. Examples of augmented orthoses include a reciprocating gait orthosis (RGO) augmented by computer directed muscle stimulators [31, 32] and the RGO with a sensory feedback system (SFS) [33, 34]. These devices provided mobility assistance for spinal cord paralyzed individuals.

The pneumatic muscle actuator (PMA) is another technological development. PMA's can be divided into two categories: a low-force PMA and a high-force PMA. Low-force PMA refers to a small-sized device, used in multiples of five or ten, for movement assistance under low force conditions. Some applications using low-force PMA's include functional recovery in physical therapy [35] and as the activator in a human arm orthosis [9]. The rubbertuator manufactured by Bridgestone (Japan) uses the low-force PMA in the design of a suspended robot called the SoftArm [6]. High-force PMA refers to a large-size device, used singly or in pairs, for force assistance under low displacement conditions. Applications include industrial purposes utilizing the commercially available Festo (Germany) fluidic muscle [36, 37] and rehabilitation purpose as an active orthosis [30, 38].

A significant problem with pneumatic actuators, in general, and PMA's in particular, is their inaccuracy and difficulty to control. Nonlinearities exist as the pressure changes in the bladder of the PMA because its area expands radially but the output force is translated axially. Theoretical predications of the net force produced by low-force PMA's on the environment have been made [5, 12]. To date, there has been limited research on high-force PMA orthotic applications. In order to address problems of high-force PMA control using the methods of classical control theory, a model of the plant (PMA) is required.

Utilizing this plant model, the controller can then be designed. With respect to high-force PMAs, there have been two modeling approaches: biomimetics modeling and phenomenological modeling.

Biomimetic modeling characterizes the PMA plant as a Hill-type [39] muscle model which is revised to describe the chemo-mechanical energy process and the internal-element stiffness variation during an isometric muscle contraction [16]. The biomimetic controller for this plant is a biophysical, biochemical and biomechanical model of the excitations-contractions coupling during skeletal muscle isometric contraction [17].

An evaluation of controller design has been reported with a high-force PMA system being used in a force control sense over a full cycle of operation [15]. A number of power and energy related messages are assessed in the study, including a work loop method and a power ellipsoidal method. The biomimetic controller and plant model described previously [16, 17] has been specifically evaluated by performing force tracking with a position constraint [40]. The PMA in this study performed the force tracking over a complete work loop cycle.

Phenomenological modeling of the PMA dynamics allows for the examination of tasks in which there are unconstrained length variations during which force control is necessary. A phenomenological PMA dynamic model consisting of the parallel arrangement of a spring element, a damping element and a contractile force element has been developed [7]. However, to date there has been no report of a controller design for utilizing this model. The phenomenological PMA model is discussed in more detail in section 1.2.2.3.

An important high-force application for such a control system is assisting an individual to rise from a seated position to a standing position. The inability of elderly individuals to adequately perform this function is a major limitation to their independent

living [41, 42, 43]. Such a task requires simultaneously both force control and position control.

Elderly tend to have a reduction in muscle strength and coordination ability [42]. If mobility is low, a person may be moved from independent living to an institutional facility. Therefore, it is important to assess their functional mobility. One common daily task to determine an individual's function status is the sit-to-stand (STS) motion [44]. STS has been found to be the most mechanically demanding daily task [45, 46]. The largest moment generated about the STS task is about the knee [41]. By analyzing the STS regarding the PMA, it develops a high-force PMA application and provides potential benefits to elderly. A PMA assistive orthosis incorporated with the STS task will help reduce the amount of people institutionalized.

STS is performed in three main stages. The first stage is the forward lean of the upper body. This motion contributes by generating momentum and moving the center of mass closer to the knees [45]. The second stage moves the body both in the vertical and horizontal directions. It is the stage where the lower body dynamics mostly occurs. At the center of mass, the hips and knees are simultaneously moved vertically and horizontally until the center of mass is directly over the knees. Finally, the motion of upright positioning occurs. The upper body performs a reversal movement to correct for the initial forward lean. Simultaneously, the hips line up with the knees. Sometimes arm assistance (arm pushing force), mainly in the second stage, is used to help reduce some of the moment about the knee. This is very common when elderly experience a depletion of leg strength [8].

The objective of this study is to develop a simulated control system (SCS) consisting of (1) a controller relating an input position angle to an output pressure regulator voltage, (2) a phenomenological model of the PMA with an internal dynamic force loop, (3) a physical model of a human sit-to-stand task, and (4) an external position angle feed-back loop.

2.1.2 Physical model of the task

A physical model is developed to simulate the common sit-to-stand task. In this task, the PMA acts in conjunction with the quadriceps muscle group producing a moment about the knee. The first step is to calculate the normal (required) moment about the knee to complete the sit-to-stand task. The second step is to identify human anthropometric parameters.

To calculate the required normal task knee moment, a point mass free body diagram of half the body (Figure 3) is constructed. The model approximations include constant velocity (first order equation) and a point mass analysis for half the body. By summing the moments about the knee joint, it is determined that

$$M_K = mL'^2 \ddot{\theta} - mgL' \tag{10}$$

where L' is the horizontal length from the center of mass (CM) location to the knee, M_K is the moment about the knee, m is the mass of the point mass (located at CM), $\ddot{\theta}$ is the angular acceleration and g is gravity.

Assuming a first order equation (constant velocity) which results in $\ddot{\theta}$ equal to zero, Eq. (10) simplifies to

$$M_K = mgL' \tag{11}$$

acting in the clockwise direction.

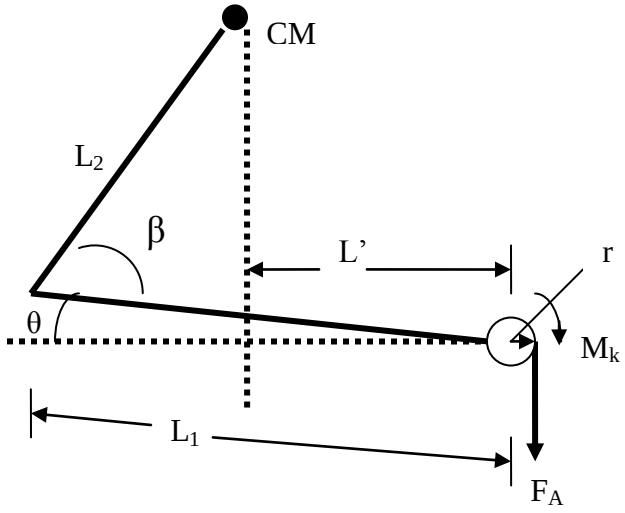

Figure 3: Sit-to-stand task free Body Diagram used to calculate the moment about the knee. Free body diagram of the point mass system where CM, L_1 and L_2 are the center of mass, length of the thigh, and length from the hip to CM respectively. L' is the distance from the CM to the knee and R is the radius of the wheel attached to the actuator system. F_A is the force generated by the pneumatic muscle actuator system. Finally, β is the fixed angle between the torso and the thigh and θ is the angle between thigh and the horizontal plane.

The second phase identifies all parameters using approximate subject values for simulation. These values can be easily altered for different subjects. The mass and height of the subject is specified as 68 kg and 1.75 meters, respectively. From anthropometric data [47], the length from the center of mass (CM) location to the hip (L_2) and thigh length (L_1) are calculated. The mass at the CM, m, is the combined weight of the head, arms and torso (HAT) acting on one leg. The knee or PMA pulley radius (r) and the fixed torso angle β are approximated to be 0.0125 m and π/5 radians, respectively. An anthropometric table of values utilized is located in Table 2. Finally, L' is calculated from the following equation:

$$L' = L_1 \cos(\theta) - L_2 \cos(\beta - \theta) \tag{12}$$

where θ ranges from zero to π/5 radians.

TABLE 2: Anthropometric Parameters

Parameter	Value
M (mass)	68 kg
H (height)	1.75 m
W (weight)	(9.8*M) N
m (mass of the point mass at CM)	(0.339*M) kg
L_1 (thigh length)	(0.245*H) m
L_2 (CM length)	(0.21698*H) m
r (knee/wheel radius)	0.025 m
α (angle between torso and thigh)	π / 3 radians

By combining Eq. (11) and Eq. (12), the equation relating the moment about the knee and the sitting angle (θ) is:

$$M_k = mg * (L_1 \cos(\theta) - L_2 \cos(B - \theta)) \quad (13)$$

The task motion proceeds from θ equal to zero until the CM location is directly over the knee (π/5 radians). The moment about the knee versus θ (from 0 to π/5 radians) is shown in Figure 4. Eq. (13) is approximated by finding the best fit line. The final mathematical equation for the required knee moment is:

$$\overline{M_k} = -85.094 * \theta - 54.774 \quad (14)$$

Eq. (14) directly relates θ and the moment about the knee, where $\overline{M}_K$ is the required moment to stand.

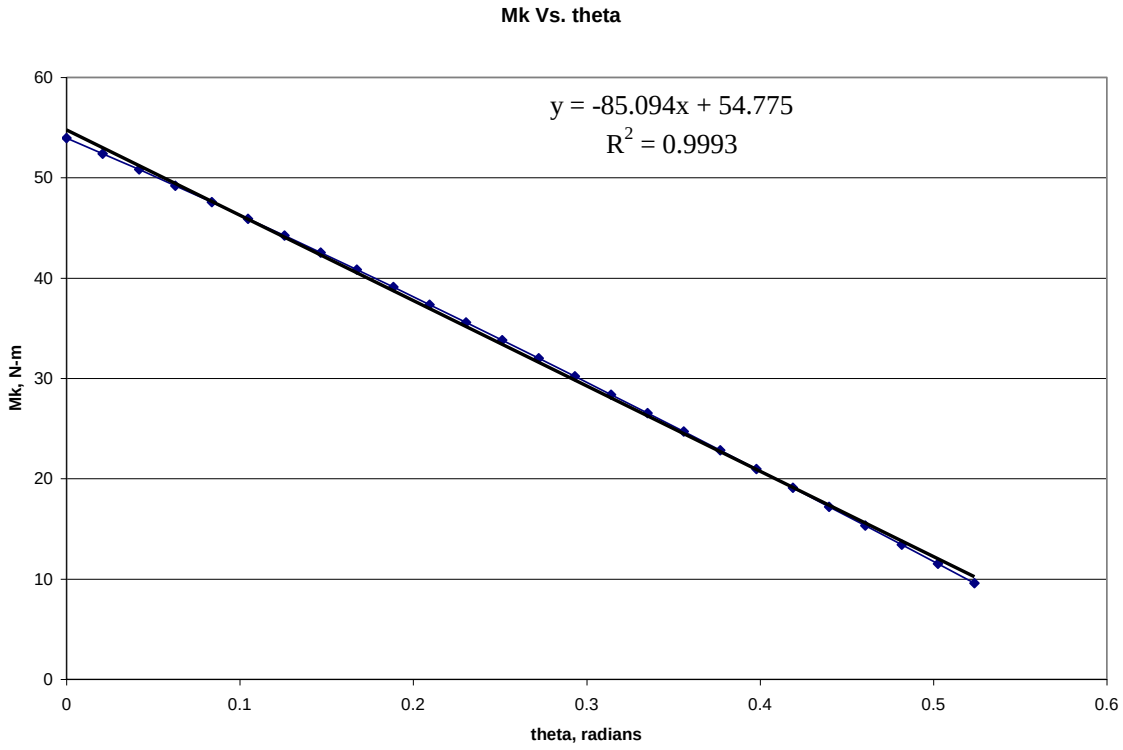

Figure 4: Sit-to-stand moment about the knee versus angle (theta) plot. The figure displays the required moment versus the angle θ (ranging from 0 to π/5 radians). M_k and theta is equivalent to y and x respectively. The best fit line estimation is displayed.

2.1.3 Controller identification: Feed-forward system

A simulated control system (SCS) is developed in a MATLAB® platform. The SCS is constructed by creating a feed-forward system with an external position control loop and an internal dynamic force loop. The feed-forward path consisted of a controller, proportional pressure regulator (PPR), PMA model and the physical model.

The goal of the SCS is to uniquely define the controller which relates required angular position, θ_r, to a voltage command, V. The PPR simply converts the voltage command to an input pressure for the PMA model.

The PMA model is based on the three element phenomenological model from [7] introduced in section 1.2.2.3. This biomimetic/biomechanical model, which is an adaptation of the Voight visco-elastic model [7], consists of a spring element (elastic), a damping element (viscous), and a contractile element. Each element is independently characterized as functions of pressure in order to predict the PMA response. The PMA moment (M_A) is calculated by modifying the phenomenological PMA model equation (Eq. (15a)) from Reynolds, et al. [7]. The modified equation (Eq. (15b)) converts forces to moments given radius, r, and removes the inertial force (F_i) due to the assumption of constant velocity. The characterized parameters from the in-house PMA in Reynolds et al. [7] are used to simulate the PMA model. The characterized PMA parameters as functions of pressure can be found in Table 3. The in-house high-force PMA from Reynolds et al. [7] is constructed with a bicycle tire tubing inner bladder (22.2 mm diameter) encased in nylon sheath used to support electrical cables [7].

$$F_A = F_{CE} - F_i - F_B - F_K \tag{15a}$$

$$M_A = F_A \cdot r = \left[F_{ce}(P) - F_K(P) - F_B(P) \right] \cdot r \tag{15b}$$

where F_i, F_{ce}, F_K and F_B are the force associated with the inertial load, the contractile element, the spring element, and the damping element as a function of pressure (P) respectively and r is the radius (moment arm) of the PMA pulley. F_B and F_K are defined in terms of B and K in Eq. (16a) and Eq. (16b), respectively.

$$F_B = B\dot{\theta} \quad (16a)$$

$$F_K = K\theta \quad (16b)$$

where B and K are defined in Table 3, $\dot{\theta}$ is angular velocity and θ is angular position. It is concluded in Reynolds et al. [7] that the phenomenological PMA model is an adequate model to describe the response of the PMA.

TABLE 3: In-house PMA Parameters as Functions of Pressure from [7]

K	5.71+0.0307P [N/mm]
B	1.01+0.00691P [N s/mm}
FCE	179.2++1.39P [N] for P>200
	2.29P [N] for P<200

The physical model approximates the human physical characteristics for a sit-to-stand (section 2.1.2). The PMA moment, M_A, corresponds to the required physical task moment, $\overline{M}_K$. The relationship between these two parameters is explained in detail in section 2.1.6.

The goal of the SCS is to define the controller block. The controller can be uniquely defined by solving for the inverse of Eq. (15b).

2.1.4 PMA time constant model: Internal dynamic force feedback loop

In order to include the dynamic force effects due to the PMA model visco-elastic time constant (τ), the value of the PMA τ is calculated as a function of pressure. The time

constant (τ), representing the servo-valve response, indicates real time PMA reaction response. It is calculated as shown in Figure 5 using Eq. (17):

$$\tau = \frac{B(P)}{K(P)} \tag{17}$$

where B and K are the damping and spring characterized pressure parameters taken from Reynolds et al. [7] in-house high-force PMA (Table 2). The time constant, τ, dynamically changes with input pressure.

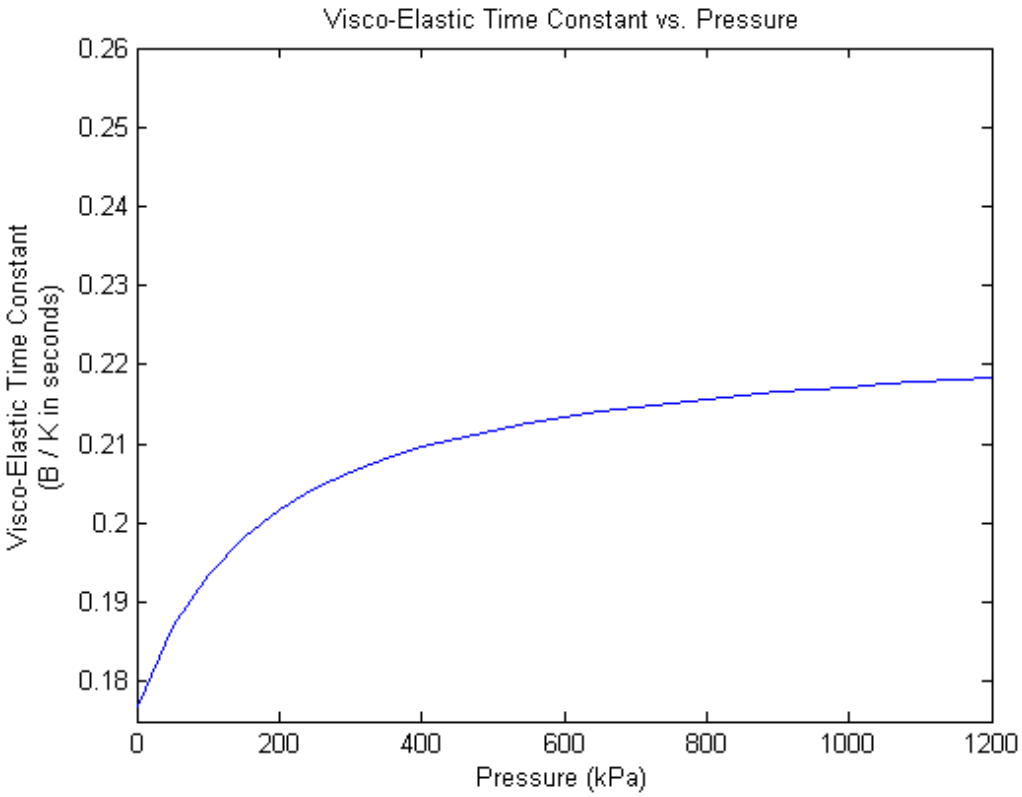

Figure 5: Visco-elastic time constant (B/K in sec)

Operationally, an internal dynamic force feedback loop is then implemented using the following equation.

$$\dot{\varepsilon} = \frac{d\varepsilon}{dt} \tag{18}$$

This internal loop simulates the time lag effect of the servo-valve with the following procedure. The difference between the PMA moments at two consecutive angles is calculated by following equation:

$$\Delta M_A = M_A(\varepsilon_{i+1}) - M_A(\varepsilon_i) \tag{19}$$

The feedback iteration process (over successive incremental time intervals dt) allows for real time calculation of an updated parameter, M_f:

$$M_f = \frac{1}{\tau}\int \Delta M_A dt = \frac{1}{\tau}\sum \Delta M_A \tag{20}$$

The updated parameter (M_f) is added to the original PMA moment (M_A) to compute an updated time dependent PMA moment referred to as M_A' (see force feedback loop in Figure 6). The schematic in Figure 6 displays the complete SCS configuration including the feed-forward pathway, the external position loop, and the internal dynamic force loop.

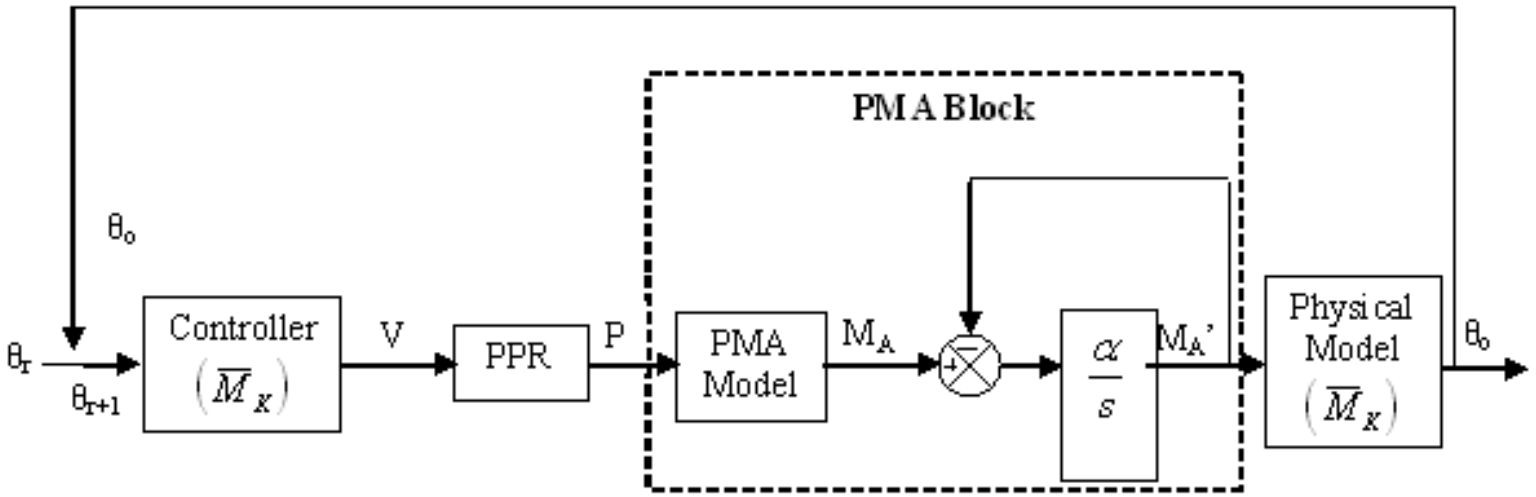

Figure 6: Schematic of the assistive pneumatic muscle with the internal dynamic force loop and a uniquely define the controller. PPR, PMA model, and physical model are the proportional pressure regulator, proposed three element model, and the physical characteristics respectively. θ_r and θ_0 are the required angle and output angle respectively. The following symbols are referenced to: V-voltage, P-pressure, M_A-moment generated by the PMA, M_A'- updated moment generated by the PMA and $\overline{M}_K$ - required task moment of the physical model.

2.1.5 SCS open-loop model validation

The SCS utilizing the PMA model is validated using the PMA length change and pressure raw data from Reynolds' et al. [7] Figure 10 between the time intervals of twelve and twenty-four seconds. Since the triangular input pressure wave has a long period of approximately seven seconds, the damping effects are considered negligible. Therefore, the model reduces to the contractile element and spring element in parallel. The open-loop feed-forward system is examined using the schematic in Figure 7. The length change output of the system is:

$$\Delta L = \frac{F_{ce}(P) - F_{ext}}{K(P)} \tag{21}$$

where ΔL is the PMA length change, $F_{ce}(P)$ is the contractile element force as a function of pressure, F_{ext} is the external weight applied to the system (given with the raw data), and K(P) is the spring constant as a function of pressure. The resultant calculated length change (Eq. (21)) is plotted against the actual PMA raw data of Reynolds et al. [7] in Figure 8. The method represents an external validation of the PMA model in the context of the feed-forward open-loop SCS. The oscillating change pressure results in both a measured and simulated length change.

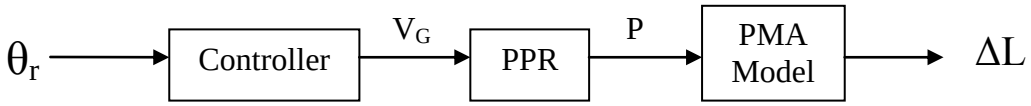

Figure 7: SCS open loop used in validation.

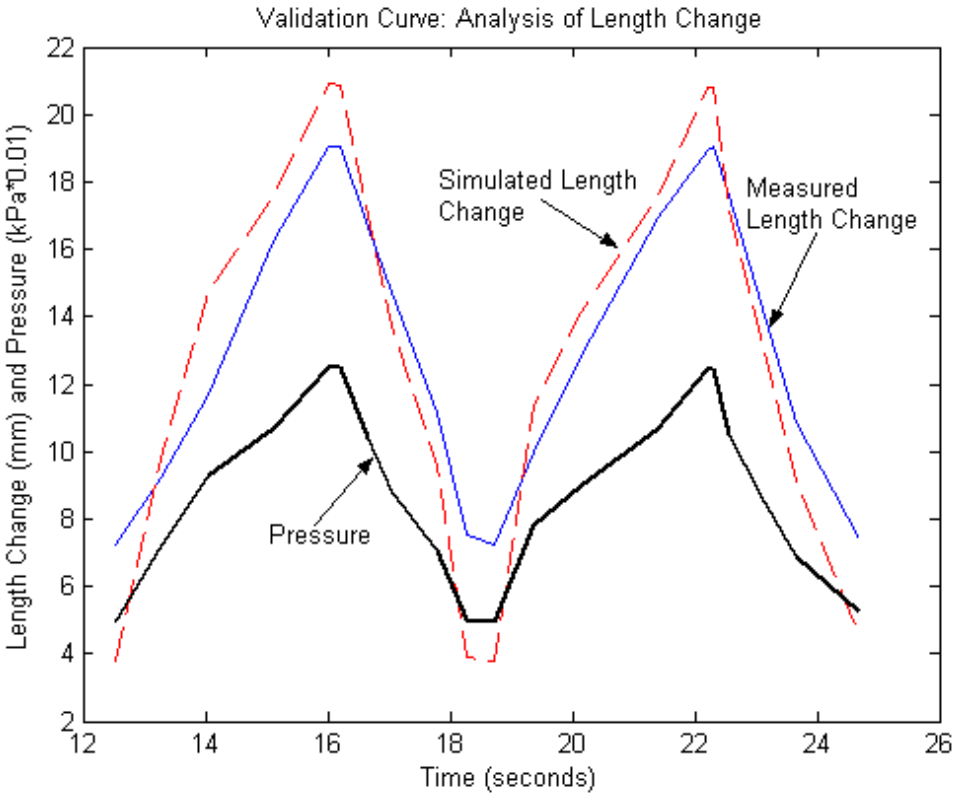

Figure 8: Phenomenological Validation curve: Measured and simulated PMA length change with corresponding input triangular pressure wave.

2.1.6 SCS Model application

The model application of the sit-to-stand physical task involves two phases and exercises four special case solutions. The sit-to-stand task is separated into two phases: phase I-static subtask and phase II-dynamic subtask. Phase I-static subtask simulates the preparation to stand where the thigh is not permitted to move (θ equals zero radians). It represents the ability to generate sufficient moment required before dynamic motion can occur. Phase II-dynamic subtask is the dynamic standing movement where θ ranged from 0 to $\pi/5$ radians.

Within each phase, cases are identified based on the amount of assistive moment required from the PMA. Case 1 is defined as a person capable of generating the total required moment (no PMA assist). Case 2 is defined as a person capable of generating enough moment initially (PMA assist only required during phase II) with/without the aid of a pushing force from the arms. Case 3 is defined as a person not capable of generating the required moment to stand even with the aid from a push (PMA assist for both phase I and phase II).

Since the PMA model is characterized from an in-house PMA, certain restrictions are placed upon the PMA input pressure. The pressure is restricted to the range of 100 kPa and 600 kPa due to the non-linearity of the PMA operating range. As a result, there is an upper and lower limit to the moment generated by the PMA system. This pressure range allows the definition of the three cases described above in terms of the percent amount of moment the human capability (with both the leg muscle and arm pushing effort).

2.1.6.1 Phase I – static phase

Since phase I is static, only the force contractile element is used to calculate the PMA moment (M_A). There is no position or velocity terms in the PMA model equation (Eq. (16b)) due to no actual movement. A high PMA assistive moment, M_A, corresponds to a low human effort and a low PMA assistive moment, M_A, corresponds to a high human effort.

The identification of the three previously discussed cases for phase I are as follows:

Case I.1: $\hat{M}_K = 100\% \ \overline{M_K}$ (No PMA assist)

Case I.2: $\hat{M}_K = 100\% \ \overline{M_K}$ (No PMA assist)

Case I.3-1: $\hat{M}_K = 90\% \ \overline{M_K}$ (Best Case, 10% PMA assist)

Case I.3-2: $\hat{M}_K = 72\% \ \overline{M_K}$ (Worst Case, 28% PMA assist)

Where $\hat{M}_K$ is the approximated function of total moment the human can generate and $\overline{M}_K$ is the required moment to stand determined in section 2.1.2. The PMA is not activated for 100% human capability, $\overline{M}_K$ (Case I.1 and Case I.2).

2.1.6.2 Phase II – dynamic phase

The three cases for the dynamic phase are divided into two time intervals. The first time interval is from t_i (initial time) to t_p (end of the push moment). This is the time from initial sitting position of zero radians until the push moment from the arms ends. The second time interval is from t_p (end of the push moment) to t_f (final time) of the PMA

assist. The final time, t_f, occurs when the person reached the angle of $\pi/5$ radians. θ_P is the angle at which t_p occurs.

The push moment is modeled as an approximated function of constant input step. The push moment value is defined as a percentage of $\overline{M}_K$. The value of 18% is taken from literature as an expression of the minimal push moment generated by capable elderly humans [8, 48]. The theta angle (θ_P) for the push moment is estimated to be $\pi/36$ radians. The approximated time interval from t_i to t_p corresponds to zero to $\pi/36$ radians.

The moment time periods for the phase II cases are shown diagrammatically in Figure 9. Note that actual moment values would vary over these time periods.

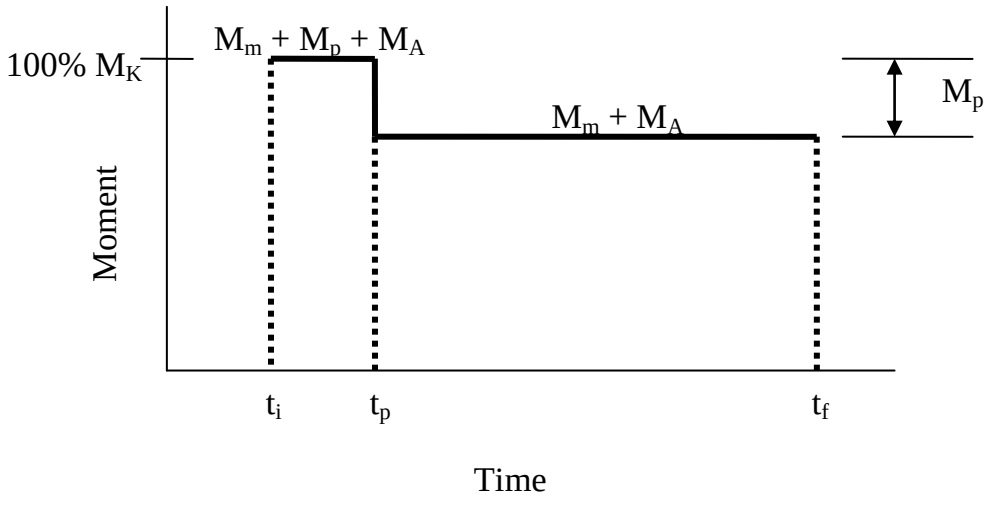

Figure 9: Moment composition for sit-to-stand phase II configuration. M_m, M_p, M_A and M_K correspond to the muscle moment, push-force moment, actuator moment and the total moment required to stand, respectively. Human capability is the combination of muscle moment and push-force moment. The initial time, end of the push-force time and the final time are indicated by t_i, t_p and t_f, respectively.

Phase II approximated the human muscle moment as continuously maximal for case 2 and case 3. θ_f is defined as the angle at which the CM of the upper body is positioned directly over the knee at a constant β of $\pi/6$ radians. θ_f is calculated using the free body diagram in Figure 10 to be $\pi/5$ radians.

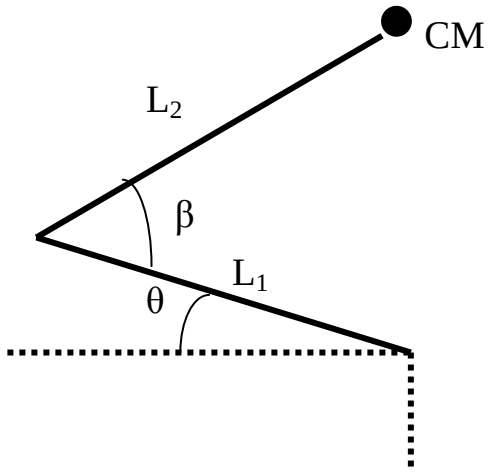

Figure 10: Free body diagram for sit-to-stand phase II where the CM of the upper body is positioned directly over the knee. This position occurs when L' is equal to zero on figure 2. L_1 and L_2 are the length of the thigh segment and length from the hip to the CM, respectively. θ and β correspond to the angle between the knee and the horizontal plane and the angle between the torso and the thigh, respectively.

The case identifications for phase II are the following:

Case II.1: $\hat{M}_K = 100\% \ \overline{M_K}$ from 0 to $\pi/6$ or t_i (initial time) to t_f (final time) (No PMA assist)

Case II.2-1: $\hat{M}_K = 100\% \ \overline{M_K}$ from t_i to t_p (end of push) and $\hat{M}_K = 90\% \ \overline{M_K}$ from t_p to t_f. (Best Case, PMA assist after t_p)

Case II.2-2: $\hat{M}_K = 100\%\ \overline{M_K}$ from t_i to tp and $\hat{M}_K = 82\%\ \overline{M_K}$ from t_p to t_f. (Worst Case, PMA assist after t_p)

Case II.3-1: $\hat{M}_K = 90\%\ \overline{M_K}$ from t_i to t_p and $\hat{M}_K = 72\%\ \overline{M_K}$ from t_p to t_f. (Best Case, continuous PMA assist)

Case II.3-2: $\hat{M}_K = 80\%\ \overline{M_K}$ from t_i to t_p and $\hat{M}_K = 62\%\ \overline{M_K}$ from t_p to t_f. (Middle case, continuous PMA assist)

Case II.3-3: $\hat{M}_K = 72\%\ \overline{M_K}$ from t_i to t_p and $\hat{M}_K = 54\%\ \overline{M_K}$ from t_p to t_f. (Worst case, continuous PMA assist)

The maximum percentage difference between the initial time (t_i) and final time (t_f) correspond to the 18% arm push moment discussed earlier. The complete sit-to-stand task combines phase I and phase II case identifications. The appropriate phase I and phase II combinations correspond to the matching percentage between phase I and time t_i and t_p in phase II.

2.1.6.3 SCS with human assist

The SCS of Figure 6 is revised to account for the human effort during the sit-to-stand task. The revised SCS is shown in Figure 11. The physical model now accounts for the human effort with the following equation:

$$\overline{M}_K' = \overline{M}_K - \hat{M}_K \tag{22}$$

Where $\hat{M}_K$ is the moment the human is capable of generating, $\overline{M}_K$ is the required moment to complete the task, and $\overline{M}_K^{'}$ is the moment not accounted for by the human. The controller has to be redefined for the new physical model by substituting $\overline{M}_K^{'}(\phi)$ for $\overline{M}_K(\Theta)$ in Figure 6.

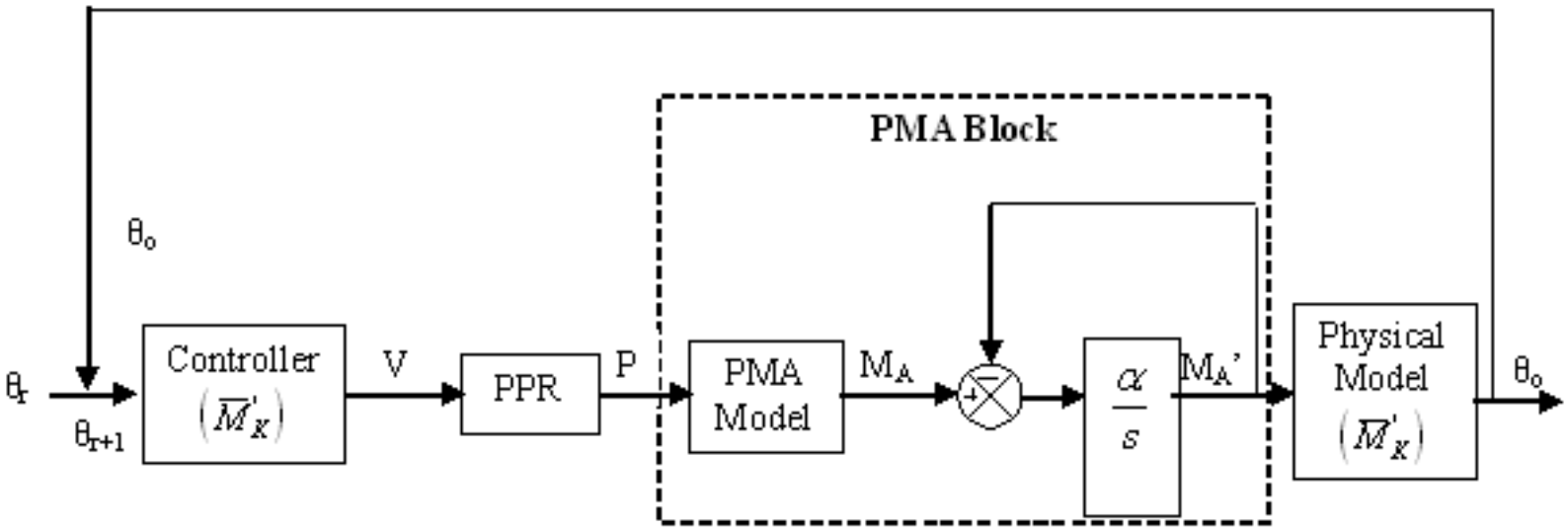

Figure 11: Complete SCS schematic of the assistive pneumatic muscle. PPR, PMA model, and physical model are the proportional pressure regulator, proposed three element model, and the physical characteristics respectively. θ_r and θ_0 are the required angle and output angle respectively. The following symbols are reference to V_G-voltage, P-pressure, M_A-moment generated by the PMA, $\hat{M}_K$-moment generated by the human, $\overline{M}_K$-required task moment, $\overline{M}'_K$ -difference between the required task moment $\overline{M}_K$ and moment generated by the human $\hat{M}_K$, α-time constant.

2.2 The Evaluation of Industrial Pneumatic Muscle Actuator Control Based on a Computational Simulated Control System

A computational simulated control system (CSCS) is constructed to (1) utilize a physical model of a physical therapy (PT) knee extension task, (2) incorporate feedback information regarding position and moment, (3) characterize PMA model variations and human operator perturbations, (4) evaluate with respect to position feedback control and moment/force feedback control and (5) evaluate with respect to adaptive control.

2.2.1 Introduction and Background

An important task for an assistive control system is the physical therapy (PT) knee extension task. Many clinical situations require restoration and/or maintenance of thigh muscle strength [49]. Specifically, quadriceps muscle group strength is necessary for the stability of the knee; and, the knee extension task focuses on that particular muscle group [50]. The knee extension task requires dynamic concentric contractions in an isokinetic motion. In an isokinetic task, the muscle contracts at a constant velocity despite changing force/load requirements. Isokinetics offers faster outcomes, proper kinematics, and safety [49].

Prior work with an assistive control system for knee extension (quadriceps strengthening) exercise has involved functional electrical stimulation (FES) with feedback position control [51, 52]. Significant exercise effects were demonstrated with neurologically impaired individuals [53, 54] that subsequently allowed these individuals

to ambulate [55, 56]. However, position control alone has been shown to degrade with progressive muscle fatigue [57].

The goal of this study is to develop a computational simulated control system (CSCS) that satisfies five objectives. First, the CSCS will utilize a physical model of a PT knee extension task. Second, the CSCS will incorporate feedback information regarding position and moment. Third, the CSCS will characterize PMA model variations and human operator perturbations. Fourth, the CSCS will be evaluated with respect to position feedback and moment feedback control. Fifth, the CSCS will be evaluated with respect to adaptive control.

2.2.2 Physical Model of the Task

Knee extension, a common PT task, is analyzed as the physical model. The task extends the lower leg at the knee joint using the quadriceps muscle group. The PMA will work in parallel with the quadriceps muscle group shown in Figure 12. Information regarding PMA force/moment and position is potentially collected from the load cell and potentiometer, respectively. The required knee moment is calculated using the joint-by-joint analysis method [58], anthropometric data, and the free body diagram shown Figure 12. The joint-by-joint method is analyzed for a constant velocity task in which an additional weight is located directly at the ankle joint. The symbolic knee moment equation is represented in Eq. (23).

$$M_K = \left[9.81\left(0.465m - m_L\right) + R_{YA}\right]\left(0.435\,L_{LL}\sin\theta\right) + M_A - \left(R_{YA} - 9.81m_L\right)\left(0.565\,L_{LL}\sin\theta\right) \quad (23)$$

Where M_K and M_A are the knee moment and PMA moment, respectively; m and m_L are the mass of the human and mass of the additional load, respectively; L_{LL} is the length of the lower leg (function of human height), R_{YA} is the reaction force at the ankle in the y-direction, and θ is the movement angle (0 to π/2 radians). The knee angle, θ, references the vertical axis as zero radians and the horizontal axis as π/2 radians.

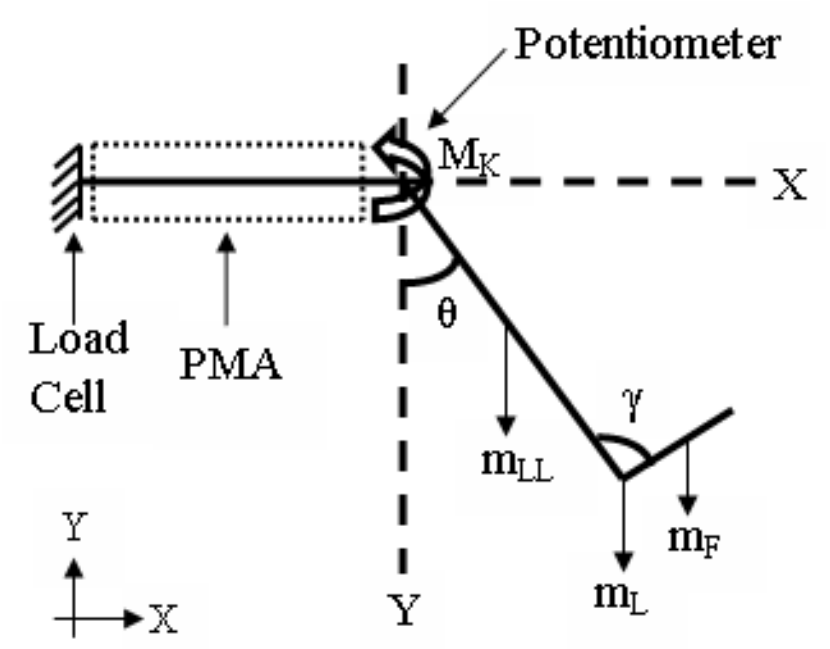

Figure 12: Knee Extension Free Body Diagram with PMA and Human Interaction.

For this application, nominal values are chosen for the anthropometric data (Table 4). This allows the knee moment in Eq. (23) to simplify into Eq. (24) see Appendix B.

$$\overline{M}_K = -29.147\sin\theta - 0.33\cos\left(\theta - \frac{\pi}{18}\right) \tag{24}$$

The required knee moment, $\overline{M}_K$, continuously increases as a function of knee angle, θ, given the knee movement constraints.

TABLE 4: Knee Extension Anthropometric Parameters

Parameter	Value
M (mass)	68 kg
H (height)	1.75 m
M_L (load mass)	2.27 kg
γ (ankle angle)	5π / 9 radians

2.2.3 Control System Modeling and Simulation

The computational simulated control system (CSCS) is developed in a MATLAB® platform [59]. The CSCS consist of two systems: a feed-forward system and a feedback system. The feed-forward system outputs position information and contains an internal dynamic pressure loop. The feedback system contains error information from an external position control loop and an internal PMA moment control loop. The CSCS diagram can be found in Figure 13.

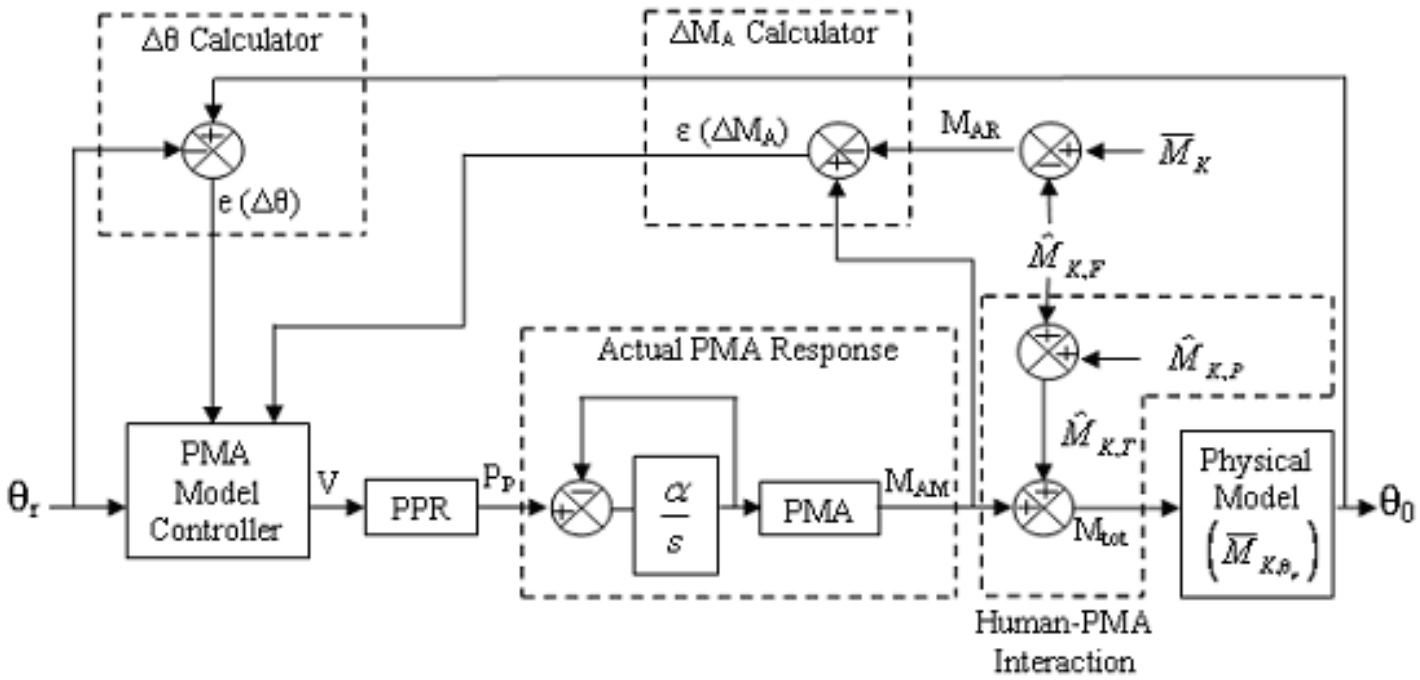

Figure 13: Computational Simulated Control System (CSCS).

2.2.3.1 Feed forward system

The feed-forward system consists of the PMA model controller, the proportional pressure regulator (PPR), the actual PMA response, the human-PMA interaction, and the physical model.

The PMA phenomenological model developed by Reynolds et al. [7] predicts the response of the PMA. The PMA force can be calculated from Eq. (25).

$$F_A = F_{CE}(P) - F_K(P) - F_B(P) \tag{25}$$

Where F_A, F_{CE}, F_K, and F_B are the PMA force, contractile element force, spring element force, and damping element force, respectively. Each element is defined a function of pressure (P).

The PMA model controller utilizes the inverse of the PMA model in Eq. (25) given that F_{CE}, F_K, and F_B are characterized individually by linear functions of pressure. Eq. (26) and Eq. (27) are the governing equations used in the PMA model controller to predict the input system pressure (P_P).

$$P_P = \left[\frac{\left(M_{AR}/r\right) - a - a' r\dot{\epsilon} - a'' r\epsilon}{b - b' r\dot{\epsilon} - b'' r\epsilon} \right]^{-} \quad for\ P_p \geq 200 \tag{26}$$

$$P_P = \left[\frac{\left(M_{AR}/r\right) - a' r\dot{\epsilon} - a'' r\epsilon}{c - b' r\dot{\epsilon} - b'' r\epsilon} \right]^{-} \quad for\ P_p \leq 200 \tag{27}$$

where P_P is the predicted pressure; M_{AR} is the required PMA moment; r is the radius of the PMA pulley; a, b, and c are F_{CE} piecewise parameters; a', and b' are F_B parameters; a" and b" are F_K parameters; θ_r and $\dot{\epsilon}$ are position and velocity information, respectively. The pressure is constrained by the characteristics of the PMA. For the PMA parameters given in Table 4, the equations are valid for pressures between 0 kPa and 600 kPa.

The predicted pressure is inputted into the 'Actual PMA Response' block. In this block, an internal dynamic pressure loop iterates the pressure, Eq. (29), via the viscoelastic time constant (τ), Eq. (28), to produce real time response. The time constant is defined as a function of the damping (B) and spring (K) parameters.

$$\tau = \frac{B(P)}{K(P)} \tag{28}$$

$$\sigma = \frac{dt}{\tau} \tag{29}$$

Where B and K are functions of pressure taken from the defined PMA block discussed in the following paragraph; and, dt is the incremental sampling rate of the system.

In the 'Actual PMA Response' block, the PMA response block is defined as a variation from the predictive PMA model (PMA model block). This variation represents fluctuations in the PMA model which can cause fluctuations in the system response. The PMA response block variation is represented by calculating ± 1 standard deviations (SD)

and ± 0.5 standard deviations (SD) from the F_{CE}, B and K parameters, individually. The values for each of the four cases plus the predictive PMA model can be found in Table 5.

TABLE 5: PMA Parameter Fluctuations for the Simulation of the Actual PMA Response

	F_{CE}			B		K	
	a	b	c	a'	B'	a''	B''
Predicted	179.1	1.39	2.29	1.01	0.0069	5.71	0.0307
	a_2	B_2	c_2	a_2'	b_2'	a_2''	b_2''
+1 SD	252.21	1.408	2.67	1.95	0.0069	6.74	0.0311
-1 SD	101.55	1.377	1.88	0.09	0.0067	3.83	0.0331
+0.5 SD	202.07	1.43	2.44	1.484	0.00697	6.035	0.0314
-0.5 SD	144.87	1.37	2.09	0.56	0.00679	5.078	0.0306

The 'Actual PMA Response' block outputs a force (F_A) generated by the PMA using Eq. (30) and Eq. (31). It is then converted to a corresponding moment (M_{AM}) using Eq. (32).

$$F_A = \left[a_2 P_P\right] - \left[\left(a_2' - b_2' P_P\right) \dot{\theta}_r\right] - \left[\left(a_2'' - b_2'' P_P\right) \dot{\theta}_r\right] \quad \text{for } P_P \le 200 \tag{30}$$

$$F_A = \left[a_2 - b_2 P_P\right] - \left[\left(a_2' - b_2' P_P\right) \dot{\theta}_r\right] - \left[\left(a_2'' - b_2'' P_P\right) \dot{\theta}_r\right] \quad \text{for } P_P > 200 \tag{31}$$

where P_P is the predicted pressure per Eq. (26) or Eq. (27); F_{CE} parameters are a_2, b_2, and c_2; the F_B parameters are a_2' and b_2'; the F_K parameters are a_2'' and b_2''; r is the moment arm of the PMA pulley located at the knee; and, angle position and velocity are θ_r and $\dot{\theta}_r$, respectively.

$$M_{AM} = F_A r \tag{32}$$

The PMA response (M_{AM}) and the total human operator ($\hat{M}_{K,T}$) are incorporated in the 'Human-PMA Interaction' block. The $\hat{M}_{K,T}$ consist of the human operator function $\left(\hat{M}_{K,F}\right)$ defined as 90%, 80% or 70% $\overline{M}_K$, and the human operator perturbation (defined as $\hat{M}_{K,P}$). The human operator perturbation is simulated using random white noise with zero mean. The M_{AM} and $\hat{M}_{K,T}$ are summed together resulting in a total moment (M_{tot}) defined by Eq. (33) where $\hat{M}_{K,T}$ is the addition of $\hat{M}_{K,F}$ and $\hat{M}_{K,P}$. The M_{tot} is equated to the physical model $\left(\overline{M}_K\right)$ defined by Eq. (24). Equation (34) outputs the position result θ_0.

$$M_{tot} = M_{AM} + \hat{M}_{K,T} \tag{33}$$

$$\theta_0 = f^{-1}\left(\overline{M}_K\right) \tag{34}$$

where $\overline{M}_K = M_{tot}$.

2.2.3.2 Feedback system

The feedback system contains the error position calculator and error moment calculator. The error position (e) calculator outputs the position feedback between the position output (θ_0) and required position (θ_r) via Eq. (35).

$$e = \theta_0 - \theta_r \tag{35}$$

The error moment (ε) calculator outputs the moment feedback between the generated PMA moment (M_{AM}) and the required PMA moment (M_{AR}) using Eq. (36). Both the position error and moment error are feed directly into the PMA model controller.

$$\varepsilon = M_{AM} - M_{AR} \tag{36}$$

where $M_{AR} = \bar{M}_K - \hat{M}_K$ and both $\bar{M}_K$ and $\hat{M}_K$ are model-predicted parameters.

2.2.4 Model Application

The CSCS is designed to allow the comparison of feedback responses given the PT knee extension task and the human predicted model. By utilizing negative feedback error, Eq. (37) and Eq. (38) are the updating equations for the PMA model controller.

$$\theta_{r_{NEW}} = \theta_r(\ ) - e(\ ) \tag{37}$$

$$M_{A\,NEW} = M_{AR}(\ ) - \varepsilon(\ ) \tag{38}$$

The computational control system in Figure 13 is implemented for the cases of no feedback (open loop), position feedback only (Eq. (37)), moment feedback only (Eq. (38)), and the combination of pure position and moment feedback (Eq. (37) and Eq. (38)).

Each case is executed at three human operator function levels (90%, 80%, and 70% of $\overline{M}_K$) and at the four PMA model fluctuations (± 1 standard deviations and ± 0.5 standard deviations). This allows for twelve different combinations at each of the three feedback control methods.

The analysis is conducted at five different randomly generated human operator perturbation (HOP) levels. In order for comparison, the five HOP levels are held constant for each scenario. The five HOP level values used can be found in Table 6. For analysis of each HOP level, a mean error value is calculated. Then a mean square error (MSE) value is calculated from the combination of the mean error values, per Eq. (39).

$$MSE = \frac{1}{T}\int_0^T e^2(t)\,dt \tag{39}$$

The percent deviation denotes the absolute average error from the ideal response given the sampling position interval of 0.087266 radians (5 degrees). An accuracy criterion of 10% is specified before implementation of the CSCS. This provides an accuracy of ±0.0087266 radians (±0.5 degrees). If the accuracy value is equal to or below 10%, the correction method sufficiently rectified the effects of model fluctuations and human operator perturbations.

TABLE 6: Randomly Generated Human Operator Perturbations (HOP) Levels

Human Operator Perturbation Levels				
HOP1	HOP2	HOP3	HOP4	HOP5
0.1184	-1.0091	0.0327	-0.9499	-0.2012
0.3148	-0.0195	1.8705	0.7812	-0.0205
1.4435	-0.0482	-1.209	0.569	0.2789
-0.351	0	-0.7826	-0.8217	1.0583
0.6232	-0.3179	-0.7673	-0.2656	0.6217
0.799	1.095	-0.1072	-1.1878	-1.7506
0.9409	-1.874	-0.9771	-2.2023	0.6973
-0.9921	0.4282	-0.964	0.9863	0.8115
0.212	0.8956	-2.3792	-0.5186	0.6363
0.2379	0.731	-0.8382	0.3274	1.3101
-1.0078	0.5779	0.2573	0.2341	0.3271
-0.742	0.0403	-0.1838	0.0215	-0.673
1.0823	0.6771	-0.1676	-1.0039	-0.1493
-0.1315	0.5689	-0.117	-0.9471	-2.449
0.3899	-0.2556	0.1685	-0.3744	0.4733
0.088	-0.3775	-0.5012	-1.1859	0.1169
-0.6355	-0.2959	-0.7051	-1.0559	-0.5911
-0.5596	-1.4751	0.5082	1.4725	-0.6547
0.4437	-0.234	-0.4209	0.0557	-1.0807

2.2.5 Adaptive Controller

The adaptive controller is constructed from the MIT reference model adaptive controller technique [60]. It updates the parameters in the PMA model controller block. The position and moment information are updated to respond to the fluctuations in the actual PMA response.

A more robust derivation of this method can be found in [60]. The following description highlights major MIT model reference adaptive control concepts and assumptions. The equations are formulated for position error analysis and can be altered in the same fashion for moment error analysis. The adaptive controller objective for

position is to track $\theta_0(t)$ to $\theta_r(t)$. This is done by minimizing the mean square error (MSE). The basic equation for MSE can be found in Eq. (39).

For this particular application, the error equation is defined in Eq. (35). Only the minimization of the present error is necessary; therefore, the minimized updating parameter $\dot{K}_C$ is approximated by Eq. (40) which utilizes negative feedback error.

$$\dot{K}_C \approx -\frac{\partial}{\partial K_C} e^2(t) \tag{40}$$

where K_C is the updated parameter block.

By assuming the updated parameter block (K_C) is a constant at a particular time (discrete time analysis), the minimized updated parameter $\dot{K}_C$ simplifies to Eq. (41).

$$\dot{K}_C = -g\, e(t)\frac{\partial e(t)}{\partial K_C} \tag{41}$$

where g is an arbitrary positive scalar gain that determines the adaptive speed [60].

The adaptive control process is independently executed on both the error position calculator output (e) per Eq. (35) and error moment calculator output (ε) per Eq. (36). Each process contains individual updating equations $\dot{K}_{C1}, \dot{K}_{C2}$ and gain values (g_1, g_2). Equation (42) is the updating equation for position information (θ_r); and, Eq. (43) is the updating equation for moment information (M_{AR}).

$$\dot{K}_{C1} = -g_1\, e(t)\frac{\partial e(t)}{\partial K_C} \tag{42}$$

$$\dot{K}_{C2} = g_2(e(t), M_{AR}(t)) \tag{43}$$

$\dot{K}_{C1}$ and $\dot{K}_{C2}$ are used in updating the input PMA model parameters θ_r and M_{AR} via Eq. (44) and Eq. (45).

$$\theta_{NEW} = \theta_r(t) - (\dot{K}_{C1}(t) * dt) \tag{44}$$

$$M_{A\,NEW} = M_{AR}(t) - (\dot{K}_{C2}(t) * dt) \tag{45}$$

where θ_{NEW} and M_{ANEW} are the new input parameters and dt is the sampling rate of the system. These updated values are then directly inputted into the PMA model controller block via Figure 14.

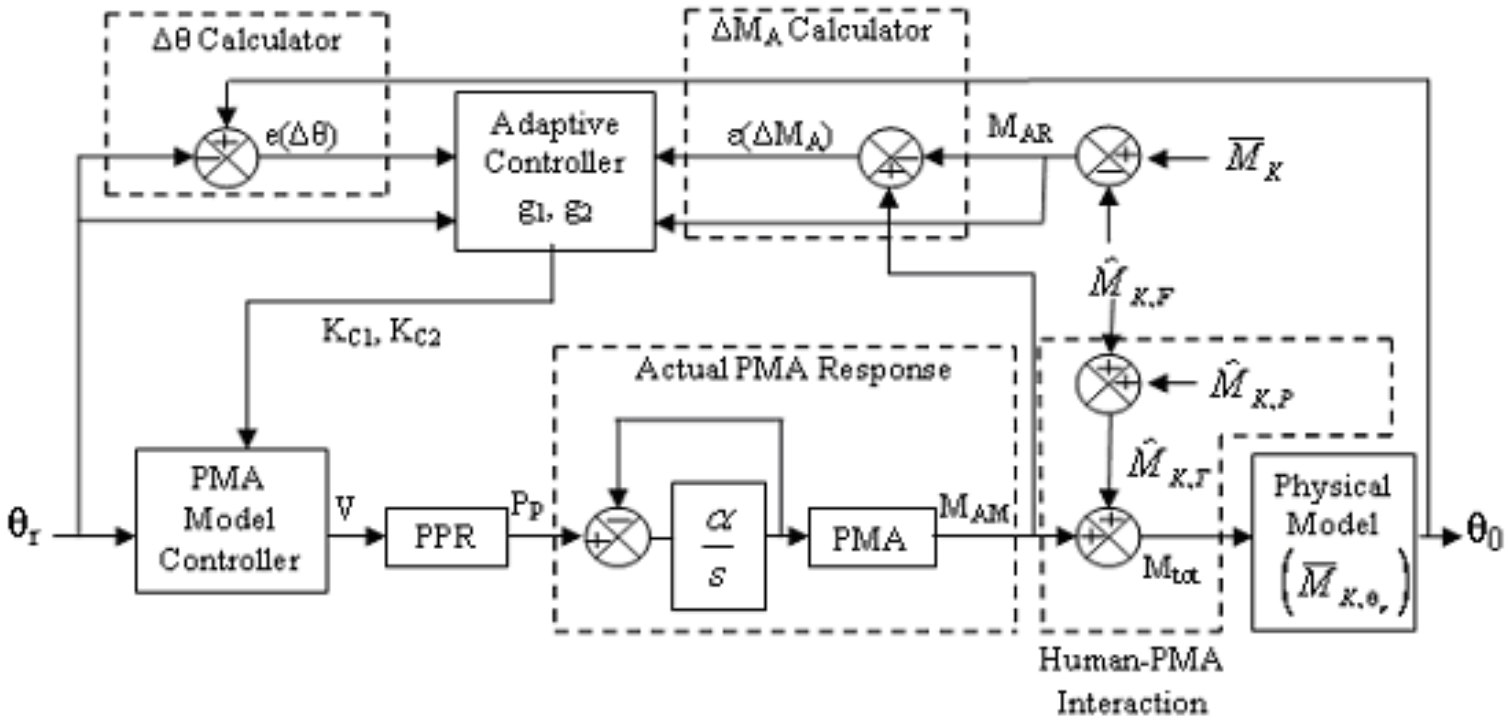

Figure 14: Adaptive Simulated Control System.

The adaptive control is implemented for the worst case scenarios where model fluctuations for F_{ce}, B and K are not equal. From Reynolds et al. [7], B and K parameter values are determined independently while F_{ce} parameter values are dependent on the B and K parameters values. Therefore, the analysis at varying model fluctuations is configured into four cases. B and K parameters vary at different SD levels while F_{ce} matches the SD level of either B or K. Only ±1 SD is analyzed because it provides the worst case scenario. The four different cases include:

1. F_{ce} +1 SD, B -1 SD, K +1 SD
2. F_{ce} +1 SD, B +1 SD, K -1 SD
3. F_{ce} -1 SD, B -1 SD, K +1 SD
4. F_{ce} -1 SD, B +1 SD, K -1 SD

The constant gain values (g_1 and g_2) utilize in the simulation consist of:

1. $\hat{M}_K$ = 70% $g_1 = 0.5$ and g2 = 1.5
2. $\hat{M}_K$ = 80% $g_1 = 0.5$ and $g_2 = 2$
3. $\hat{M}_K$ = 90% and $\varepsilon \leq -0.5$ $g_1 = 0.5$ and $g_2 = 4.5$
4. $\hat{M}_K$ =90% and $\varepsilon > -0.5$ $g_1 = 0.5$ and $g_2 = 3.5$

2.3 Closed Loop Moment (Force) Feedback Control versus Open Loop Control for a Commercial Pneumatic Muscle Actuator Utilizing a Dynamic Test System

A moment/force feedback control system is utilized with a commercially available PMA for a high force application. The moment/force feedback controller is evaluated on a dynamic PMA test system and compared to open loop control.

2.3.1 Introduction and Background

Pneumatic muscle actuators (PMAs) contain advantages over other traditional actuator systems. PMAs are low cost, quick response time and high power to weight and high power to volume ratios which are ideal for high force applications. However, PMAs exhibit system nonlinearities [40] causing challenges in accurate modeling and control.

Pneumatic muscle actuators utilize pressure as an activation parameter causing it to contract. This mechanical action is similar to biological muscle behavior. PMA are constructed from an inner rubber bladder surrounded by a high strength fiber shell. One end of the PMA is sealed while the other provides a gas inlet/outlet. The high strength fiber shell provides both stability and contraction mechanism [7, 14]. The shell's fibers are intertwined in a cross woven pattern. As the gas enters the PMA, it causes the inner bladder to expand. The inner bladder interacts with the fiber shell resulting also in expansion. Due to the fiber arrangement, the fiber shell and the inner bladder expand in the radial direction as the gas volume increases [7, 9, 14, 40]. This causes the length of the PMA to contract (shorten) resulting in a longitudinal force.

Advantages of PMAs provide feasibility to high force application. Due to the similarities to biological muscle, it has gained interest in human interaction applications.

One major concern with human interaction applications is safety; however, PMAs contain soft failure characteristics eliminating risk. Various areas of PMA application include robotic control, physical therapy, and parachute landing systems [9, 11, 35, 61].

High force generating pneumatic muscle actuators have been commercially available since the 1980s. Three companies have marketed a form of PMA: Bridgestone (Japan), Shadow Robot Company (UK) and Festo Corporation (Germany).

In the 1980's, Bridgestone created a braided muscle called Rubbertuators (Rubber-Actuators) [6]. The design improved on the McKibben muscle by providing durability and performance [6]. Two industrial robots were created using the Rubbertuator: the RASC (horizontal robot) and the SoftArm (suspended robot). Even though the Rubbertuator application has diminished, researchers have explored control via neural networks for the SoftArm robot [62, 63].

The Shadow Robot Company developed an Air Muscle about the same time as the Rubbertuator. Air Muscles are comprised of an inner rubber tube encased in an outer plastic weave. This product is still currently available in various sizes [64]. The Air Muscle has been used in the construction of a robotic arm. This robotic arm contains 36 Air Muscles and replicates movement of the human hand [65].

Festo Corporation manufactures a PMA referred to as fluidic muscle. It is constructed with a three-dimensional rhomboidal woven layer embedded in a rubber bladder providing a more robust design [37, 66]. It is available in three basic diameters (10mm, 20mm and 40mm) with a maximum contraction of approximately 25% of the nominal length [66]. The fluidic muscle has industrial applications in paper punches, assembly tables, presses, lifting equipment and medical equipment [36, 37]. A

collaboration among Festo AG and the Technical University of Berlin applied fluidic muscles to a bionic upper body capable of mimicking human abilities [67].

Pneumatic muscle actuator control schemes have been limited due to modeling errors [14]. A summary of previous control schemes can be found in section 1.2.3.3. Most attempted control systems assume linear analysis and step reference inputs which are not ideal for dynamic application. Additionally, the models used in many control methods insufficiently characterize the nonlinear dynamics of the PMA. The methods that actually address the PMA nonlinear dynamics lacks actual physical application and are implemented through pure simulation. It is important that an accurate model, which incorporates the PMA's dynamics, formulates the foundation for a controller and that the controller is evaluated on a dynamic test system.

This research (1) introduces a control system for a commercially available PMA utilizing an industrial (high force) application, (2) evaluates a moment feedback controller on a dynamic PMA test system, and (3) compares moment feedback control to open loop control.

2.3.2 Mathematical Characterization of the Phenomenological Model

Other PMA models for low-force applications have been previously summarized in Reynolds et al. [7]. This research applies the PMA phenomenological three-element model to a commercially available high force Festo PMA. The phenomenological three-element model is a biomimetic/biomechanical model consisting of a spring element (elastic), damping element (visco) and contractile element in a parallel configuration.

The governing equation (Eq. (46)) of motion for the phenomenological model [7], assuming y is the displacement, is

$$m\ddot{y} + B\dot{y} + Ky = F_{CE} - F_A \tag{46}$$

where m is the mass of the moving components, B is the damping coefficient, K is the spring coefficient, F_{ce} is the contractile force coefficient and F_A is the force exerted by the PMA.

Since the dynamic system (described in the methods section) is configured horizontally and the moving component mass (m) is determined to be negligible, the governing equation can be simplified by eliminating the inertial term. Using this simplification and by solving for the force exerted by the PMA (F_A), the following equation (Eq. (47)) is acquired.

$$F_A = F_{CE} - B\dot{y} - Ky \tag{47}$$

The phenomenological model is characterized for a medium size (20mm) commercial Festo pneumatic muscle actuator within the operating pressure range between 150-550 kPa (21.8-79.8 psi). The spring coefficient, damping coefficient, and contractile force coefficient are determined independently as piecewise functions of pressure using ramp perturbations and contraction studies [38]. This procedure is similar to the method described in [7]. Table 7 contains the characterized phenomenological

Festo muscle model parameters as a function of pressure [38]. This characterized model is predetermined to be a reasonable dynamic model for this particular Festo muscle [38].

TABLE 7: Characterized Phenomenological Festo Muscle Model Parameters

Spring Coefficient, K (N/mm)	
K = 0.256P+101	150<P>253 kPa
K = -0.0468P+47.8	253<P>550 kPa
Contracting Damping Coefficient, B (Ns/mm)	
B = 0.009P+6.77	150<P>550
Contractile Force Coefficient, Fce (N)	
Fce = 2.3481P+407.4	150<P>418
Fce = 1405	418<P>550

2.3.3 Moment/Force Feedback Control

Conventional feedback control is utilized to design a moment/force feedback controller. Even though position is the performance parameter for the dynamic test system, the major components interact via moment/force parameters. The basic schematic of the control system is found in Figure 15.

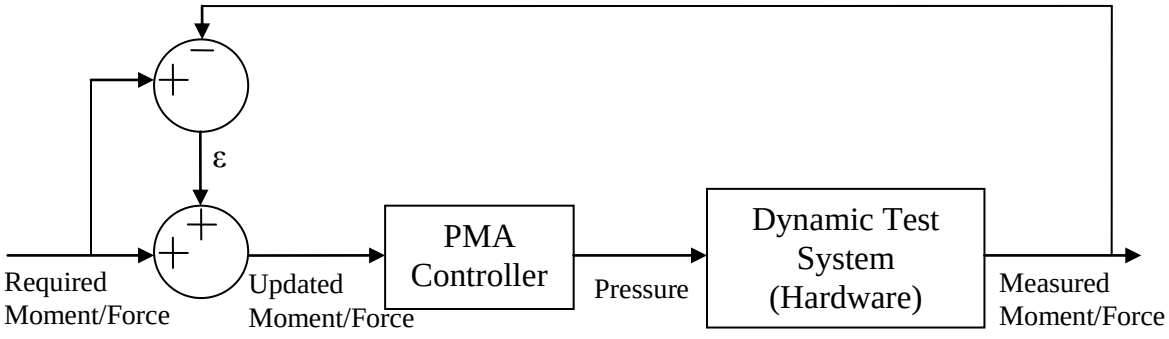

Figure 15: Moment/Force Feedback Controller Schematic

In the dynamic test system, the required torque/force is the resistive torque/force that the PMA acts against. This required torque/force is commanded via software. The PMA controller, consisting of the inverse of the characterized phenomenological Festo muscle model equation (Eq. (47)), converts the updated moment/force into a PMA pressure command. As a result of the commanded required moment/force and pressure, the dynamic test system outputs a measurable moment/force placed on the PMA. The following are the governing moment/force feedback equations (Eq. (48a) and Eq. (48b)):

$$\varepsilon(t) = M_{AM}(t) - M_{AR}(t) \tag{48a}$$

$$M_{A,NEW}(t) = M_{AR}(t) - \varepsilon(t) \tag{48b}$$

Where ε is the moment error, M_{AM} is the measured moment, M_{AR} is the required Moment, and $M_{A,NEW}$ is the updated moment sent to the PMA controller.

The required moment/force also exerts a position displacement on the dynamic test system in the opposite direction of the PMA contraction. The pressure from the PMA controller activates the PMA allowing it to contract with axial displacement. When the measured moment matches the required moment, there is no displacement in the system. This provides an external validation of the moment feedback control system. The dynamic test system description is located in the following section.

2.3.4 Experimental Procedure and System Components (Hardware and Software)

The dynamic PMA test system is constructed in a horizontal configuration. The pneumatic muscle actuator (Festo Corporation, Hauppauge, NY, model: MAS-20-250N-AAMCK) resting parameters include an inner diameter of 20 mm (0.79 in.) and a length of 250 mm (9.84 in). It is rated for a maximum force of 1200N (270 lb), maximum pressure of 600 kPa (87.2 psi) and a maximum contraction of 25% of the initial length [66]. The pressure inlet/outlet end of the PMA is fastened to a load cell using an L-shaped aluminum bracket; while, the closed end of the PMA is connect to a pulley on the shaft of a DC servo motor via a cable. The load cell (Transducer Techniques, Temecula, CA, model: LPU-500) measures the load placed on the PMA and has a maximum capacity of 2224 N (500 lb). The DC servo motor (Pacific Scientific, Rockford, IL, model: PMA 45N-00100-00) is operated in torque mode to apply various resistive moments/loads to the system. The nitrogen gas pressurizing the PMA is controlled by a proportional pressure regulator (Festo, Corporation, Hauppauge, NY, model: MPPE-3-1/8-6-010-B). The proportional pressure regulator (PPR) has a response time of 0.22 seconds. The actually pressure in the inner bladder of the PMA is monitored using a pressure transducer (Festo, Corporation, Hauppauge, NY, model: SDE-1-D10-G2-W18-L-PU-M8). Both the PPR and the pressure transducer are connected to the inlet/outlet end of the PMA. The closed end of the PMA is connected via an aluminum slide to a linear variable differential transducer (LVDT) (Honeywell-Sensotec, Columbus, OH, model: JEC-060-G317-03). The LVDT measures the linear PMA/Cable displacement. The load required to overcome static friction in the LVDT is 1.96 N (0.44 lb) and dynamic friction

1.47 N (0.33 lb). Since these loads are comparably less then the loads applied to the system, the aluminum slide friction is considered negligible. A more detailed component description of the PMA dynamic test system components can be found in Appendix C. A schematic of the dynamic test system can be found in Figure 16.

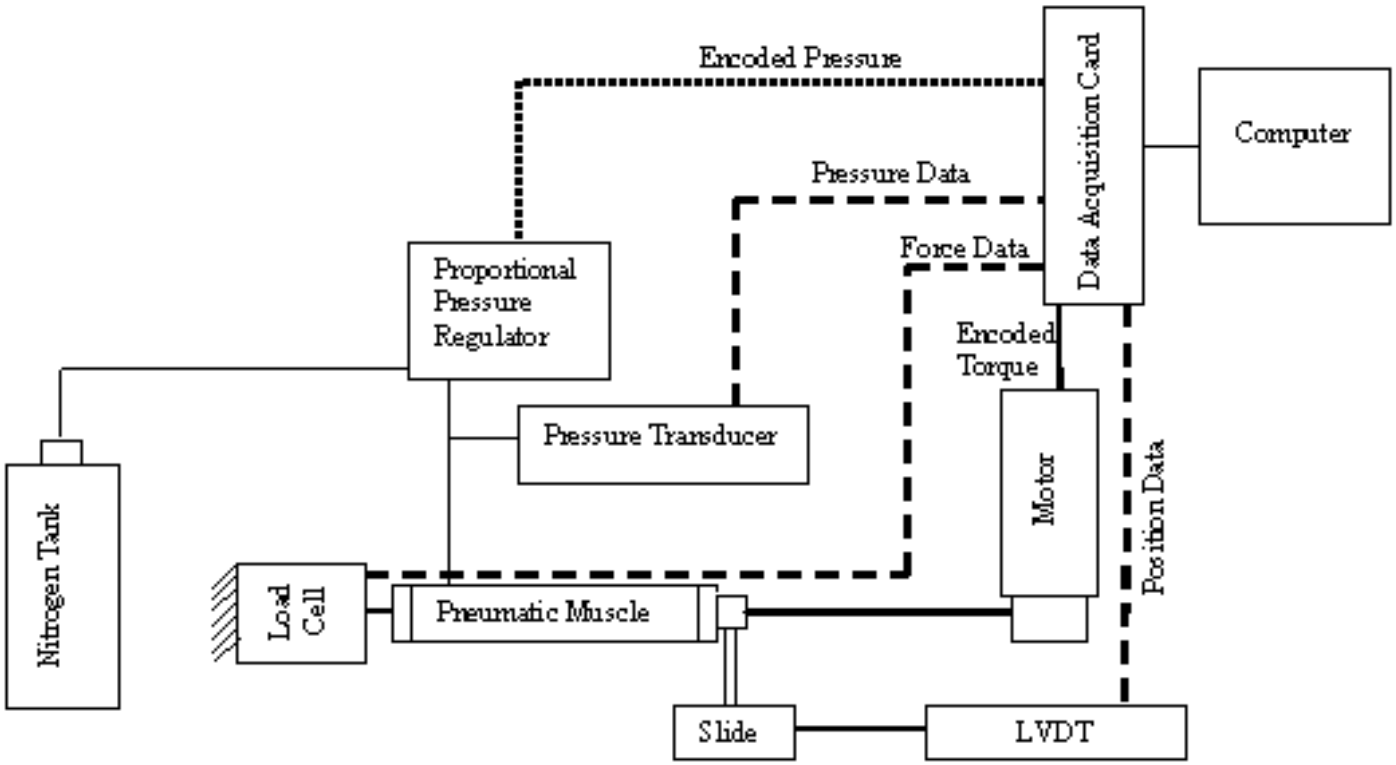

Figure 16: Dynamic Test System Schematic

The communication between the dynamic test system hardware and the LabVIEW 8.0 software (National Instruments, Austin, TX) is performed utilizing a data acquisition card (National Instruments, Austin, TX, model: PCI-6025). The software controls the two output parameters: the moment/force commanded to the DC Servo motor and the pressure commanded via the proportional pressure regulator to the PMA. It also allows the data collection of the three main input sensors: load cell, pressure transducer, and LVDT. All output and input parameters are communicated via calibrated voltages. The data collection sampling frequency is set at 100 Hz.

2.3.4.1 Case Study

In order to test a control system on the dynamic test system, a simulated practical application utilizing the PMA as an assistive device in the physical therapy (PT) knee extension task is developed. The subject performing the task starts in a seated position with their feet on the floor and extends one of the lower legs via the knee pivot point. This motion isolates the quadriceps muscle group. The isokinetic motion (constant velocity with changing load/force) in this task provides maximum building of muscle strength [49, 50].

As an assistive device, the PMA would be attached parallel to the quadriceps muscle group. This configuration allows the PMA to provide an additional assistive force for impaired subjects. A joint-by-joint analysis [58] is conducted to calculate the knee moment versus knee angle movement. Figure 17 displays the graphical representation of the task.

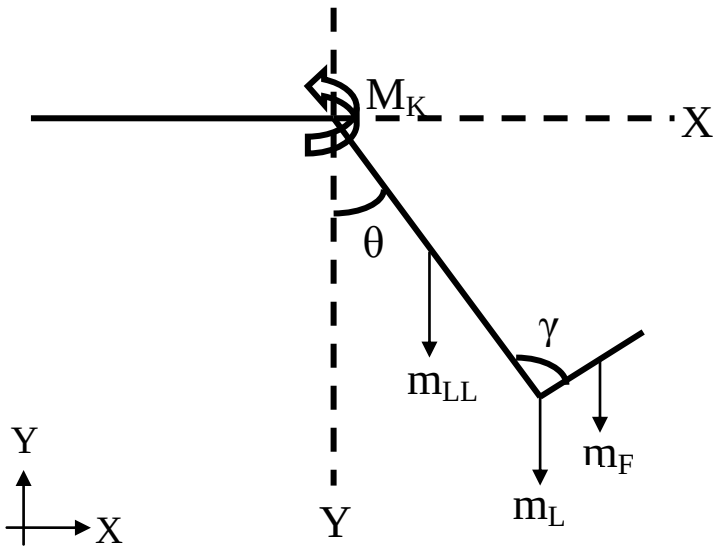

Figure 17: Physical Therapy Knee Extension Task, Joint-by-Joint Free Body Diagram

The mathematical Eq. (49) relates knee angle to knee moment utilizing the joint-by-joint analysis. The derivation of the equation can be found in Appendix B. The analysis assumes constant angular velocity representing isokinetic motion.

$$M_K = \left[9.81\left(0.465m - m_L\right) + R_{YA}\right]\left(0.435\,L_{LL}\sin\theta\right) + M_A - \left(R_{YA} - 9.81m_L\right)\left(0.565\,L_{LL}\sin\theta\right) \quad (49)$$

Where M_K and M_A are the knee moment and PMA moment, respectfully; m and m_L are the mass of the human and mass of the additional load, respectfully; L_{LL} is the length of the lower leg (function of human height), R_{YA} is the reaction force at the ankle in the y-

direction, and θ is the movement angle (0 to π/2 radians). The knee angle, θ, references the vertical axis as zero radians and the horizontal axis as π/2 radians.

For this application, nominal values are chosen for the anthropometric data (Table 8). The simplified equation utilizing the anthropometric data can be found in Eq. (50).

TABLE 8: Knee Extension Anthropometric Parameters

Parameter	Value
M (mass)	68 (kg)
H (height)	1.75 (m)
M_L (load mass)	2.27 (kg)
γ (ankle angle)	5π / 9 (radians)

$$M_K = -29.147\sin\theta - 0.33\cos\left(\theta - \frac{\pi}{18}\right) \tag{50}$$

The required knee moment (Eq. (50)) to successfully complete the leg extension task without PMA assist is located in Figure 18.

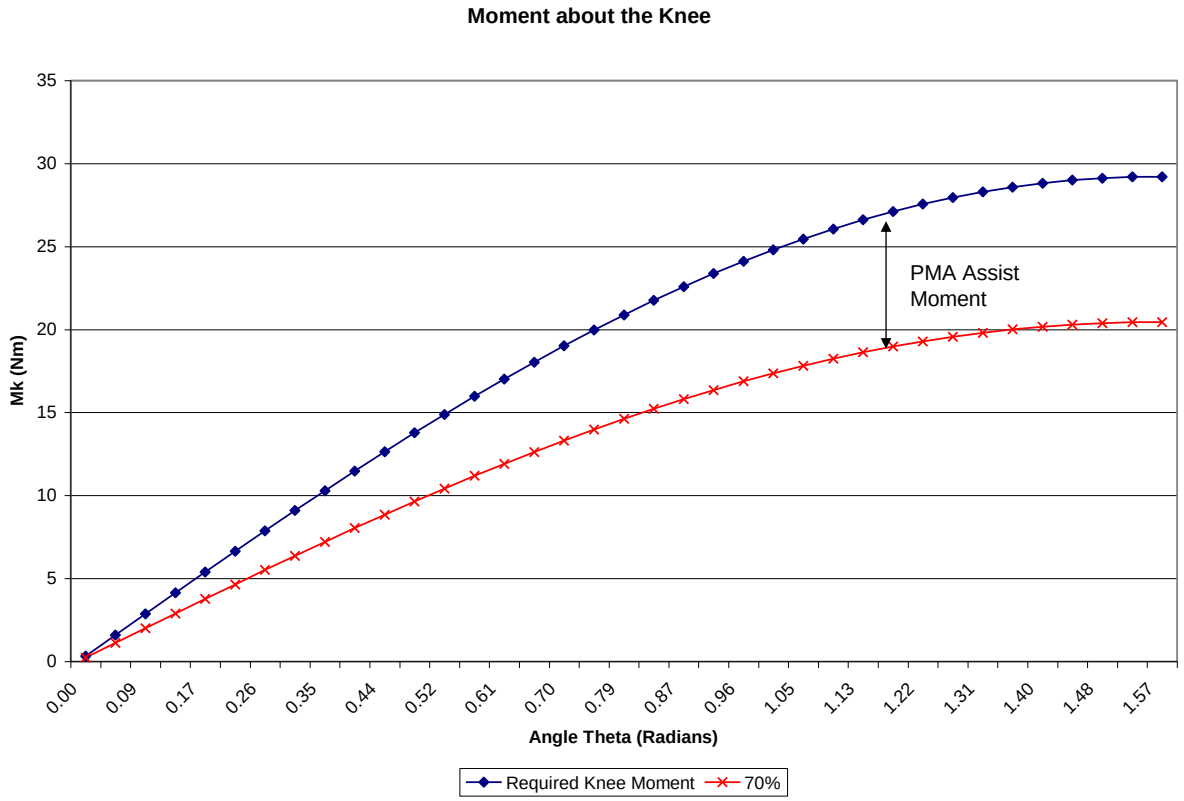

Figure 18: Required Knee Moment versus Knee Angle (represents 70% application only).

The amount of PMA assist is calculated using human capability percentages of the total required knee moment. Three assistive scenarios are analyzed: human capability of 70%, 80%, and 90% which corresponds to 30%, 20%, and 10% PMA assist, respectively. The 70% scenario can be seen on Figure 18.

Since the dynamic test system only contains one motor, only the PMA assist portion of the simulated leg extension task is analyzed. This refers to the difference between the required knee moment and the human capability curves in Figure 18. The PMA assist portion in Figure 18 demonstrates the amount of moment/force the PMA must generate to successfully complete the task. In reference to the horizontal dynamic

test system, the PMA represents the PMA assistive device. The pulley connected to the shaft of the motor symbolizes the knee joint. Finally, the resistive moment/force generated by the DC servo motor corresponds to additional moment the PMA assist has to generate, i.e. the PMA assist moment in Figure 18.

2.3.4.2 Closed Loop Study

A closed loop study is conducted using LabVIEW to communicate between the hardware and software of the dynamic test system. Real time calculations of the required pressure into the PPR are calculated via a moment/feedback control system described in the theory section. The LabVIEW programming code (Appendix G) commands the assistive PMA moment/force (Figure 18) to the motor hardware component. The feedback information obtained from the difference between the required moment/force (motor output force) and the measured moment/force (load cell input force) is utilized in the characterized phenomenological Festo muscle model. This error is inputted into the PMA controller to calculate the PPR pressure. The real time PPR pressure is then sent to the hardware via the DAQ card. Additional input parameters collected include LVDT data and pressure transducer data. The closed loop study is conducted for the 70%, 80%, and 90% PT human capability cases.

The test performance parameter is the LVDT of the dynamic test system. Since both the output commands (motor profiles and pressure profiles) are dynamically changing over time, a constant response in the LVDT indicates that the PMA is generating equal and opposite moment/force compared to the DC servo motor resistive moment/force. Thus, it demonstrates the capability of adequately controlling the PMA

nonlinearities not accounted for in the characterized phenomenological Festo muscle model.

2.3.4.3 Open Loop Study

In order to evaluate the closed loop study (moment/force feedback controller), an open loop comparison is conducted. In the open loop study, the pressure commanded to the PPR is predefined utilizing the inverse of the characterized phenomenological Festo muscle model discussed in section 1.2.2.3. This model provides a direct software time-dependent command signal to the PPR responding to the required motor software time-dependent output. Both signals are directly commanded via LabVIEW to the system hardware components while the measurable input sensors data is collected. The Labview code can be found in Appendix F.

2.3.5 Statistical Analysis

2.3.5.1 Linear Fit (Slope Analysis)

A linear regression with an analysis of variance is performed on the open loop study data and closed loop study data separately. The analysis of variance examines the following model and tests the stated null hypothesis.

$$\text{Model: } E(Y) = \beta_0 + \beta_1 t \tag{51}$$

Where Y is the angular position, t is time, β_0 is the intercept and β_1 is the slope

$$\text{Null Hypothesis: } H_o\text{: } \beta_1 = 0 \tag{52}$$

$$\text{Alternative Hypothesis: } H_a\text{: } \beta_1 \neq 0 \tag{53}$$

2.3.5.2 Root Mean Square Error Analysis

The root mean square error (RMSE) is calculated using the absolute deviation of the open loop study and closed loop study data from the ideal constant LVDT output of 42 mm. Eq. (54) is used to calculate the RMSE.

$$RSME = \sqrt{\frac{\sum (x - y_i)^2}{n}} \tag{54}$$

Where x is the open loop/closed loop data, y_i is the ideal LVDT output, and n is the number sample points.

3.0 Results: Model Application

3.1 A computational simulated control system for a high-force pneumatic muscle actuator: System definition and application as an augmented orthosis

3.1.1 Results for phase I

The result for Case I.1 ($\hat{M}_K = 100\% \overline{M_K}$) and Case I.2 ($\hat{M}_K = 100\% \overline{M_K}$) are illustrated in Figure 19. Both cases result in constant zero voltage profile because the PMA is inactive. Case I.3-1 ($\hat{M}_K = 90\% \overline{M_K}$) and Case I.3-2 ($\hat{M}_K = 72\% \overline{M_K}$) result in an increasing voltage ramp due to the activation of the PMA as shown in Figure 20. Since the phase I is static, the person is given an infinite amount of time for preparation. Therefore, the x-axis is given in code iterations.

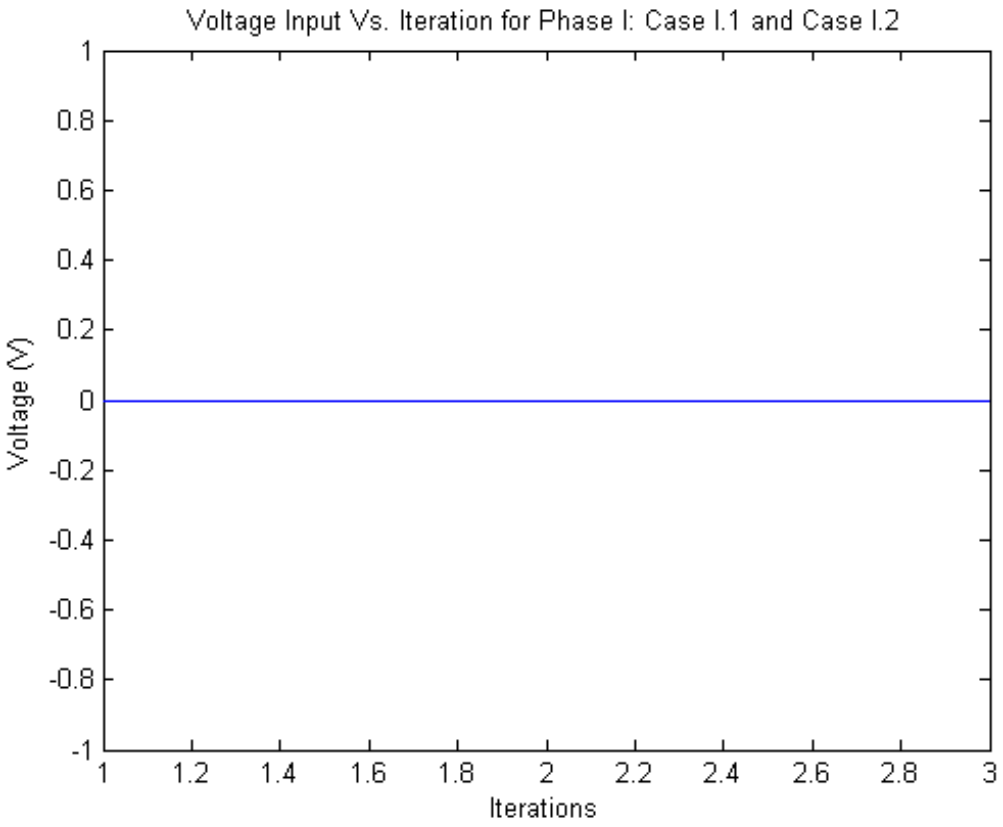

Figure 19: Voltage profile for phase I Case I.1 and Case I.2. Case I.1and Case I.2 are defined as $\hat{M}_K = 100\% \overline{M_K}$, *where* $\hat{M}_K$ *is the moment generated by the human and* $\overline{M_K}$ *is the required moment to stand.*

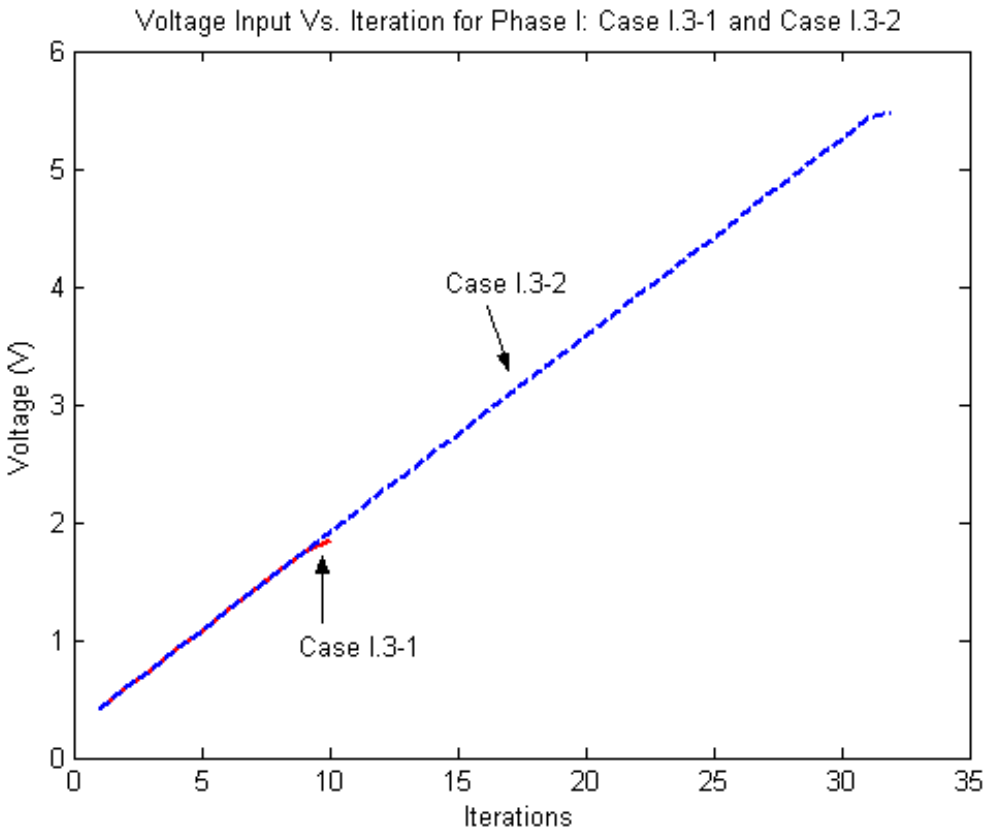

Figure 20: Voltage profile for phase I: Case I.3-1 $\hat{M}_K = 90\% \overline{M_K}$ *and Case I.3-2* $\hat{M}_K = 72\% \overline{M_K}$

3.1.2 Results for phase II

Figure 21 illustrates the result for Case II.1 ($\hat{M}_K = 100\% \overline{M_K}$). There is a constant zero voltage profile corresponding to no PMA assist. Initially for Case II.2-1 and Case II.2-2 (Figure 22), there is a voltage profile of zero until time t_p in which the voltage jumps increasingly and then decays with time. Case II.3-1, Case II.3-2, and Case II.3-3(Figure 23) produce an initial voltage corresponding to the final voltage in phase I. This voltage then decays until time t_p in which an increase jump in voltage occurs. As time

continues, the voltage decays again from the time period of t_p to t_f. All profiles remain below the upper pressure limit of 600 kPa (10.26 volts).

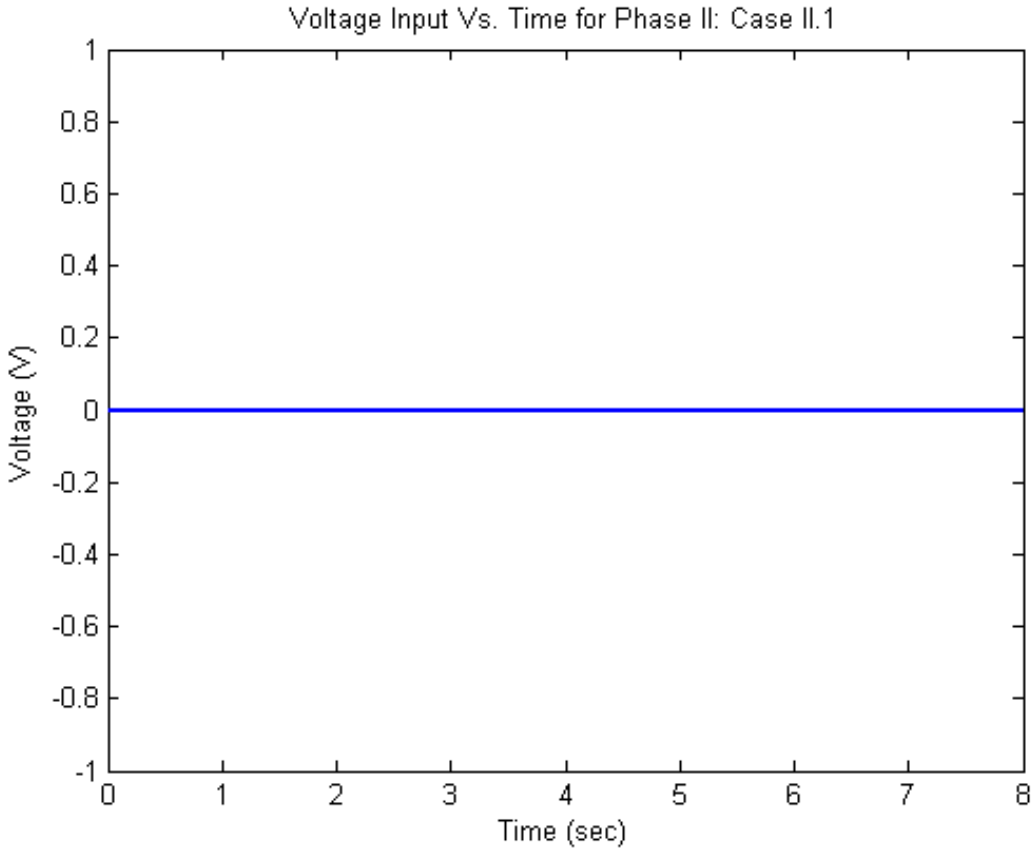

Figure 21: Voltage profile for phase II: Case II.1 $\hat{M}_K = 100\% \overline{M_K}$ *from 0 to π/6 or* t_i *(initial time) to* t_f *(final time)*

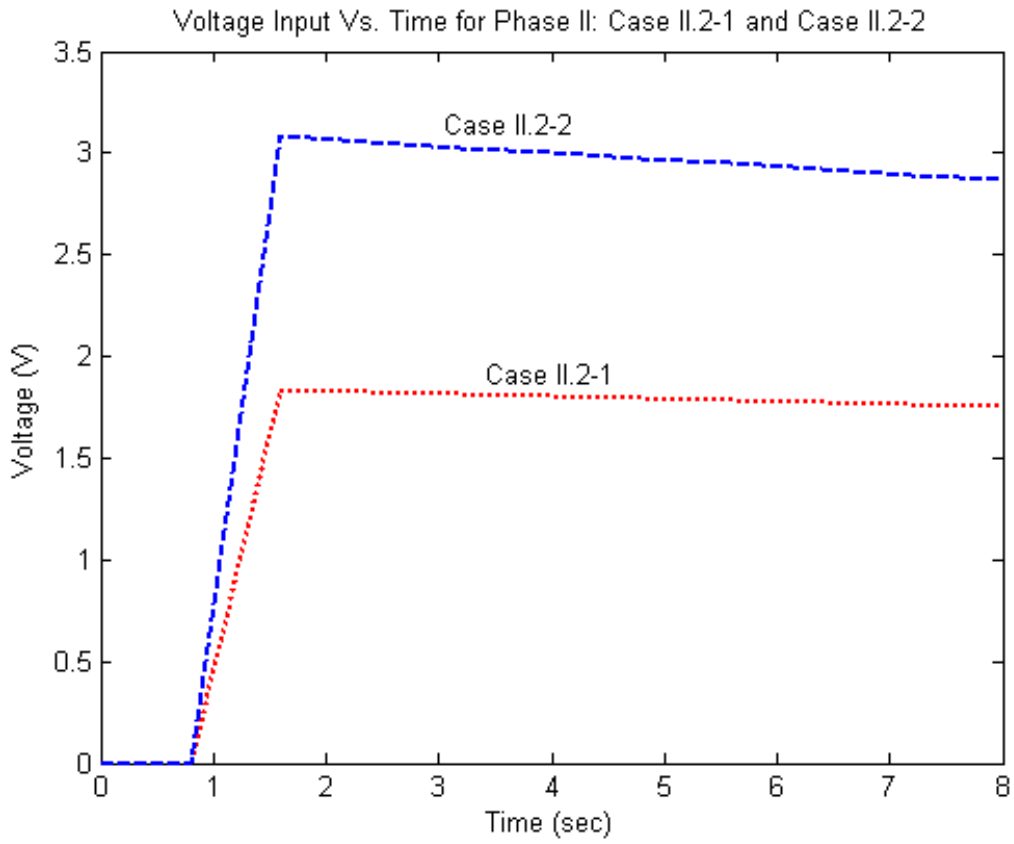

Figure 22: Voltage profile for phase II: Case II.2-1 $\hat{M}_K = 100\% \overline{M_K}$ *from 0 to π/6 and* $\hat{M}_K = 90\% \overline{M_K}$ t_i *(initial time) to* t_f *(final time) and Case II.2-2* $\hat{M}_K = 100\% \overline{M_K}$ *from 0 to π/6 and* $\hat{M}_K = 82\% \overline{M_K}$ t_i *(initial time) to* t_f *(final time)*

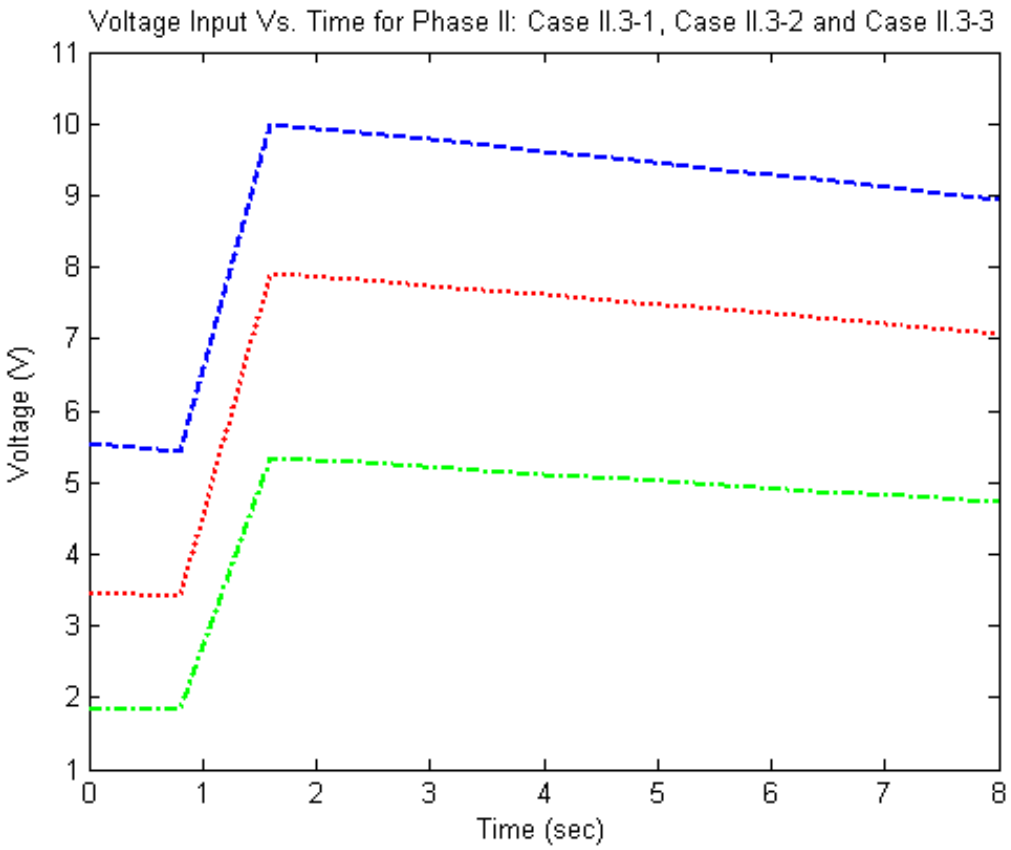

Figure 23: Voltage profile for phase II: Case II.3-1 $\hat{M}_K = 90\%\ \overline{M_K}$ *from 0 to π/6 and* $\hat{M}_K = 72\%\ \overline{M_K}$ t_i *(initial time) to* t_f *(final time), Case II.3-2* $\hat{M}_K = 80\%\ \overline{M_K}$ *from 0 to π/6 and* $\hat{M}_K = 62\%\ \overline{M_K}$ t_i *(initial time) to* t_f *(final time) and Case II.3-3* $\hat{M}_K = 72\%\ \overline{M_K}$ *from 0 to π/6 and* $\hat{M}_K = 54\%\ \overline{M_K}$ t_i *(initial time) to* t_f *(final time)*

3.2 The Evaluation of Industrial Pneumatic Muscle Actuator Control Based on a Computational Simulated Control System

3.2.1 CSCS Numerical Results

Table 9 provides numerical results for the open loop configuration and the three correction methods: position feedback only, moment feedback only and the combination of position and moment feedback. The MSE values reported indicate the average absolute deviation from the ideal response. A smaller MSE corresponds to less deviation.

The accuracy in terms of percent deviation is also reported in Table 9. A smaller percentage corresponds to greater accuracy. Accuracy below 10% is bolded.

TABLE 9: CSCS Numerical Results for the cases of open loop, pure position feedback, pure moment feedback, and the combination of position and moment feedback. Accuracies under 10% are indicated in bold.

		Open Loop		Position Only		Moment Only		Position & Moment	
	%	MSE	Accuracy (%)	MSE	Accuracy (%)	MSE	Accuracy (%)	MSE	Accuracy (%)
1SD	90	2.22E-03	49.09	1.55E-02	137.97	2.21E-05	**5.39**	1.52E-04	11.51
	80	2.46E-03	55.92	1.82E-03	48.89	1.68E-05	**4.7**	2.97E-05	**6.23**
	70	1.87E-03	48.98	1.52E-03	44.69	1.94E-05	**5.04**	2.65E-05	**5.89**
-1SD	90	3.55E-03	67.38	2.47E-03	56.91	2.43E-04	17.88	1.38E-03	42.35
	80	2.73E-03	58.74	2.28E-03	54.64	1.61E-04	14.55	8.28E-04	32.66
	70	2.29E-03	53.12	1.69E-03	47.05	7.23E-05	**9.74**	2.75E-04	18.75
0.5 SD	90	1.32E-03	41.25	1.07E-03	37.2	1.23E-05	**4.01**	2.26E-05	**5.11**
	80	1.30E-03	40.89	2.88E-04	19.43	1.23E-05	**4.01**	1.20E-05	**3.96**
	70	1.07E-03	37.38	2.57E-04	18.38	1.52E-05	**4.47**	1.51E-05	**4.45**
-0.5 SD	90	2.03E-03	50.72	8.39E-04	33.03	7.99E-07	**1.02**	3.00E-04	19.3
	80	1.38E-03	41.16	4.12E-04	23.19	7.54E-07	**0.99**	3.33E-05	**6**
	70	1.18E-03	37.24	3.42E-04	21.18	7.76E-07	**1.01**	7.83E-06	**2.51**

The output position response versus time for the PMA model disturbances of +1 SD is shown in Figure 24 for a 20% PMA assist (human operator function $\hat{M}_{K,F}$ of 80% $\overline{M}_K$). The human operator perturbation level is HOP5 (see Table 3). Figure 4 displays the required position output, the open loop output, the position feedback only output, and the moment feedback only output. Deviations from the required position output indicate error in the response.

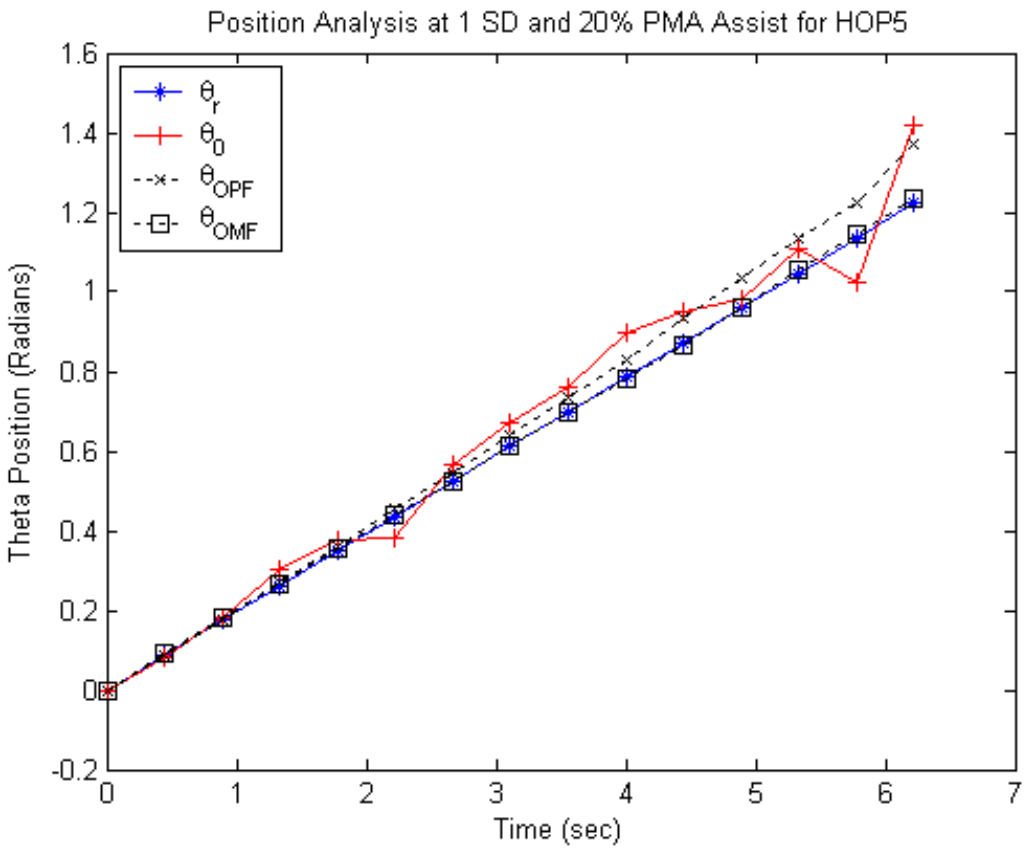

Figure 24: Position analysis at model disturbance level 1 SD and 20% PMA assist.

The output position response versus time for the PMA model disturbance of -1 SD is shown in Figure 25.

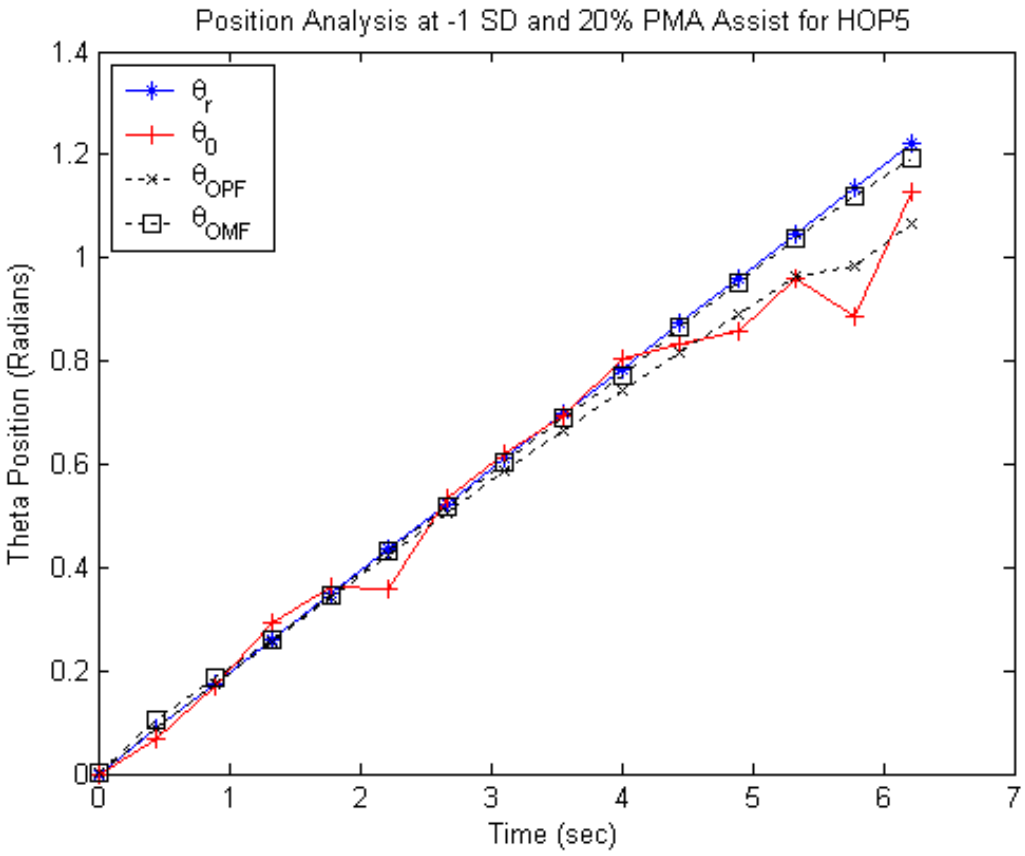

Figure 25: Position analysis at model disturbance level -1 SD and 20% PMA assist.

The output position response versus time for the PMA model disturbance of +0.5 SD is shown in Figure 26.

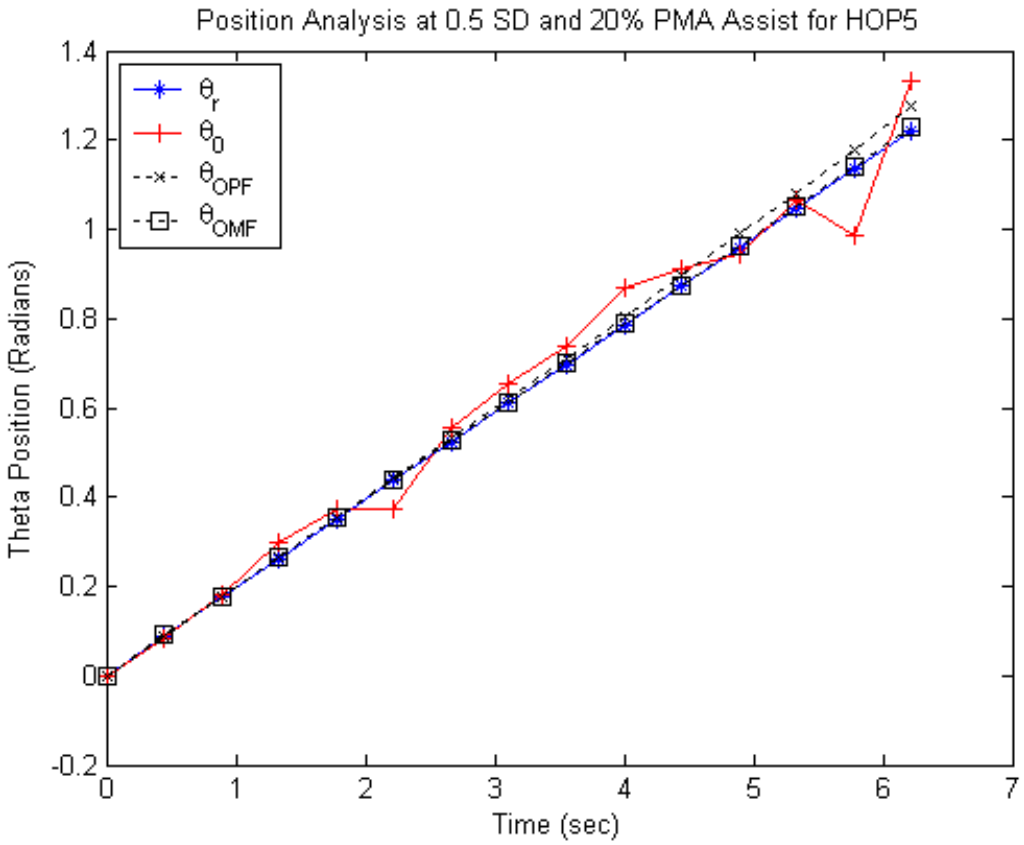

Figure 26: Position analysis at model disturbance level 0.5 SD and 20% PMA assist.

The output position response versus time for the PMA model disturbance of -0.5 SD is shown in Figure 27.

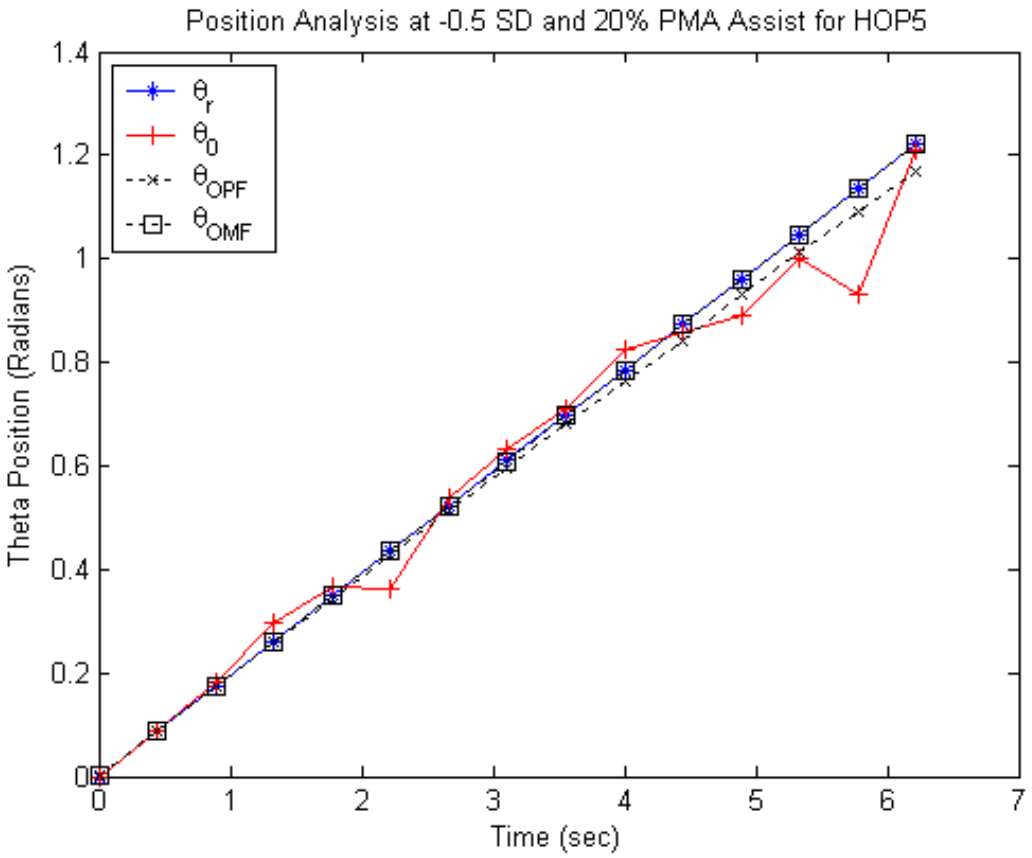

Figure 27: Position analysis at model disturbance level -0.5 SD and 20% PMA assist.

Table 10 provides the numerical results for varying model fluctuations levels. Analysis includes the four control methods: position feedback only, moment feedback only, position and moment feedback, and adaptive control. The MSE and accuracy values are determine via the same method as in Table 9. The results in bold indicate an accuracy level below 20%.

TABLE 10: Results at four different cases analyzed with adaptive control feedback, open loop, pure position feedback, pure moment feedback, and the combination of position and moment feedback. Accuracies under 20% are indicated in bold.

		Position Only		Moment Only		Position & Moment		Adaptive Control	
	%	MSE	% Acc.	MSE	% Acc.	MSE	% Acc.	MSE	% Acc.
Fce +1, B -1, K +1	90	3.62E-02	201.93	2.63E-03	58.79	5.23E-04	25.78	8.93E-05	**10.82**
	80	3.16E-03	64.33	3.84E-04	22.46	5.91E-04	27.32	1.20E-04	**12.56**
	70	2.47E-03	57	1.35E-04	**13.29**	1.55E-04	**14.28**	3.84E-05	**7.1**
Fce +1, B +1, K -1	90	8.13E-03	101.57	1.10E-04	**12.03**	1.03E-03	36.49	3.73E-04	22.12
	80	1.05E-02	115.28	1.54E-04	**14.21**	1.28E-03	40.29	2.04E-04	**16.34**
	70	6.35E-03	91.31	1.23E-04	**12.72**	1.38E-04	**13.43**	1.70E-04	**14.92**
Fce -1, B -1, K +1	90	1.02E-02	115.49	1.14E-03	38.62	4.21E-03	74.28	1.61E-03	46.02
	80	1.07E-02	118.72	6.71E-04	29.68	3.81E-03	70.52	8.48E-04	33.37
	70	6.70E-03	93.71	3.20E-04	20.51	1.73E-03	47.65	4.96E-04	25.53
Fce -1, B +1, K -1	90	3.69E-03	69.53	2.50E-04	**18.11**	1.55E-03	44.99	2.23E-04	**17.1**
	80	3.63E-03	68.94	1.19E-04	**12.49**	9.97E-04	35.91	1.87E-04	**15.68**
	70	2.65E-03	58.9	4.90E-05	**8.02**	3.31E-04	20.67	1.40E-04	**13.57**

3.3 Closed Loop Moment (Force) Feedback Control versus Open Loop Control for a Commercial Pneumatic Muscle Actuator Utilizing a Dynamic Test System

3.3.1 LVDT Results

The LVDT response to both the closed loop study and the open loop study at 70% can be found in Figure 28. The LVDT measures in millimeters the linear displacement of the dynamic test system PMA/cable/motor pulley connection.

The open loop study data analysis for 70% can be found in Figure 29 and Tables 10 and 12. The closed loop study data analysis for 70% can be found in Figure 30 and Tables 13 and 14.

The RMSE results for the open loop study and closed loop study data at 70% can be found in Table 15.

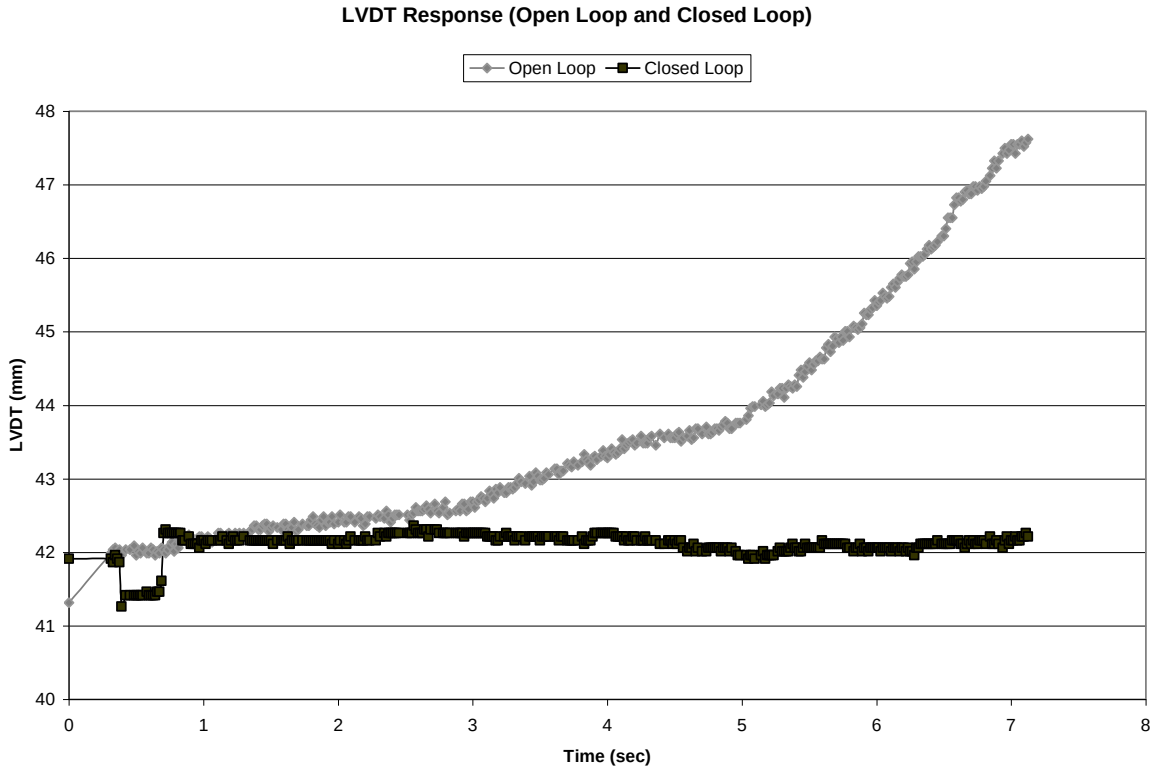

Figure 28: Open Loop Study and Closed Loop Study LVDT Data 70%

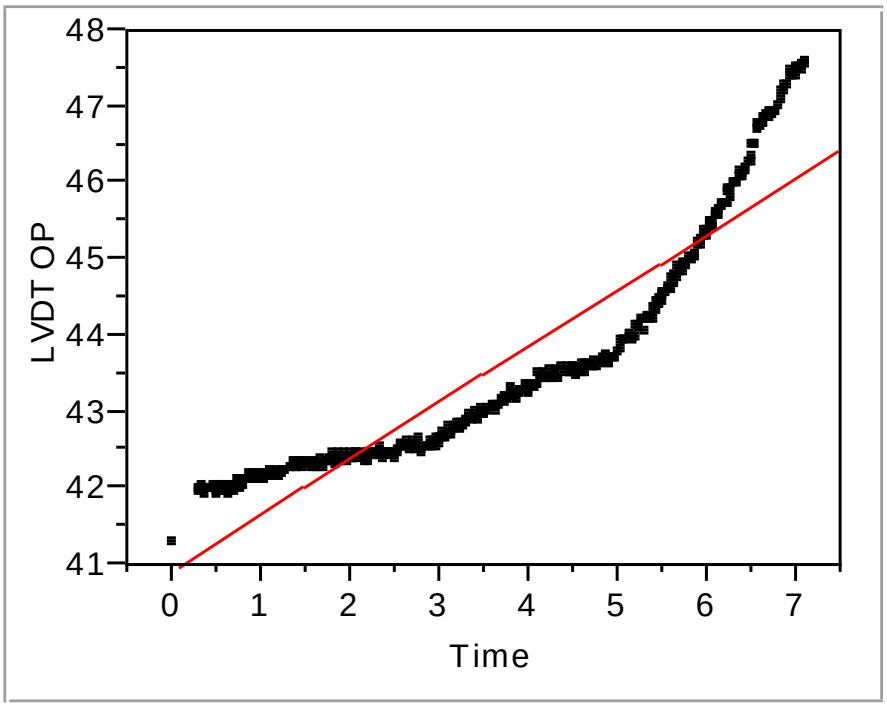

Figure 29: Open Loop Linear Regression Fit 70%
*LVDT linear equation: Open loop LVDT = 40.919294 + 0.7353207*Time. The corresponding R^2 value is 0.858448.*

TABLE 11: Analysis of Variance of the Open Loop Study

Source	DF	Sum of Squares	Mean Square	F Ratio
Model	1	827.50590	827.506	2304.519
Error	380	136.45026	0.359	Prob > F
C. Total	381	963.95616		<.0001

TABLE 12: Parameter Estimates of the Open Loop Study

Term		Estimate	Std Error	t Ratio	Prob>|t|
Intercept		40.919294	0.065737	622.47	0.0000
Time		0.7353207	0.015317	48.01	<.0001

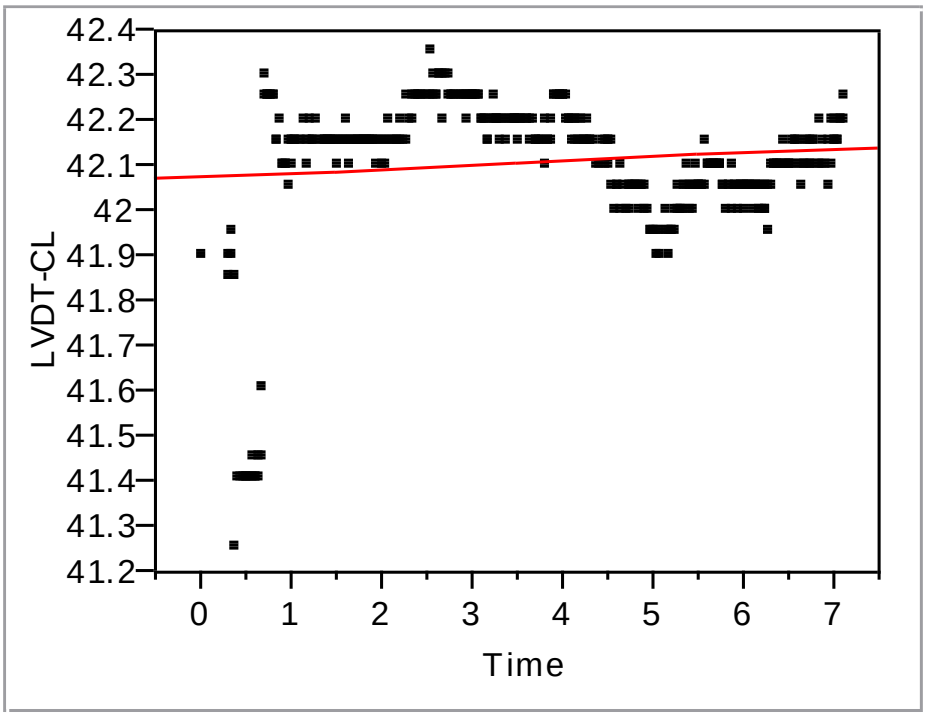

Figure 30. Closed Loop Linear Regression Fit 70%
*LVDT linear equation: Closed Loop LVDT = 42.079107 + 0.0089313*Time. The corresponding R^2 value is 0.011231.*

TABLE 13: Analysis of Variance of the Closed Loop Study

Source	DF	Sum of Squares	Mean Square	F Ratio
Model	1	0.122081	0.122081	4.3161
Error	380	10.748330	0.028285	Prob > F
C. Total	381	10.870411		0.0384

TABLE 14: Parameter Estimates of the Closed Loop Study

Term		Estimate	Std Error	t Ratio	Prob>|t|
Intercept		42.079107	0.01845	2280.7	0.0000
Time		0.0089313	0.004299	2.08	0.0384

TABLE 15: RMSE Values for Open Loop and Closed Loop Studies 70%

RMSE	
Open Loop	2.335 (mm)
Closed Loop	0.203 (mm)

The LVDT response to both the closed loop study and the open loop study at 80% can be found in Figure 31. The LVDT measures in millimeters the linear displacement of the dynamic test system PMA/cable/motor pulley connection.

The open loop study data analysis for 80% can be found in Figure 32 and Tables 16 and 17. The closed loop study data analysis for 80% can be found in Figure 33 and Tables 18 and 19.

The RMSE results for the open loop study and closed loop study data at 80% can be found in Table 20.

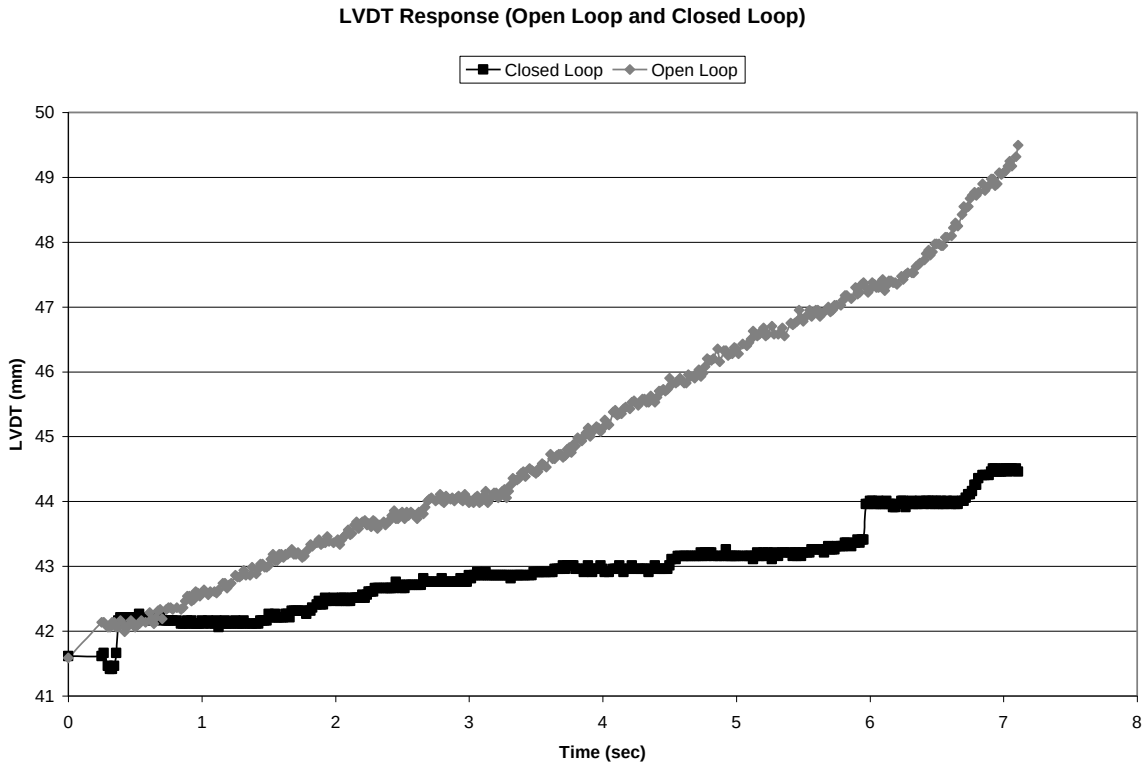

Figure 31: Open Loop Study and Closed Loop Study LVDT Data 80%

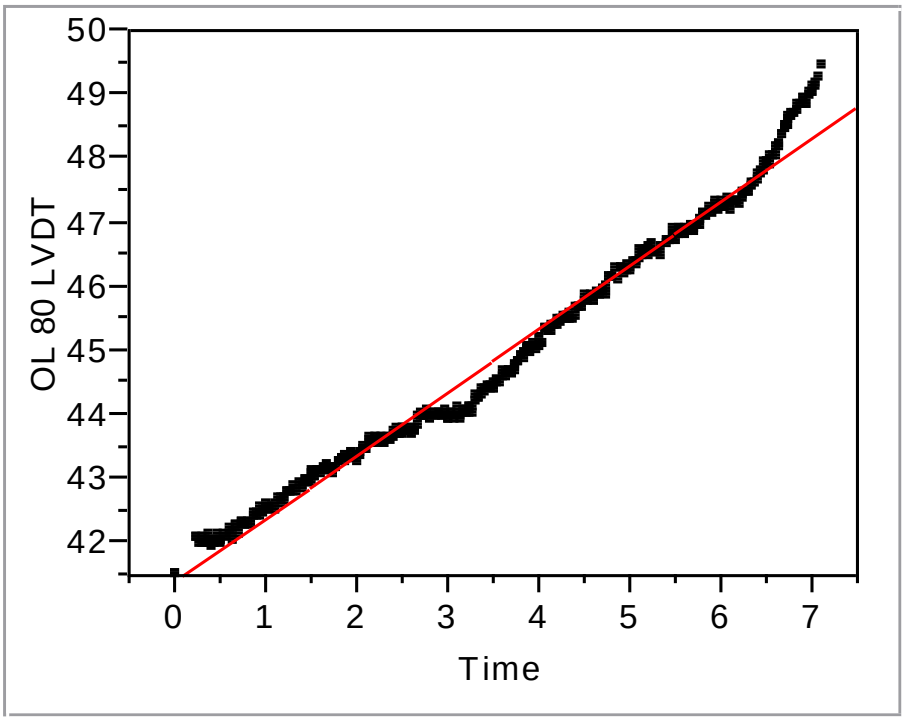

Figure 32: Open Loop Linear Regression Fit for 80%
*LVDT linear equation: Open loop LVDT (mm) = 41.379302 + 0.9982391*Time. The corresponding R^2 value is 0.982459*

TABLE 16: Analysis of Variance of the Open Loop Study 80%

Source	DF	Sum of Squares	Mean Square	F Ratio
Model	1	1508.4437	1508.44	21507.68
Error	384	26.9319	0.07	Prob > F
C. Total	385	1535.3756		0.0000

TABLE 17: Parameter Estimates of the Open Loop Study 80%

Term		Estimate	Std Error	T Ratio	Prob>|t|
Intercept		41.379302	0.028266	1463.9	0.0000
Time		0.9982391	0.006807	146.65	0.0000

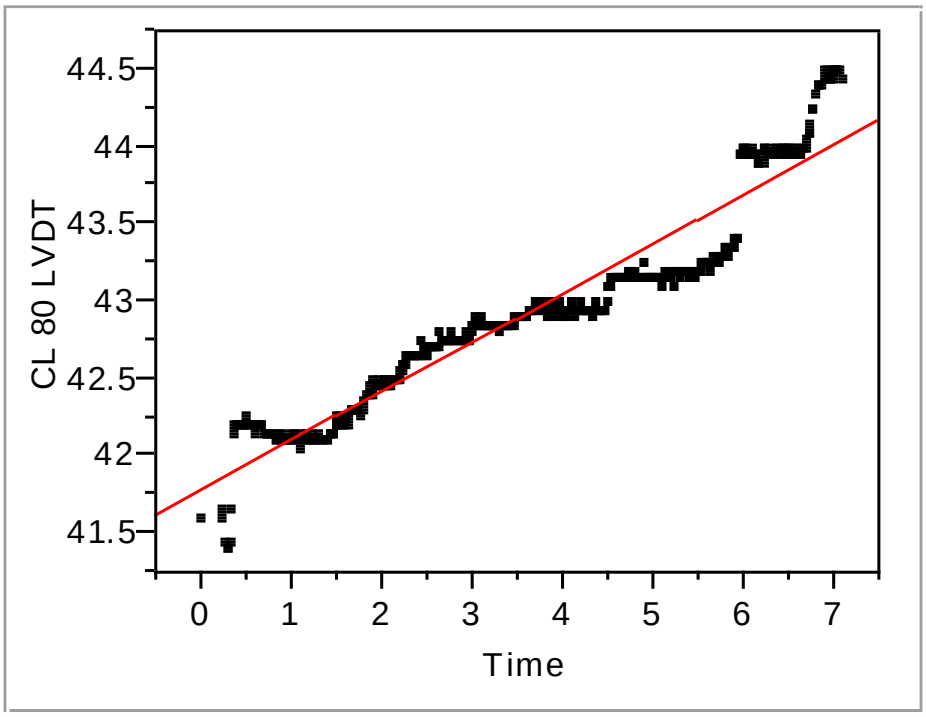

Figure 33: Closed Loop Liner Regression Fit 80%
*LVDT Linear equation: Closed Loop LVDT (mm) = 41.780582 + 0.3203549 *Time. The corresponding R^2 value is 0.913525.*

TABLE 18: Analysis of Variance of the Closed Loop Study 80%

Source	DF	Sum of Squares	Mean Square	F Ratio
Model	1	155.34585	155.346	4056.571
Error	384	14.70523	0.038	Prob > F
C. Total	385	170.05108		<.0001

TABLE 19: Parameter Estimates of the Closed Loop Study 80%

Term		Estimate	Std Error	T Ratio	Prob>|t|
Intercept		41.780582	0.020889	2000.1	0.0000
Time		0.3203549	0.00503	63.69	<.0001

TABLE 20: RMSE Values for Open Loop and Closed Loop Studies 80%

RSME	
Open Loop	3.6216 (mm)
Closed Loop	1.1589 (mm)

The LVDT response to both the closed loop study and the open loop study at 90% can be found in Figure 34. The LVDT measures in millimeters the linear displacement of the dynamic test system PMA/cable/motor pulley connection.

The open loop study data analysis for 90% can be found in Figure 35 and Tables 21 and 22. The closed loop study data analysis for 80% can be found in Figure 36 and Tables 23 and 24.

The RMSE results for the open loop study and closed loop study data at 80% can be found in Table 25.

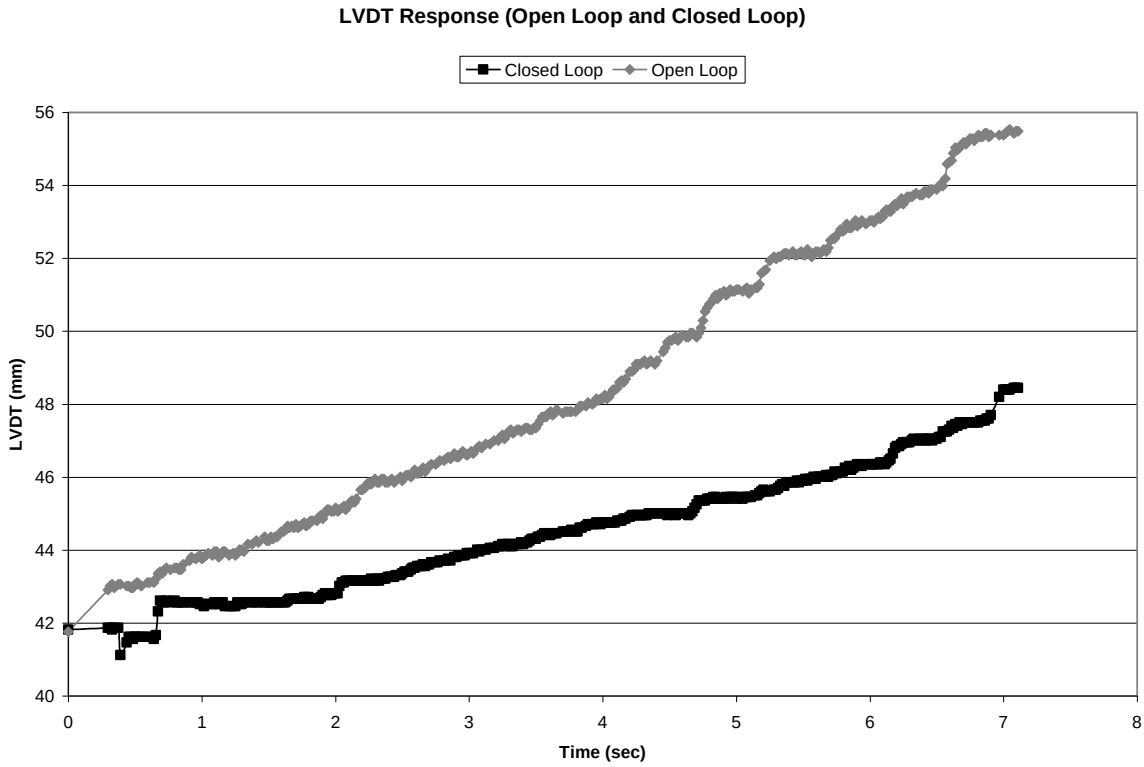

Figure 34: Open Loop Study and Closed Loop Study LVDT Data 90%

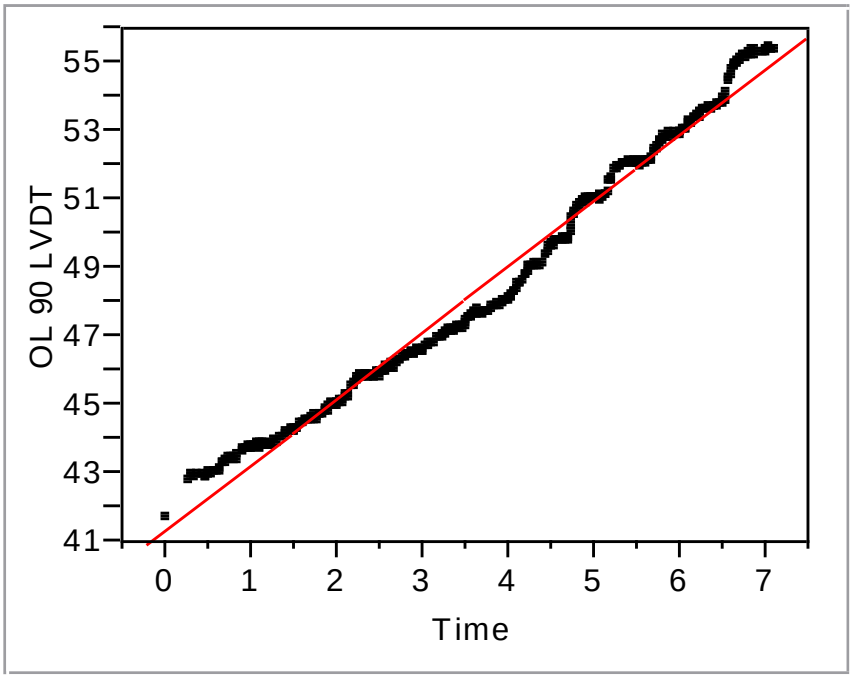

Figure 35: Open Loop Linear Regression Fit.
*LVDT linear equation: Open loop LVDT (mm) = 41.339553 + 1.9303915*Time. The corresponding R^2 value is 0.984833.*

TABLE 21: Analysis of Variance of the Open Loop Study 90%

Source	DF	Sum of Squares	Mean Square	F Ratio
Model	1	5362.8240	5362.82	24544.28
Error	378	82.5914	0.22	Prob > F
C. Total	379	5445.4154		0.0000

TABLE 22: Parameter Estimates of the Open Loop Study 90%

Term		Estimate	Std Error	t Ratio	Prob>|t|
Intercept		41.339553	0.052052	794.20	0.0000
Time		1.9303915	0.012322	156.67	0.0000

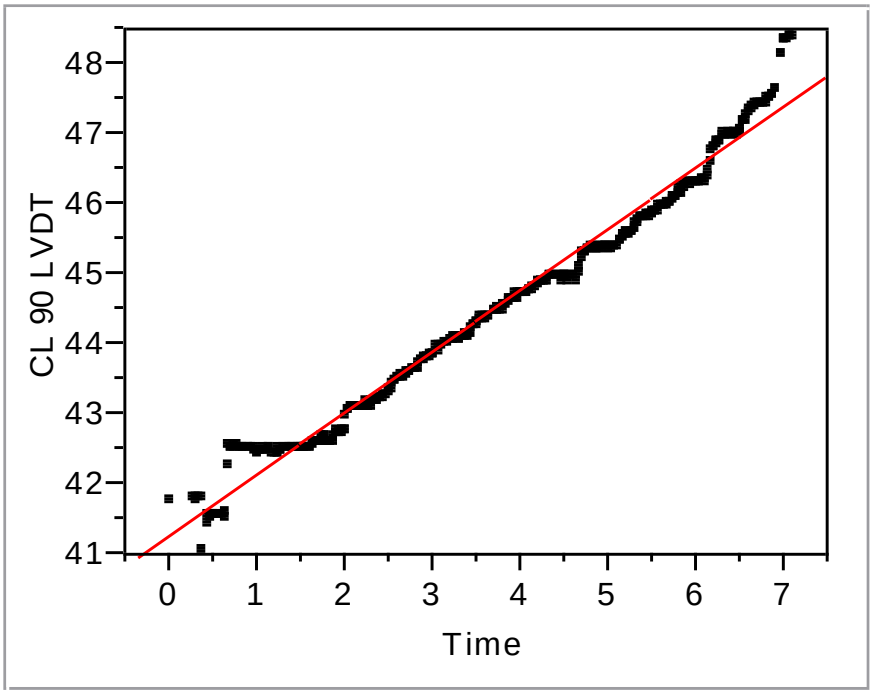

Figure 36: Closed Loop Linear Regression Fit.
*LVDT linear equation: Closed Loop LVDT (mm) = 41.28263 + 0.874286*Time. The corresponding R^2 value is 0.979709.*

TABLE 23: Analysis of Variance of the Closed Loop Study 90%

Source	DF	Sum of Squares	Mean Square	F Ratio
Model	1	1100.0365	1100.04	18251.15
Error	378	22.7829	0.06	Prob > F
C. Total	379	1122.8194		0.0000

TABLE 24: Parameter Estimates of the Closed Loop Study 90%

Term		Estimate	Std Error	t Ratio	Prob>|t|
Intercept		41.28263	0.027339	1510	0.0000
Time		0.874286	0.006472	135.10	0.0000

TABLE 25: RMSE Values for Open Loop and Closed Loop Studies 90%

RSME	
Open Loop	7.589 (mm)
Closed Loop	3.084 (mm)

4.0 Discussion

4.1 A computational simulated control system for a high-force pneumatic muscle actuator: System definition and application as an augmented orthosis

For phase I, the constant zero voltage profiles in both Case I.1 and Case I.2 (Figure 19) indicates the absence of PMA. However, Case I.3-1 and Case I.3-2 (Figure 20) require pressure to activate the pneumatic muscle actuator; thus, resulting in an increasing voltage profile. This generation of initial moment is required for the human to begin the standing process.

For phase II, a voltage change at the pressure regulator is required to achieve the desired position. Case II.1 (Figure 21) requires no voltage because of the PMA is not activated. All the other cases (Figures 22 and 23) require an increase in voltage when the push is eliminated (at t_P). After t_p, the voltage decreases with time.

The results indicate that the PMA has the potential to be an assistive device. Within the linear operating pressure range, the PMA is capable of providing up to 46% assist given the human capability of 54% in case II.3-3.

The required task moment for phase II is achieved in all cases evaluated. Figure 37 shows that the total moment generated by both the human and the PMA (M_{ktot}) is equal to the required moment ($\overline{M}_K$) to complete the task. It is concluded that the SCS is able to satisfactorily control the PMA model. This indicates that the required moment profiles essential for the human to stand is achieved.

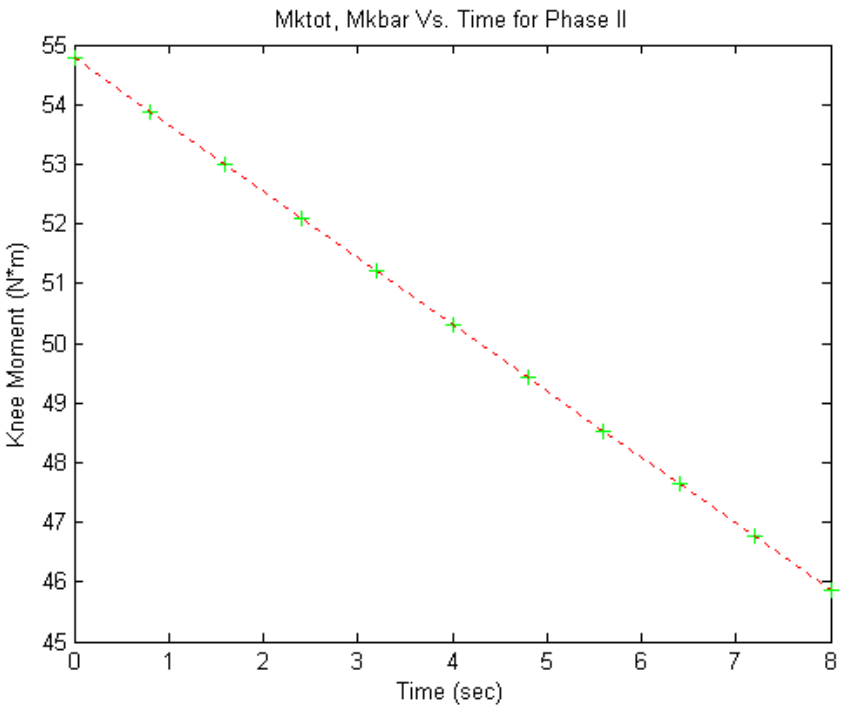

Figure 37: M_{ktot} vs. M_{kbar} for phase II.

A future application of the SCS is the implementation of a high-force PMA in a physical therapy setting. The current SCS can be altered so the PMA output is constant at the point when the push-force is eliminated (t_p). This results in a lower effort exerted by the PMA demanding additional effort from the subject. The physical therapy application strengthens the human quadriceps muscle. As the muscle gains strength, the PMA support can be altered for applicable assist.

A computational simulation model that incorporates the PMA dynamics is developed. The SCS uniquely defines the controller's transfer function for the specified cases. Future work includes implementing the SCS in a physical system. The physical system will utilize the controller profiles to active the PMA via a pressure regulator. The SCS will be evaluated by analyzing the PMA's response time and ability to control

position. A successful PMA control system will advance the field of high-force PMA technology.

The research develops a computational simulated control system for a PMA based on phenomenological modeling. The created controller profiles indicate the necessary input voltage for a proportional pressure regulator. The resultant pressures would be directly applied to the PMA. By taking into account time constant information, the SCS provides real time responses. An internal dynamic force loop is added to the PMA model for this purpose.

The sit-to-stand task is an ideal application for high-force PMAs. The PMA is found to be assistive for this task within the linear operating range of 100 kPa to 600 kPa. The results support PMA feasibility in this application and demonstrate the time constant effects. A physical therapy application of the SCS is also proposed.

4.2 The Evaluation of Industrial Pneumatic Muscle Actuator Control Based on a Computational Simulated Control System

CSCS incorporates model fluctuations and human perturbations to analyze control schemes. Figures 24-27 display the effects of both model fluctuations and human perturbations along with a general trend. Model fluctuations of positive SD (Figure 24 and Figure 26) cause the response to be greater than the required position output. Model fluctuations of negative SD (Figure 25 and Figure 27) show the opposite effect.

Human perturbations in Figure 24-27 vary the response randomly. It slightly changes the slope between sampling position points. If the human perturbations were

eliminated, the response would contain a constant slope only shifting the response up or down according to the model fluctuations.

The open loop results in Table 9 directly show how the model fluctuations and human perturbations affect the position output response. With position feedback only (Table 9), there is (on average) a slight improvement compared to the open loop results. The combination of both moment and position feedback (Table 9) improves the results more than pure position feedback only. Five out of the twelve cases for the combination of moment and position feedback are within the acceptable accuracy tolerance of 10% on Table 9 in bold. Moment feedback only (Table 9), performed the best with an MSE value 10^4 significant digits better than the open loop output position response.

From the numerical results in Table 9 and Figure 24-27, it is apparent that moment feedback alone is a best control method compared to position feedback alone or the combination of position and moment feedback. Moment feedback is able to correct all cases within the predefined criteria of accuracy below 10% except for two cases. These two cases resulted in an accuracy of 17.88% and 14.55% which corresponds to ±0.0156 radians (±0.9 degrees) and ±0.0127 radians (±0.73 degrees), respectively.

Moment feedback performs better than position feedback because moment instead of position dominates the CSCS dynamics. Although the CSCS input and output are in the position domain, the PMA component and the human component in the CSCS interact by combining moments. Therefore to correct for model fluctuations and human perturbations, it is expected that moment feedback would perform better than position feedback. This also causes pure position feedback to have little effect on the response.

This is demonstrated by comparing open loop and position feedback only MSE and accuracy values. There is little variation between these two sets of values.

For varying combination of model fluctuations (Table 10), the results indicate that none of the four control methods (including adaptive control) are able to provide an accuracy tolerance level of 10% in all cases. There is only one sub-trial in both the adaptive control method (F_{ce} +1 SD, B -1SD, K +1 SD and 70% human assist) and moment feedback only method (F_{ce} -1 SD, B +1 SD, K -1SD and 70% human assist) within this tolerance level.

However by raising the accuracy tolerance level to 20% (0.01745 radians or ± 1 degree), the adaptive control sufficiently corrects eight out of twelve sub-trials (66.67%). The moment feedback alone sufficiently corrects seven out of twelve sub-trials (58.33%). The combination of position and moment feedback corrects two out of twelve sub-trials (16.67%). Position feedback is unable to correct any of the twelve sub-trials at the new accuracy tolerance level. The values below the 20% accuracy level are indicated on Table 10 in bold.

The adaptive control and moment feedback both perform better when F_{ce} and K parameter values are at the same SD. This is a result of the PMA physical characteristics. The actual high-force in-house PMA [7], used to determine the PMA parameter values, is more analogous to an elastic spring than a damper. Since F_{ce} is dependent on B and K parameter values (and K is more dominant than B), it is reasonable that F_{ce} will naturally display the same model fluctuations as the K parameters.

In conclusion, the CSCS utilizes a physical model of a physical therapy knee extension task. It demonstrates a high-force PMA application for rehabilitation that requires a force generating task.

The CSCS examines the effects of both model fluctuations and human perturbations. Results show that moment feedback only out performs position feedback only under constant model fluctuation combinations. Moment feedback alone is capable of providing accuracy less than ±0.5 degrees. Moment feedback alone provides a robust control method for the CSCS.

Regarding different model fluctuation combinations, the addition of an adaptive controller provides somewhat better results than the moment feedback.

4.3 Closed Loop Moment (Force) Feedback Control versus Open Loop Control for a Commercial Pneumatic Muscle Actuator Utilizing a Dynamic Test System

Closed loop (moment/force feedback control) is compared to open loop control utilizing a dynamic test system with a commercially available PMA. The LVDT response to the open loop study and closed loop study for human capability of 70% is located in Figure 28. The open loop study has a maximum displacement of 6 mm. The closed loop study has a maximum displacement of less than 1 mm. The initial LVDT response (less than 1 second) for the closed loop study contains the highest displacement due to the nonlinearity of low pressures (less than 150 kPa) commanded to the PMA. It is also a result of the initially large deviation/error in the moment feedback controller. In Figure 28, it is apparent that the closed loop study improved the control of the LVDT performance parameter compared to the open loop study.

The open loop data for 70% is fitted to a regression line. The analysis of variance (Table 11) indicates the probability that the null hypothesis (the slope is zero) is less than 0.001%. The null hypothesis is rejected at 95% and 98% criteria. A 95% confidence interval for the open loop study slope is calculated to be 0.7053 mm/s to 0.7653 mm/s.

The closed loop data for 70% is also fitted to a regression line. The analysis of variance (Table 13) indicates the probability that the null hypothesis (slope is zero) is less than 3.84%. Even though this results in a rejection the null hypothesis for a 95% criteria, a 98% criteria results in a fail to reject indicating the possibility that the slope could be zero. A 95% confidence interval for the closed loop slope is calculated to be 0.0005 mm/s to 0.01714 mm/s. The R^2 value for the closed loop linear fit is considerably low due to the natural fluctuation of the data; therefore, the R^2 value is not a practical statistical inference in this case.

By comparing the 95% slope confidence intervals for both the open loop study and the closed loop study at 70%, it can be concluded that the slopes are statistically different due to the lack of corresponding ranges. This indicates that the two methods, open loop and closed loop, are statistically different.

The smaller the root mean square error (RMSE) value indicates less deviation from an ideal response. Since the RMSE (Table 15) for the closed loop study (0.203 mm) at 70% is considerably smaller than the open loop study (2.335 mm) at 70%, it can be concluded that the closed loop method improved the outcome of the dynamic test system, i.e. less deviation form the ideal response.

The LVDT response to the open loop study and closed loop study for human capability of 80% is located in Figure 31. The open loop study has a maximum

displacement of 8 mm. The closed loop study has a maximum displacement of 3 mm. In Figure 31, it is apparent that the closed loop study improved the control of the LVDT performance parameter compared to the open loop study.

The open loop data at 80% has a 95% slope confidence interval of 0.9849 mm/s to 1.0116 mm/s. A 95% confidence interval for the closed loop slope at 80% is calculated to be 0.3105 mm/s to 0.3302 mm/s. By comparing the 95% slope confidence intervals for both the open loop study and the closed loop study at 80%, it can be concluded that the slopes are statistically different due to the lack of corresponding ranges. This indicates that the two methods, open loop and closed loop, are statistically different.

Since the RMSE (Table 20) for the closed loop study (1.1589 mm) at 80% is considerably smaller than the open loop study (3.6216 mm) at 80%, it can be concluded that the closed loop method improved the outcome of the dynamic test system.

The LVDT response to the open loop study and closed loop study for human capability of 90% is located in Figure 34. The open loop study has a maximum displacement of 14 mm. The closed loop study has a maximum displacement of 6 mm. In Figure 34, it is apparent that the closed loop study improved the control of the LVDT performance parameter compared to the open loop study.

The open loop data at 90% has a 95% slope confidence interval of 1.9062 mm/s to 1.9545 mm/s. A 95% confidence interval for the closed loop slope at 90% is calculated to be 0.8616 mm/s to 0.8870 mm/s. By comparing the 95% slope confidence intervals for both the open loop study and the closed loop study at 90%, it can be concluded that the slopes are statistically different due to the lack of corresponding ranges. This indicates that the two methods, open loop and closed loop, are statistically different.

Since the RMSE (Table 25) for the closed loop study (3.084 mm) at 90% is considerably smaller than the open loop study (7.589 mm) at 90%, it can be concluded that the closed loop method improved the outcome of the dynamic test system.

The closed loop study performs better for all the three cases. The 70% outperforms the 80% and 90% because of the nonlinearity of low pressures (less than 150 kPa) commanded to the PMA. The commanded pressures at 80% and 90% are majority under 150 kPa.

The open loop results indicate that the characterized phenomenological Festo muscle model is unable to completely characterize the nonlinearities of the PMA. Since Festo PMA, similar to all pneumatic actuators, displays dynamic nonlinearities, any characterized model will display error. Therefore, improvement using a controller is necessary. The moment/force controller utilizes the dynamic interaction of the test system instead of the overall test performance parameter. High force application, like the PT application employed in this research, demonstrates greater deviation in moment/force than position.

The moment/force controller is evaluated on a dynamic test system and compared to the open loop method. The open loop method under predicts the response of the system; thus, it results in greater linear displacement (more force generated by the PMA then required). The closed loop moment/force controller, which utilizes the same characterized phenomenological Festo muscle model as the open loop method, is able to compensate for the under prediction. The closed loop controller updates the input moment/force parameter of the characterized phenomenological Festo muscle model to

better predict the PMA pressure command. The result is better position control compared to the current open loop method.

Future improvements to the moment/force feedback control system include a more robust characterized phenomenological model. Since the model is utilized in closed loop controller, less error present in the model results in less error present in the closed loop controller. The closed loop system can also be tested on more demanding tasks. In this research, the PT knee extension task exhibits constant contraction of the PMA. Another application would analyze the moment/force control of a high force relaxation application and/or a combination of contraction and relaxation application.

This research provides a moment/force feedback controller for a dynamic test system. The dynamic test system includes a commercially available Festo muscle offering reproducible results and the ability to compare other potential control schemes on similar standards. The moment/force feedback controller is capable of producing less error associated with the outcome position performance metric.

5.0 IMPLEMENTATION OF THE RESEARCH (FUTURE WORK)

5.1 Improving the PMA Model

The CSCS utilizes the phenomenological model developed by Reynolds et al. [7]. When implemented in the physical system, the PMA parameters calculated for a commercial FESTO PMA are utilized. Therefore, future improvements to the proposed model, in order to improve accuracy, will alter the estimated PMA response. The updated estimated PMA response is the foundation of the moment/force feedback control system. A more accurate characterization will improve the control system.

The complete dynamic test system can be modeled by characterizing the PMA and the motor response simultaneously. This would improve open loop PMA control; however, the characterization is unique to the dynamic test system.

5.2 Future Application of the Physical System

Another useful application for the PMA would be to implement it as an aerospace zero-G exercise machine. Since the PMA is driven by air pressure, it is capable of generating a resistance force in a zero-G environment. The practical application allows astronauts to exercise in space at varying resistance with minimal equipment. Exercise limits the potential of muscle atrophy in space. In order to implement this applicant on the dynamic test system, complete system characterization is required (PMA and motor) and the addition of a rotary potentiometer to monitor motor shaft movement is required.

6.0 CONCLUSIONS

This research analyzes, develops, implements and validates a dynamic high-force PMA control system for an augmented orthosis. The feasibility of the PMA as an augmented orthosis is first analyzed using the in-house characterized phenomenological model from Reynolds et al. [7]. It is determined that the PMA is able to generate assistive forces within the PMA operational pressure range.

Knowing the PMA is feasible as an assistive orthosis, different control systems are developed and analyzed utilizing a PT knee extension task. PMA control has limited the application of PMAs. This research, unlike other control methods, explores different control methods utilizing the phenomenological PMA model. A moment/force feedback, position feedback, moment/force and position combination feedback, and adaptive control are analyzed. In regards to model fluctuations and human perturbation, moment/force feedback and adaptive control equally perform the best. Since moment/force feedback is the simpler in structure, it is implemented in the PMA dynamic test system.

The moment/force feedback control system is implemented via LabView in the dynamic test system. The PT knee extension task is analyzed. The PMA dynamic test system includes a FESTO® PMA, pressure transducer, proportional pressure regulator (PPR), load cell, LVDT and DC servo motor. The closed loop (moment/force feedback control system) is compared to an open loop (pure phenomenological model) controller. The results indicate that the moment/force feedback control system (closed loop)

improved the response of the system for all cases (human capabilities levels of 70%, 80% and 90%). The amount of improvement is related to the operational pressure range.

This research provides a dynamic (time dependent) control system utilizing a dynamic test system with a commercially available PMA. Other control systems previously explore mostly static and in-house PMAs. The control system is capable of improving the control of the PMA response versus time. It also implements a commercially available PMA for the reproducibility of results. Ultimately, this research, due to control improvements, may lead to implementation of PMA in rehabilitation and assistive devices.

7.0 Research Funding

Research was funded in part by NSF grant no. DGE-0504438*; IGERT: An Interdisciplinary Initiative on Technology–based Learning with Disability/*

Appendix A

List of Publications and Conference Presentation Resulting from Dissertation

Journal Publications

Gerschutz, M. J., C. A. Phillips, D. B. Reynolds, and D. W. Repperger. A computational simulated control system for a high-force pneumatic muscle actuator: System definition and application as an augmented orthosis. *Computer Methods in Biomechanics and Biomedical Engineering* (Submitted).

Gerschutz, M. J., C. A. Phillips, D. B. Reynolds, D. W. Repperger, and J. L. Serres. The Evaluation of Industrial Pneumatic Muscle Actuator Control Based on a Computational Simulated Control System. *Medical Engineering & Physics* (Submitted).

Gerschutz M. J., C. A. Phillips, D. B. Reynolds, D. W. Repperger, and J. L. Serres. Closed Loop Moment (Force) Feedback Control versus Open Loop Control for a Commercial Pneumatic Muscle Actuator Utilizing a Dynamic Test System. *Medical Engineering & Physics* (Submitted).

Peer-Reviewed Journal Abstracts

Phillips, C. A., M. J. Gerschutz, D. B. Reynolds, D. W. Repperger, J. L. Serres, and S. Mohler. Dynamic control modeling of an antagonist pneumatic muscle when performing a simulated knee extension task. *Aviation, Space and Environmental Medicine* (In Press).

Conference Presentations

Gerschutz M. J., C. A. Phillips, and D. B. Reynolds. Application of an adaptive Simulated Control System for Industrial Pneumatic Muscle Actuators. *3rd Annual Dayton Engineering Sciences Symposium*. Oct. 29, 2007.

Gerschutz M. J., C. A. Phillips, and D. B. Reynolds. Dynamic Control System Modeling for an Assistive Pneumatic Muscle. *2nd Annual Dayton Engineering Sciences Symposium*. Oct. 2006.

Gerschutz M. J., Assistive Pneumatic Muscle Simulation Utilizing a Dynamic Control System. *BioOhio Conference 2006 Student Poster Competition*. Oct. 2006.

Appendix B

Mathematical Derivation of Knee Extension Task

The physical therapy knee extension task analyzes a single leg utilizing the joint-by-joint method. Each segment is analyzed individually starting at the distal end (foot). After the moment about the knee is determined, assumptions are applied to the model.

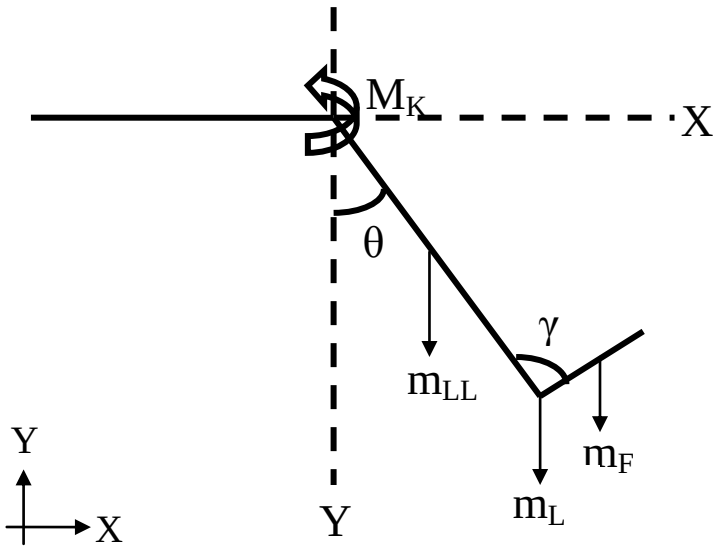

Figure B1: Free body diagram of the knee extension task. M_K is the moment about the knee; m_{LL}, m_F and m_L are the mass of the lower leg, mass of the foot and mass of external load respectively; θ and γ are the angle of the lower leg and angle of the ankle respectively.

Foot Segment

From the foot segment free body diagrams, the forces in the x and y directions and the moment about the foot are calculated. The resultant equation is the moment about the ankle which is used in analyzing the lower leg segment.

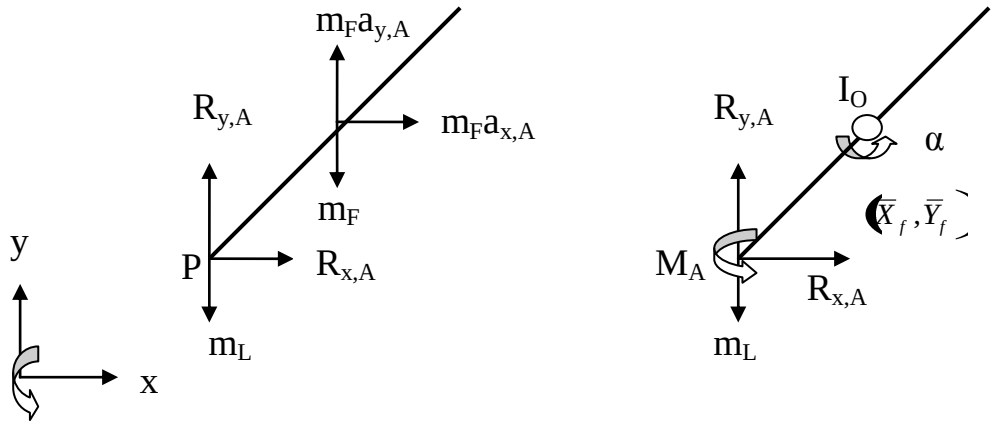

Figure B2: Foot Segment Analysis. $(\bar{X}_f, \bar{Y}_f)$ *is the center of mass location of the foot.*

Summation of forces in the y-direction:

$$\sum F_y = m_f a_{y,A} = R_{y,A} - m_f g - m_L g \qquad \text{(B1a)}$$

$$R_{y,A} = m_f a_{y,A} - m_f g - m_L g = m_f a_{y,A} - (m_f - m_L) g \qquad \text{(B1b)}$$

Summation of forces in the x-direction:

$$\sum F_X = m_f a_{x,A} = R_{x,A} \tag{B2a}$$

$$R_{x,A} = m_f a_{x,A} \tag{B2b}$$

Summation of moments about the foot center of mass $(\bar{X}_f, \bar{Y}_f)$. $Y_{p,f}$ and $X_{p,f}$ are the proximal location of the segment.

$$\sum M_O = I_O \alpha = M_A + R_{x,A}(\bar{Y}_f - Y_{p,f}) - R_{y,A}(\bar{X}_f - X_{p,f}) + m_L g(\bar{X}_f - X_{p,f}) \tag{B3a}$$

$$I_O \alpha = M_A + R_{x,A}(\bar{Y}_f - Y_{p,f}) - (m_L g - R_{y,A})(\bar{X}_f - X_{p,f}) \tag{B3b}$$

$$M_A = I_O \alpha - R_{x,A}(\bar{Y}_f - Y_{P,f}) - (m_L g - R_{y,A})(\bar{X}_f - X_{p,f}) \tag{B3c}$$

Lower Leg Segment

From the lower leg segment free body diagrams, the forces in the x and y directions and the moment about the leg are calculated. The resultant equation is the moment about the knee.

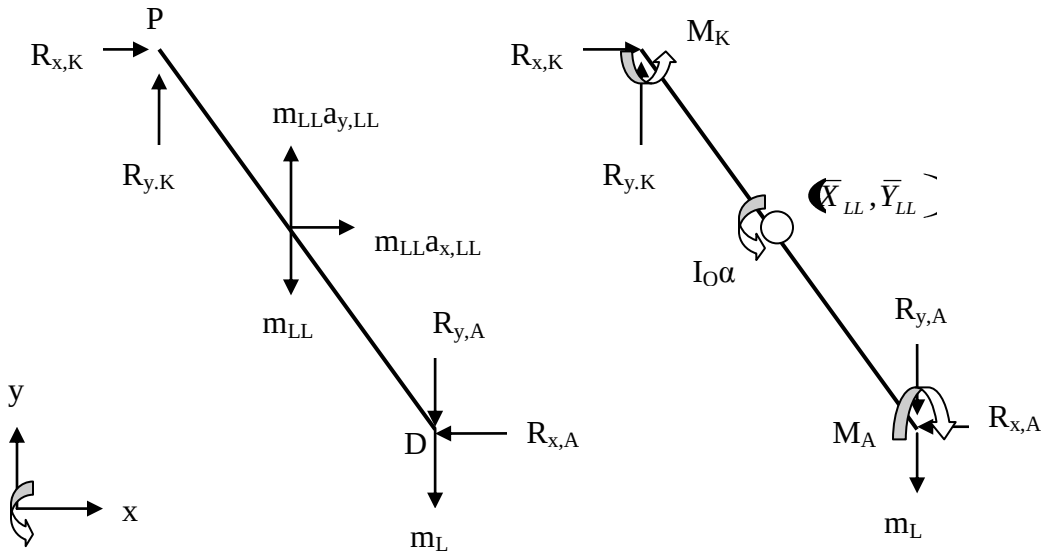

Figure B3: Lower Leg Segment Analysis. $(\bar{X}_{LL}, \bar{Y}_{LL})$ *is the center of mass location of the foot.*

Summation of forces in the y-direction:

$$\sum F_y = m_{LL}a_{y,LL} = R_{y,K} - m_{LL}g - m_L g - R_{y,A} \quad \text{(B4a)}$$

$$R_{y,K} = m_{LL}a_{y,LL} + m_{LL}g + m_L g = m_f a_{y,A} + R_{y,A} \quad \text{(B4b)}$$

$$R_{y,K} = m_{LL}a_{y,LL} + (m_{LL} + m_L)g + R_{y,A} \quad \text{(B4c)}$$

Summation of forces in the x-direction:

$$\sum F_X = m_{LL} a_{x,LL} = R_{x,LL} - R_{x,A} \tag{B5a}$$

$$R_{x,LL} = m_{LL} a_{x,LL} + R_{x,A} \tag{B5b}$$

Summation of moments about the lower leg center of mass $(\bar{X}_{LL}, \bar{Y}_{LL})$. $Y_{P,LL}$ and $X_{P,LL}$ are the proximal location of the segment and $Y_{D,LL}$ and $X_{D,LL}$ are the distal location of the segment.

$$\begin{aligned}\sum M_O = I_O \alpha = M_K + R_{x,K}(Y_{P,LL} - \bar{Y}_{LL}) - R_{y,K}(\bar{X}_{LL} - X_{P,LL}) - M_A \\ - R_{x,A}(\bar{Y}_{LL} - Y_{D,LL}) - R_{y,A}(X_{D,LL} - \bar{X}_{LL}) - m_L g(X_{D,LL} - \bar{X}_{LL})\end{aligned} \tag{B6a}$$

$$\begin{aligned}M_K = I_O \alpha + R_{x,K}(Y_{P.LL} - \bar{Y}_{LL}) + R_{y,K}(\bar{X}_{LL} - X_{P,LL}) + M_A \\ + R_{x,A}(\bar{Y}_{LL} - Y_{D,LL}) + (R_{y,A} + m_L g)(X_{D,LL} - \bar{X}_{LL})\end{aligned} \tag{B6b}$$

Application of Assumptions

The assumptions for the model include:

1. Constant angular velocity resulting in no angular acceleration
    a. $\alpha = 0$
    b. $a_{y,A} = 0$; $a_{x,A} = 0$; $a_{y,LL} = 0$; $a_{x,LL} = 0$
2. Constant ankle angle

Foot Segment Equations with Assumptions Applied

Summation of forces in the y-direction:

$$R_{y,A} = (m_f - m_L)g \quad \text{(B7)}$$

Summation of forces in the x-direction:

$$R_{x,A} = 0 \quad \text{(B8)}$$

Summation of moments about the foot center of mass $(\bar{X}_f, \bar{Y}_f)$. $Y_{p,f}$ and $X_{p,f}$ are the proximal location of the segment.

$$M_A = -(m_L g - R_{y,A})(\bar{X}_f - X_{p,f}) \quad \text{(B9)}$$

Lower Leg Segment Equations with Assumptions Applied

Summation of forces in the y-direction:

$$R_{y,K} = (m_{LL} + m_L)g + R_{y,A} \tag{B10}$$

Summation of forces in the x-direction:

$$R_{x,LL} = 0 \tag{B11}$$

Summation of moments about the lower leg center of mass $(\bar{X}_{LL}, \bar{Y}_{LL})$. $Y_{P,LL}$ and $X_{P,LL}$ are the proximal location of the segment and $Y_{D,LL}$ and $X_{D,LL}$ are the distal location of the segment.

$$M_K = R_{y,K}(\bar{X}_{LL} - X_{P,LL}) + M_A + (R_{y,A} + m_L g)(X_{D,LL} - \bar{X}_{LL}) \tag{B12}$$

Parameter Identification

Anthropometric values are used in calculating the segments lengths, center of mass locations and moment distances. The anthropometric values are of a female. All calculations are functions of height (H) and mass (M) of the female.

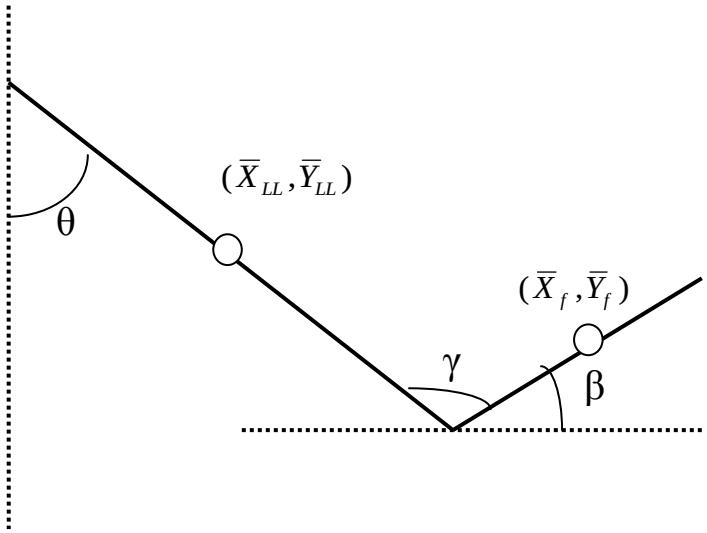

Figure B4: Knee Extension task with angle identification and center of mass identification.

Segment Identification

$$L_{LL} = 0.246\ H \tag{B13}$$

$$L_f = 0.039\ H \tag{B14}$$

$$m_f = 0.0145\ M \tag{B15}$$

$$m_{LL} = 0.0465\ M \tag{B16}$$

Center of Mass Identification

The center of mass values are functions of the segment parameters. It is not necessary to calculate $\bar{Y}_{LL}$ because it was eliminated from the moment equations.

$$\bar{X}_f = 0.5L_f \tag{B17}$$

$$\bar{Y}_f = 0.5L_f \tag{B18}$$

$$\bar{X}_{LL,P} = 0.435L_{LL} \tag{B19}$$

$$\bar{X}_{LL,D} = 0.565L_{LL} \tag{B20}$$

Moment Distance Identification

The moment distances are the distances from the center of the mass to either the proximal or distal end of a segment. In order to calculate the moment distances, the angle β is calculated in terms of γ and θ.

$$\beta = 90 - \theta - \gamma \tag{B21}$$

$$(\bar{X}_f - X_{p,f}) = 0.5L_f \cos(90 - \theta - \gamma) \tag{B22}$$

$$(\bar{Y}_f - Y_{p,f}) = 0.5L_f \sin(90 - \theta) \quad \text{(B23)}$$

$$(\bar{X}_{LL,P} - X_{P,LL}) = 0.435L_{LL} \sin\theta \quad \text{(B24)}$$

$$(X_{D,LL} - \bar{X}_{LL,D}) = 0.565L_{LL} \sin\theta \quad \text{(B25)}$$

Foot Segment Calculation Identifications

The segment equations utilize the segment identifications, center of mass identifications, and moment distance identifications. It also uses the value of gravity (g) as 9.81 [m/s^2]

$$R_{y,A} = (0.0145M - m_L) \cdot 9.81 \text{ [N]} \quad \text{(B26)}$$

$$R_{x,A} = 0 \text{ [N]} \quad \text{(B27)}$$

$$M_A = -(m_L - (0.0145M - m_L) \cdot 9.81 \cdot (0.5L_f \cos(90 - \theta)) \text{ [Nm]} \quad \text{(B28)}$$

Lower Leg Segment Calculation Identification

$$R_{y,K} = (0.0465M + m_L) \cdot 9.81 + R_{y,A} \text{ [N]} \quad \text{(B29)}$$

$$R_{x,LL} = 0 \text{ [N]} \quad \text{(B30)}$$

$$M_K = [(0.465M + m_L) \cdot 9.81 + R_{y,A}](0.435L_{LL} \sin\theta) + M_A - (R_{y,A} + m_L \cdot 9.81)(0.565L_{LL} \sin\theta) \text{ [Nm]} \quad \text{(B30)}$$

Calculation using Numerical Values

The anthropometric values and constant values include:

1. H = 1.75 [m]
2. M = 68 [kg]
3. mL = 2.27 [kg] (5 lbs)
4. γ = 100 degrees
5. θ ranges from 0 degrees to 90 degrees
6. $L_f = 0.039 \cdot 1.75 = 0.06825$ [m]
7. $L_{LL} = 0.246 \cdot 1.75 = 0.4305$ [m]

Foot Segment Numerical Calculation

The foot segment equations are calculated using the equations in the identification section and the previous numerical values.

$$R_{Y,A} = 31.94136 \text{ [N]}$$

$$M_A = 0.33\cos(\theta - 10°) \text{ [Nm]}$$

Lower Leg Segment Numerical Calculation

The lower leg segment equations are calculated using the equations in the identification section and the previous numerical values.

$$R_{y,K} = 85.22928 \text{ [N]}$$

$$M_K = 29.147\sin\theta + 0.33\cos(\theta - 10°) \text{ [Nm]}$$

Appendix C

Hardware Components

The physical system models the PMA force, the resistant force required to stand, and the human capability. The total system is controlled and monitored using the LabVIEW software system. The physical system picture can be found in Figure C1.

The physical system hardware can be separated into two categories: the PMA and motor. The PMA and motor are connected via a pulley and cable system. The PMA is controlled by a servo-valve that allows nitrogen gas to flow into the PMA. The motor provides a back EMF that corresponds to the human resistive force.

LabVIEW is able to command, via voltages, the proportional pressure regulator (PPR) and the motor. It receives pressure data from the pressure transducer, force data from the load cell, and position data from the linear variable differential transformer (LVDT).

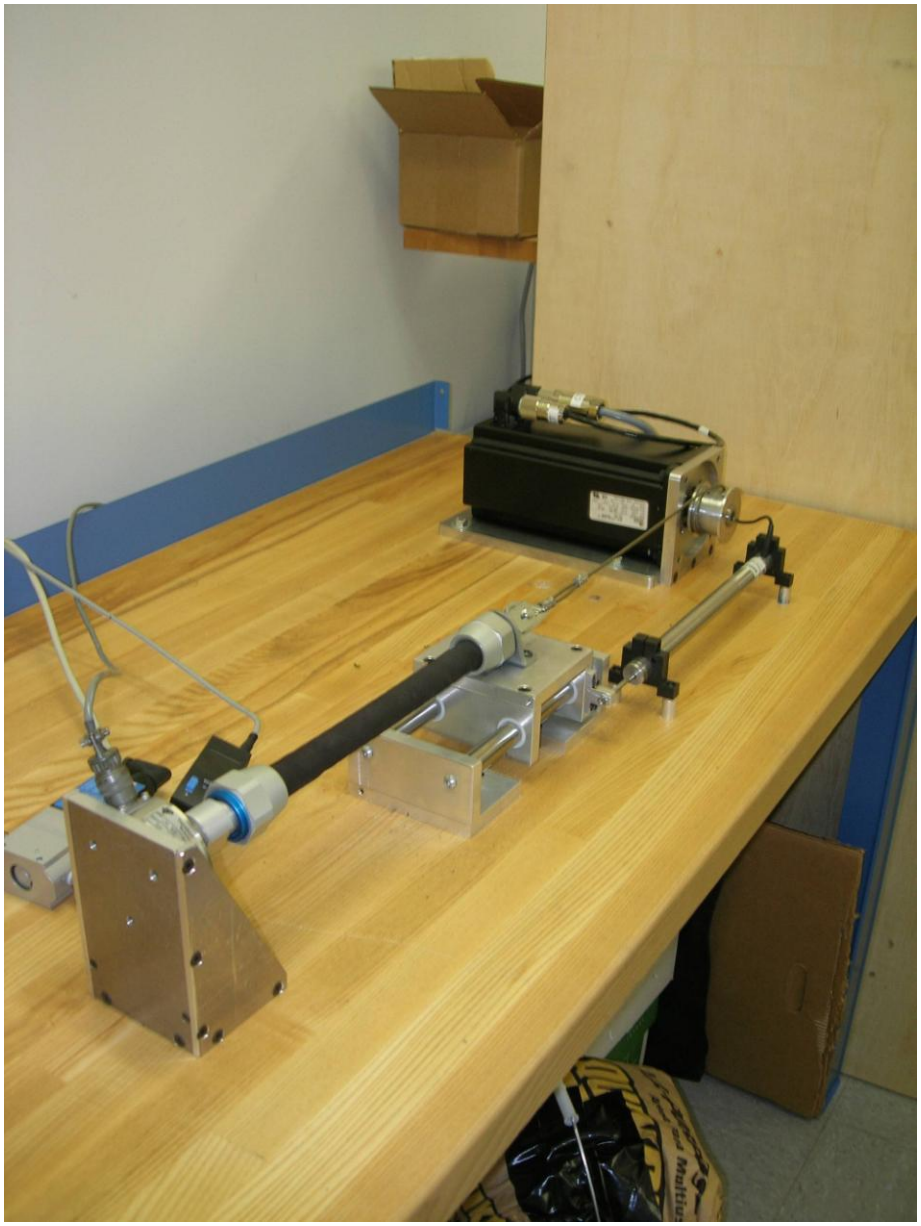

Figure C1: Physical System Picture

PMA

The PMA was purchased from FESTO (FESTO MAS-20-N254-AA-MCHK). The dimensions are described by the inner diameter and length of the contractive rubber section. The inner diameter is 20 mm and the elastic length is 254 mm.

Figure C2: FESTO® Pneumatic Muscle Actuator

PPR (Proportional Pressure Regulator)

The PPR was also purchased from FESTO (MPPE-3-1/8-6-010B). The maximum flow rate is 800 L/min which is limited by the diameter of the input and exhaust ports. The PPR is controlled by voltage inputs. It has a closed loop mechanism that shuts off the air flow when is reaches the specified set point. The main purpose of the PPR is to regulate the pressure entering the PMA. This is controlled by LabVIEW commands and communicates through a data acquisition card.

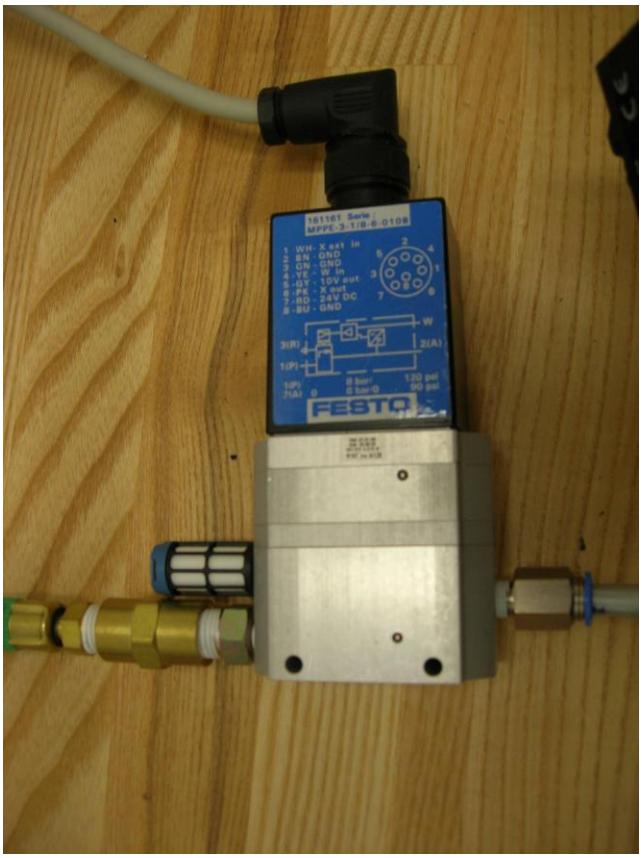

Figure C3: Proportional Pressure Regulator

Load Cell

The load cell (Transducer Techniques, Temecula, CA) is a 4 bridge element of strain gauges. It is mounted inline to the PMA on the fixed surface. The load cell measures the force exerted by the PMA. It communicates through a signal conditioner that outputs a voltage to LabVIEW.

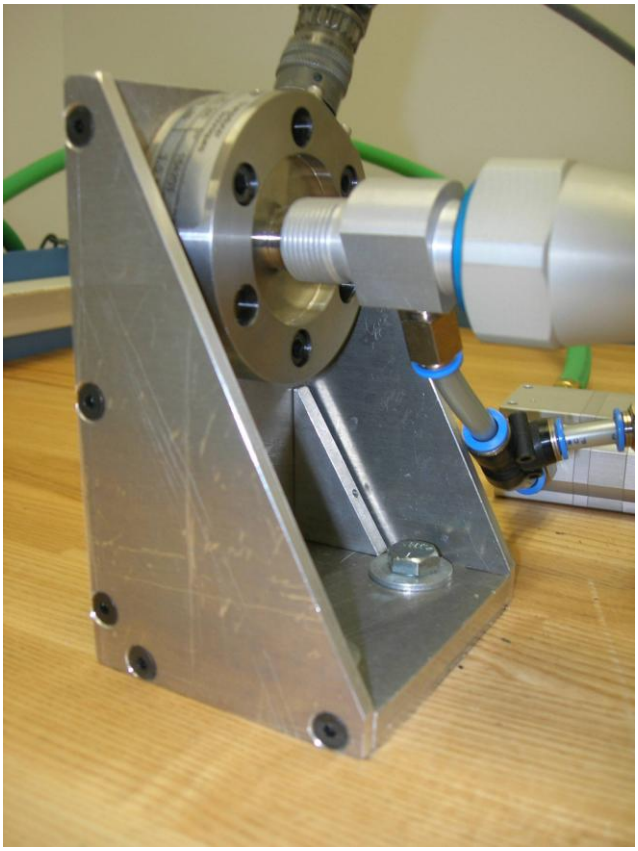

Figure C4: Load Cell

LVDT

The linear variable differential transformer (LVDT) from Sensotec, Columbus, OH measures the linear displacement of the PMA. The measurements are referenced to the starting length of the PMA instead of an internal zero position. The maximum length change is constrained to ± 2 inches.

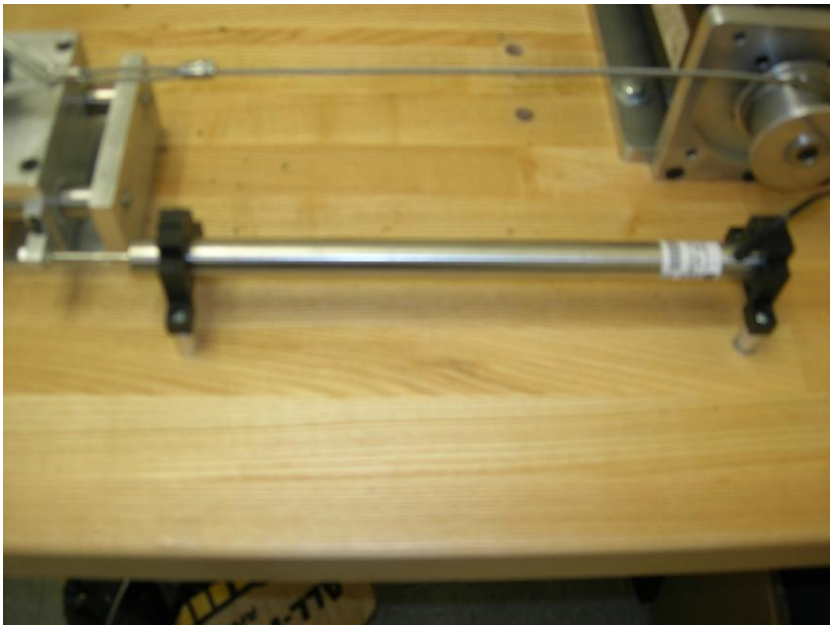

Figure C5: LVDT

Air Pressure Transducer

The air pressure transducer (FESTO SDE1-D10-G2-W18-L-PU-M8) outputs the pressure data entering the PMA. The data ranges from 0-10 volts corresponding to 0-10 bars. The data is read into LabVIEW.

Figure C6: Pressure Transducer

Power Supply

The power supply contains three 24 volt DC configured in one power supply box.

Figure C7: Power Supply

Data Acquisition Card (DAQ)

The data acquisition card (National Instruments) communicates between the computer and the system in terms of voltages. It contains 16 input channels and 2 output channels. The output channels allow for the control of the PMA and the motor. The input channels receive information from the pressure transducer, load cell, and LVDT. The signals send and receive information in the form of analog voltages. The voltages can be converted into useful information in LabVIEW.

Motor

The motor (Pacific, PMA45N-00100-00) contains a driving shaft and a pulley. It allows the application of a resistant force against the PMA. The motor controls two torque directions, positive and negative, referring to the clockwise and counter-clockwise motion.

Figure C8: DC Servo Motor

Software

National Instruments' LabVIEW will be used to monitor and collect the data imported through the DAQ card. It will also dispatch the control profiles for both the PPR and motor. LabVIEW allows for the dynamic collection of data.

Nitrogen Air Supply

A nitrogen air supply is used to inflate the PMA. It was chosen due to non-flammable properties and cleanliness.

TABLE C3: Categorized Component List

Component List	
PMA	Festo Muscle
	PPR
	Nitrogen Tank
	Load cell
	LVDT
	Pressure Transducer
	Power Supply
Motor 1	Pulley
	Cable
Computer	LabVIEW
	DAQ

Appendix D

SCS MATLAB CODE

%MatLab Function: input the case percentage for ti to tp then tp to tf.

```
function PMAcontroller(percentMkhat1,percentMkhat2)
    percentMkhat1=percentMkhat1/100;
    percentMkhat2=percentMkhat2/100;
%Constants
    tt=20; ii=11; A=(pi/2)/tt;
    M=68; What=0.678*9.8*M; WL=(What/2);
    H=1.75; L2=1.142*0.19*H; L1=0.245*H; rw=0.025; alpha=pi/3;
%Fce parameters
    %coeff. for P greater than 200
    a=179.2; b=1.39;
%Coeff. for P less than 200
    c=2.29;
%Dashpot parameters
    aa=1.01*1000; bb=0.0069*1000;
%Spring parameters
    aaa=5.71*1000; bbb=0.0307*1000;
%initial conditions
    %Desired theta value
    thetar=0;
    %pressure
    P(1)=0;
    %initial parameters
    theta(1)=0;
    dt=(2*tt/5)/((ii-1)*4);
    %Case identification
    for i=1:ii     %tp set at 1/6 of the total angle. (5 degrees = pi/36)
        n=round(ii/6);
        if i<=n
            thetar(i) =pi*(i-1)/300;
            %Calculation of Mkbar
            Mkbar(i)=-85.094*thetar(i)+54.775;
            %Calculation of Mkhat
            Mkhat(i) = percentMkhat1*Mkbar(i);
            Mf(i)=0;
        else
            thetar(i) =pi*(i-1)/300;
            %Calculation of Mkbar
            Mkbar(i)=-85.094*thetar(i)+54.775;
            %Calculation of Mkhat
            Mkhat(i) = percentMkhat2*Mkbar(i);
            Mf(i)=0;
        end
```

```
    Mkbarprime(i)=Mkbar(i)-Mkhat(i);
    %PMA Model Block
    if P(i) <= 200
        Fa=(c*P(i))-((aa+bb*P(i))*rw*A)-((aaa+bbb*P(i))*rw*theta(i));
    else
        Fa=(a+b*P(i))-((aa+bb*P(i))*rw*A)-((aaa+bbb*P(i))*rw*theta(i));
    end
    %Condition: Fa can not be negative
    if Fa <=0
        Fa=0;
    end
    %Actuator Force conversion to Moment
    Ma(i)=Fa*rw;
    Maprime(i)=Ma(i)+Mf(i);
    for x=1:4
        %Time constant information
        deltaMa(i) = Mkbarprime(i)-Maprime(i);
        Mf(i)=Mf(i)+deltaMa(i);
        tau=(aa+(bb*P(i))) / (aaa+(bbb*P(i)));
        Madd(i)=(dt/tau)*Mf(i);
        Maprime(i)=Ma(i)+Madd(i);
    end
    P(i)=[(Maprime(i)/rw)-(a)+(aa*rw*A)+(aaa*rw*theta(i))] / [b-(bb*rw*A)-
    (bbb*rw*theta(i))];
    if P<=200;
        P(i)=[(Maprime(i)/rw)+(aa*rw*A)+(aaa*rw*theta(i))] / [c-(bb*rw*A)-
        (bbb*rw*theta(i))];
    end
    if Maprime(i)== 0
        P(i)=0;
    end
    Mtot(i) = Maprime(i) + Mkhat(i);
    theta(i) = (Mtot(i)-54.775)/(-85.094);
    theta(i+1)=theta(i);
    P(i+1)=P(i);
    %Voltage Response
    V(i)=(P(i)+14.929)/59.929;
    if V(i)<0.25
        V(i)=0;
    end
end
```

Appendix E

CSCS MATLAB Code

%CSCS MATLAB Code

```
%analysis for +-1,+-0.5 SD g1 and g2 defined by percentage input
%close all;
clear all;
percentMkhat=90;
limit=17;
limit2=19-limit;
percentMkhat=percentMkhat/100;

%Constants
   tt=8;
   ii=19;
   A=(pi/2)/tt;
   M=68;
   H=1.75;
   r=0.025;

   %Fce parameters
   %coeff. for P greater than 200
   a=179.2;
   b=1.39;
   a2=252.21;
   b2=1.408;
   %Coeff. for P less than 200
   c=2.29;
   c2=2.67;

   %Dashpot parameters
   aa=1.01*1000;
   bb=0.0069*1000;
   aa2=1.95*1000;
   bb2=0.0069*1000;

   %Spring parameters
   aaa=5.71*1000;
   bbb=0.0307*1000;
   aaa2=6.74*1000;
   bbb2=0.0311*1000;

   %initial conditions
      %Values for Mkbar and Theta output for the interpolation process;
         %where x=Mkbar and y=theta at double the sample rate; This is
         %used in the controller definition section;
          %Weight at the ankle equal to 2.27 kg (5 Lbs)
```

```
            x=[-2.22 -0.949 0.32498 1.599 2.869 4.134 5.391 6.638 7.873 9.092 10.294
11.476 12.637 13.773 14.884 15.987 17.017 18.036 19.021 19.97 20.88 21.751 22.581
23.367 24.109 24.805 25.454 26.055 26.605 27.106 27.554 27.95 28.293 28.582 28.817
28.997 29.122 29.191 29.205 29.373 29.541 29.709 30.213 30.717];
            y=[(-pi/36) (-pi/72) 0:(pi/72):(pi/2) (2*pi/3) (5*pi/6) pi (3*pi/2) (2*pi)];

      %pressure
         Po(1)=0;
      %initial parameters
         theta(1)=0; %Output theta

         dt=(tt)/((ii-1)*4);
         %U=randn(1,ii);
         %U1
         U=[0.1184 0.3148 1.4435 -0.3510 0.6232 0.7990 0.9409 -0.9921 0.2120 0.2379 -
1.0078 -0.7420 1.0823 -0.1315 0.3899 0.0880 -0.6355 -0.5596 0.4437];
         %U2
         %U=[-1.0091 -0.0195 -0.0482 0.0000 -0.3179 1.0950 -1.8740 0.4282 0.8956
0.7310 0.5779 0.0403 0.6771 0.5689 -0.2556 -0.3775 -0.2959 -1.4751 -0.2340];
         %U3
         %U=[0.0327 1.8705 -1.2090 -0.7826 -0.7673 -0.1072 -0.9771 -0.9640 -2.3792 -
0.8382 0.2573 -0.1838 -0.1676 -0.1170 0.1685 -0.5012 -0.7051 0.5082 -0.4209];
         %U4
         %U=[-0.9499 0.7812 0.5690 -0.8217 -0.2656 -1.1878 -2.2023 0.9863 -0.5186
0.3274 0.2341 0.0215 -1.0039 -0.9471 -0.3744 -1.1859 -1.0559 1.4725 0.0557];
         %U5
         %U=[-0.2012 -0.0205 0.2789 1.0583 0.6217 -1.7506 0.6973 0.8115 0.6363
1.3101 0.3271 -0.6730 -0.1493 -2.4490 0.4733 0.1169 -0.5911 -0.6547 -1.0807];


      for i=1:ii-limit2
         thetar(i) =pi*(i-1)/(2*(ii-1));
         %Calculation of Mkbar (required moment about the knee)
            Mkbar(i)=29.147*sin(thetar(i))+0.33*cos(thetar(i)-(pi/18)); %2.27 kg weight at
the ankle
            %Mkbar(i)= 9.973*sin(thetar(i))+0.33*cos(thetar(i)-(pi/18)); %0 kg weight at
the ankle
         %Calculation of Mkhat
            Mkhat(i) = percentMkhat*Mkbar(i);
         %Intergal time constant information
            Pfm(i)=0;
         %Amount of moment required by the actuator
            Mar(i)=Mkbar(i)-Mkhat(i);


         %Pressure Prediction using the PMA model
```

```
        %Required Pressure Profile
            Pp(i)=[(Mar(i)/r)-(a)+(aa*r*A)+(aaa*r*thetar(i))] / [b-(bb*r*A)-
(bbb*r*thetar(i))];
              if Pp<=200;
                 Pp(i)=[(Mar(i)/r)+(aa*r*A)+(aaa*r*thetar(i))] / [c-(bb*r*A)-
(bbb*r*thetar(i))];
              end
              if Mar(i)<= 0
                 Pp(i)=0;
              elseif Pp(i)>=600
                 Pp(i)=600;
              else
                 Pp(i)=Pp(i);
              end


      %Simulated Actual Data
         %Time lag information
            deltaPp=0;
         %White Noise generator
            %U(i)=0;

         %PMA Model Block (SD change)
            Ppressure(i)=Po(i);
               for xxx=1:4
                   %Additional time lag effects
                  if xxx<=deltaPp
                     Ppressure(i)=Po(i);
                  else
                     %Analysis of preformance
                     difPm(i) = Pp(i)-Ppressure(i);
                     Pfm(i)=Pfm(i)+difPm(i);
                     tau=(aa2+(bb2*Pp(i))) / (aaa2+(bbb2*Pp(i)));
                     Paddm(i)=(dt/tau)*Pfm(i);
                     Ppressure(i)=Po(i)+Paddm(i);
                     if Ppressure(i) <= 0
                        Ppressure(i)=0;
                     end
                  end
               end
               Po(i+1)=Ppressure(i);
            %Calculation of PMA force after pressure iteration
            if Ppressure(i) <= 200
               Fam(i)=(c2*Ppressure(i))-((aa2+bb2*Ppressure(i))*r*A)-
((aaa2+bbb2*Ppressure(i))*r*thetar(i));
            else
```

```
            Fam(i)=(a2+b2*Ppressure(i))-((aa2+bb2*Ppressure(i))*r*A)-
((aaa2+bbb2*Ppressure(i))*r*thetar(i));
        end


            %Condition: Fa can not be negative
              if Fam(i) <=0
                 Fam(i)=0;
              end

        %Actuator Force conversion to Moment
           Mam(i)=Fam(i)*r;

        %Physical Plant
           Mtot(i) = Mam(i) + Mkhat(i)+ U(i);
           theta(i) = interp1(x,y,Mtot(i));
           if theta(i)<=0
              theta(i)=0;
           end
           theta(i+1)=theta(i);
        %Adaptive Filter Constants


     %Adaptive Controller
        %Position Error Information
           e(i)=theta(i)-thetar(i);
%                 g1(i)=0.5;
%
%                %updating position law
%                 kc1(i)=-g1(i)*e(i)*thetar(i);
%                 thetanew(i)=thetar(i)+kc1(i)*dt;

     %Calculation of position feedback (if g1 = 1 pure position feedback, if g1=0
     %              no position feedback)
           g1(i)=0;
           kc1(i)=-g1(i)*e(i);
           thetanew(i)=thetar(i)+kc1(i);

        %Moment Error Information
           epsilon(i)=Mam(i)-Mar(i);
%            if percentMkhat == 0.7
%               g2(i)=1.5;
%            elseif percentMkhat == 0.8
%               g2(i)=2;
%            elseif percentMkhat == 0.9 & epsilon(i) <= -0.5
%               g2(i)=4.5;
```

```
%                elseif percentMkhat == 0.6
%                   g2(i)=1.2;
%                elseif percentMkhat == 0.5
%                   g2(i)=1.1;
%                elseif percentMkhat == 0.4
%                   g2(i)=1.05;
%                else
%                   g2(i)=3.5;
%                end


                 %updating moment law
%                      kc2(i)=-g2(i)*epsilon(i)*Mar(i);
%                      Manew(i)=Mar(i)+kc2(i)*dt;
              %Calculation of moment feedback (if g2 = 1 pure moment feedback, if g2=0
%                 no moment feedback)
                 g2(i)=1;
                 kc2(i)=-g2(i)*epsilon(i);
                 Manew(i)=Mar(i)+kc2(i);

          %Controller Definition
            %Required Pressure Profile
               P(i)=[(Manew(i)/r)-(a)+(aa*r*A)+(aaa*r*thetanew(i))] / [b-(bb*r*A)-
(bbb*r*thetanew(i))];
                 if P<=200
                    P(i)=[(Manew(i)/r)+(aa*r*A)+(aaa*r*thetanew(i))] / [c-(bb*r*A)-
(bbb*r*thetanew(i))];
                 end
                 if Manew(i)<= 0 | P(i)<=0
                    P(i)=0;
                 elseif P(i) >= 600
                    P(i)=600;
                 else
                    P(i)=P(i);
                 end
                 P(i+1)=P(i);

          %Check actual Ma and theta
               if P(i) <= 200
                    Fam2(i)=(c2*P(i))-((aa2+bb2*P(i))*r*A)-
((aaa2+bbb2*P(i))*r*thetanew(i));
               else
                    Fam2(i)=(a2+b2*P(i))-((aa2+bb2*P(i))*r*A)-
((aaa2+bbb2*P(i))*r*thetanew(i));
               end
```

```
            if P(i)<=0
               Fam2(i)=0;
            end

          %Condition: Fa can not be negative
            if Fam2(i) <=0
               Fam2(i)=0;
            end
          %Actuator Force conversion to Moment
            Mfm2(i)=Fam2(i)*r;
            Mam2(i)=Mfm2(i);


          %Physical Plant
            Mtot2(i) = Mam2(i) + Mkhat(i);
            theta2(i) = interp1(x,y,Mtot2(i));
          if g1(i)==0 & g2(i)==0
            theta2(i)=theta(i);
          end
        end
          dtheta=theta2-thetar;
          mean(abs(dtheta(1:limit)))

    %Plotting Results
      t=0:(tt)/(ii-1):(((i-1)*tt)/(ii-1));

%       figure(1)
%       plot(t,Pp,'-b*',t,Ppressure, '-r+',t,P(1:i),'-gs');
%       title(['Predicted Pressure, Input Pressure and Required Pressure vs. Time:
M_k_h_a_t percentage ', num2str(percentMkhat)]);
%       xlabel('Time (sec)');
%       ylabel('Pressure (kPa)');
%       legend('Predicted Pressure','Input Pressure','Required Pressure',2);
%
%       figure(2)
%       plot(t,thetar,'-b*',t,theta(1:i),'-r+',t,theta2(1:i),'-gs');
%       title(['\theta_r, \theta_0, \theta_O_2 Vs. Time: M_k_h_a_t percentage ',
num2str(percentMkhat)]);
%       xlabel('Time (sec)');
%       ylabel('\theta Position (Radians)');
%       legend('\theta_r', '\theta_0','\theta_O_2',2);
%
%        figure(3)
%       plot(t,Mar,'-b*',t,Mam,'-r+',t,Mam2,'-gs');
%       title(['Required M_A, Measured M_A_2 Vs. Time: M_k_h_a_t percentage ',
num2str(percentMkhat)]);
```

```
%       xlabel('Time (sec)');
%       ylabel('PMA Moment (N*m)');
%       legend('Required M_A','Measured M_A','Measured M_A_2',2);
```

Appendix F

LabVIEW Code for Open Loop Study

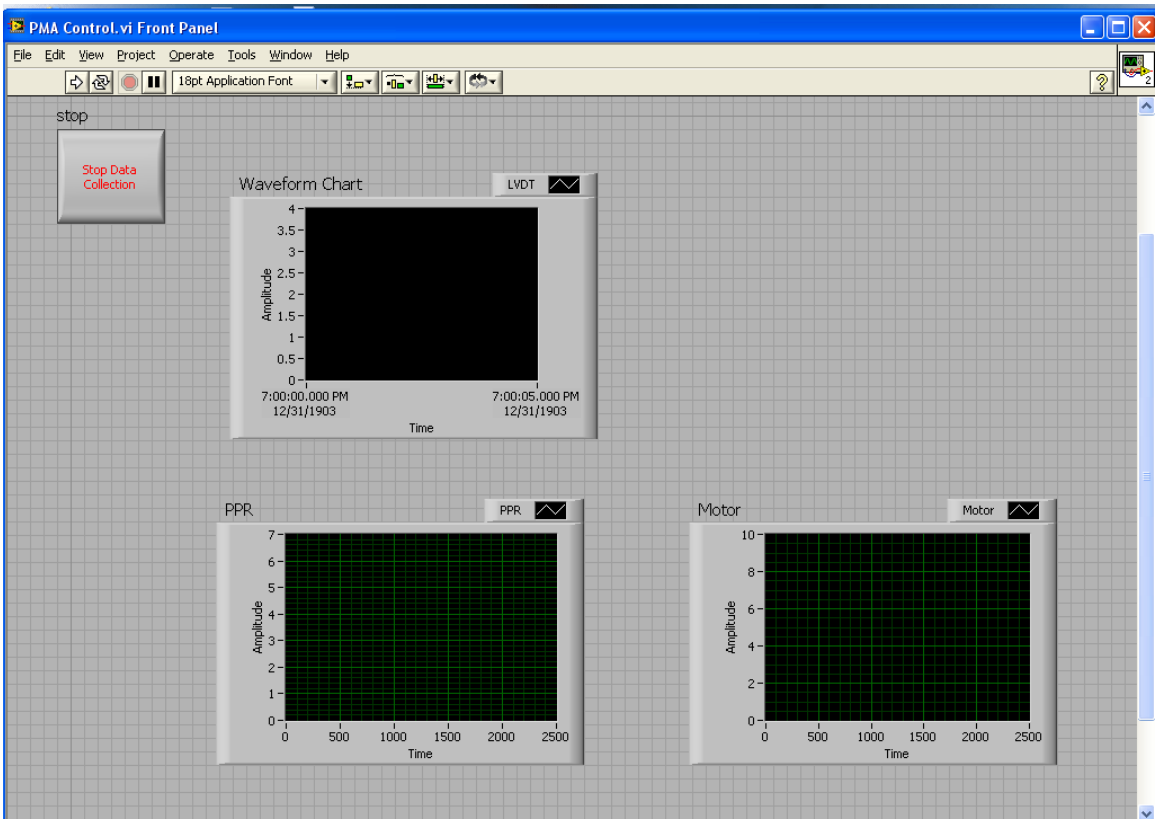

Figure F1: Open Loop LabView Code Front Panel

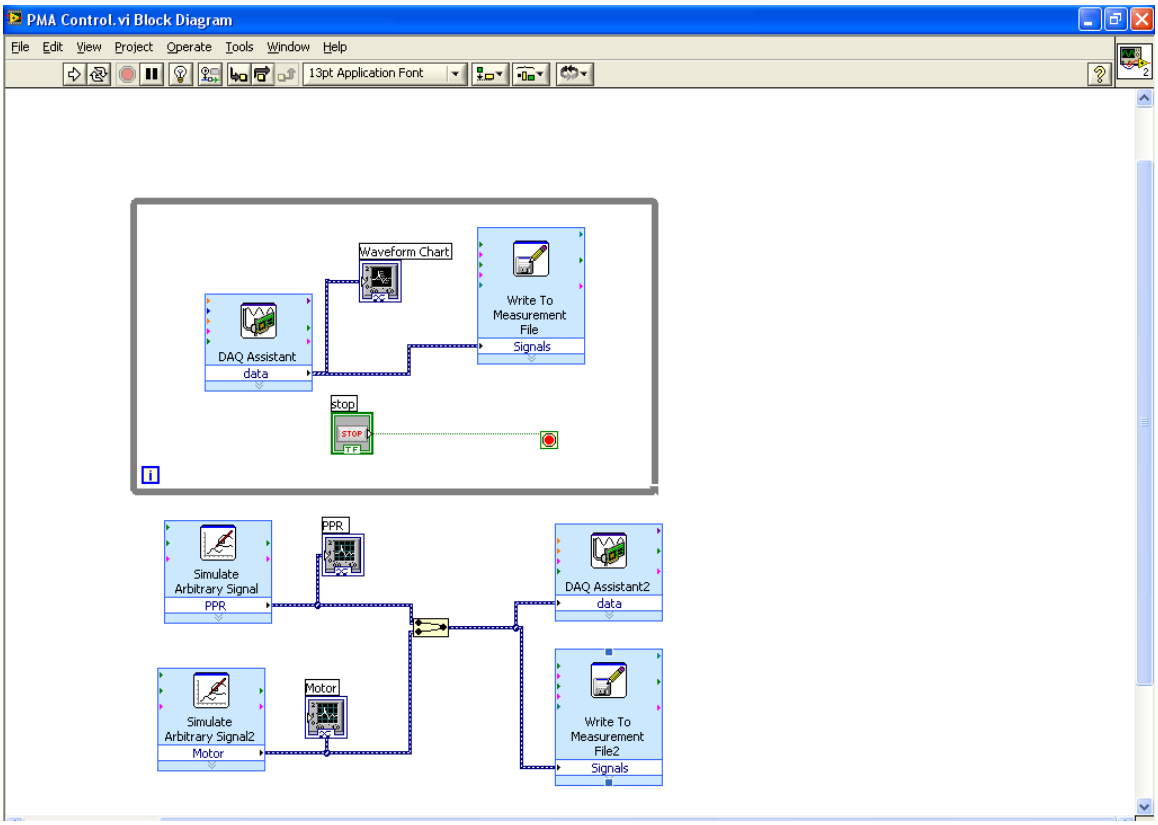

Figure F2: Open Loop LabView Code Block Diagram

Appendix G

LabView Code for Closed Loop Study

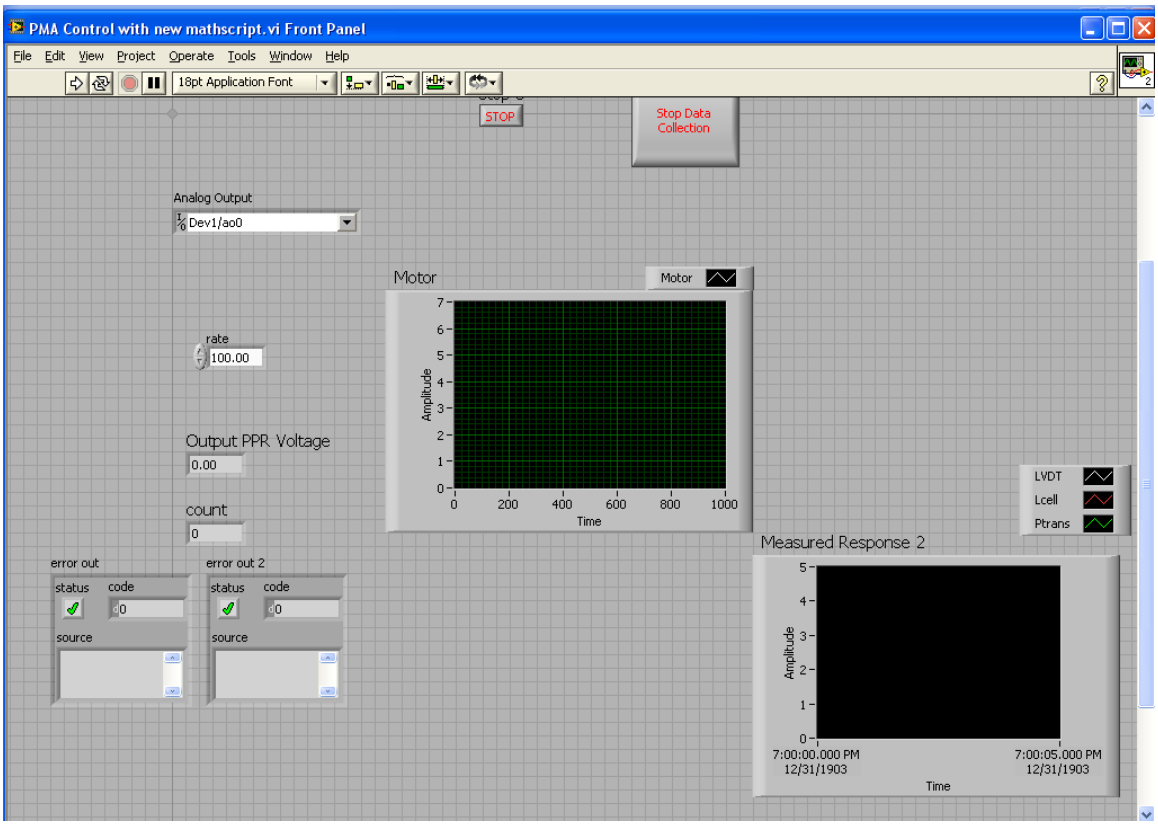

Figure G1: Closed Loop LabView Code Front Panel

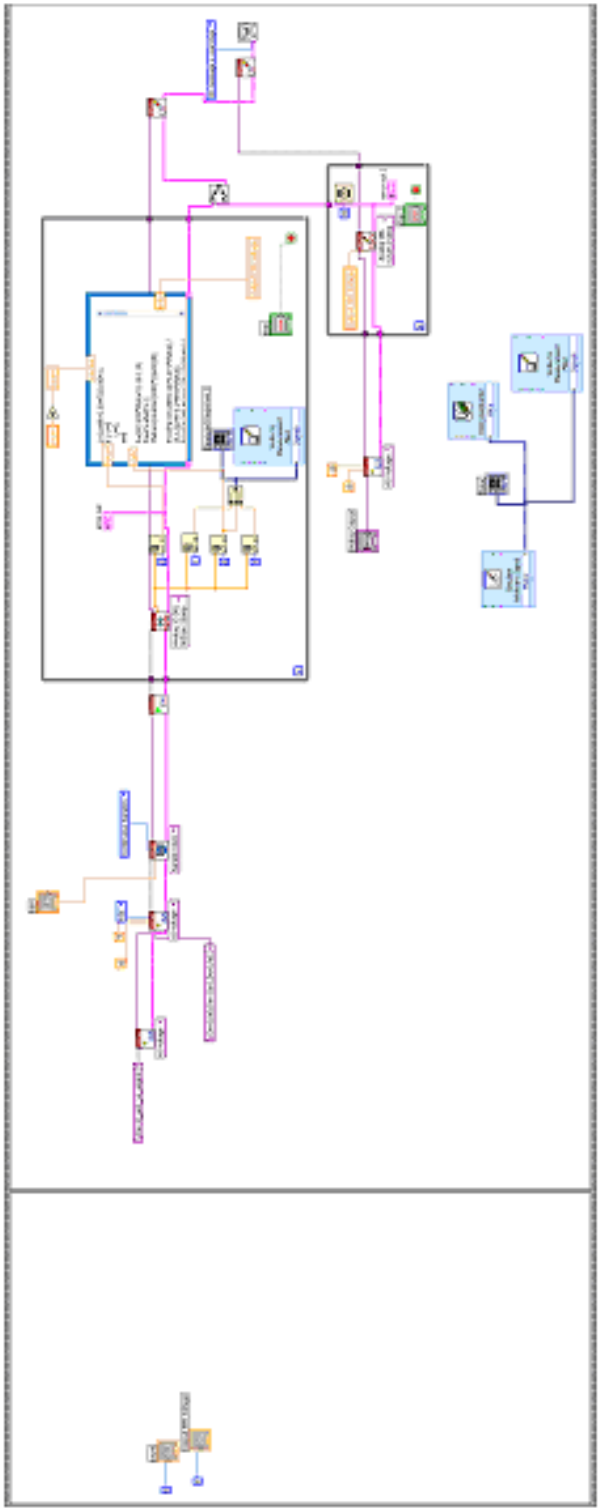

Figure G2: Closed Loop LabView Code Block Diagram

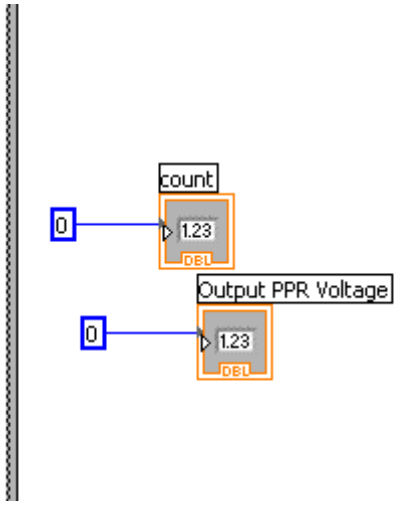

Figure G3: Closed Loop LabView Code Block Diagram Initial Conditions

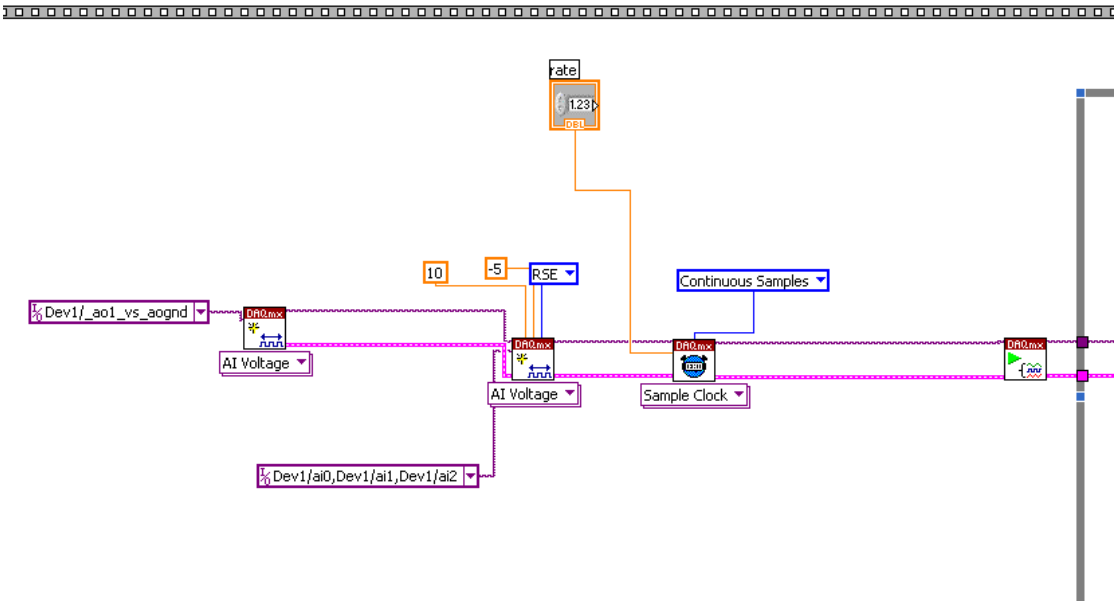

Figure G4: Closed Loop LabView Code Block Diagram Physical Channel Definition

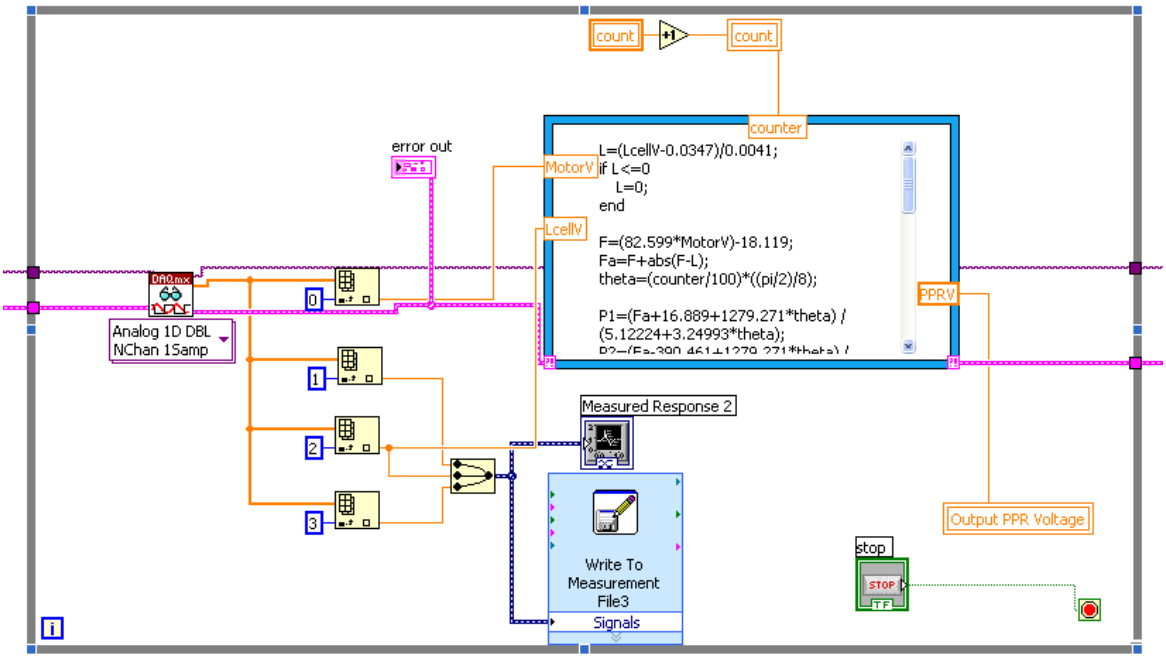

Figure G5: Closed Loop LabView Code Block Diagram Sensor Collection and Mathscript Calculation

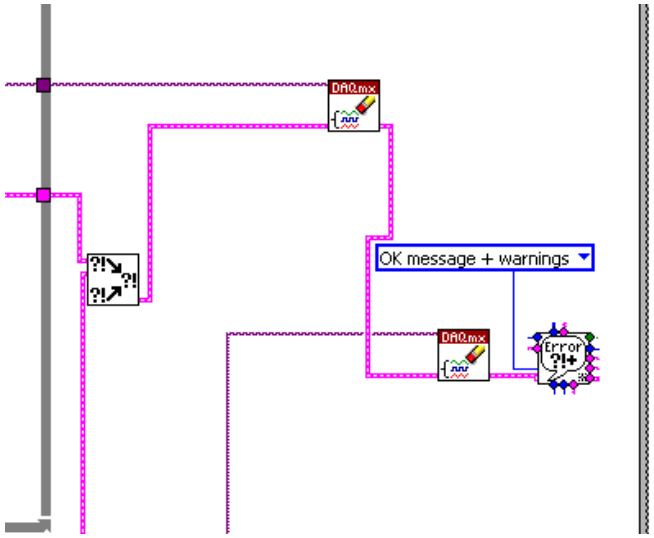

Figure G6: Closed Loop LabView Code Block Diagram Error and Warning Displays

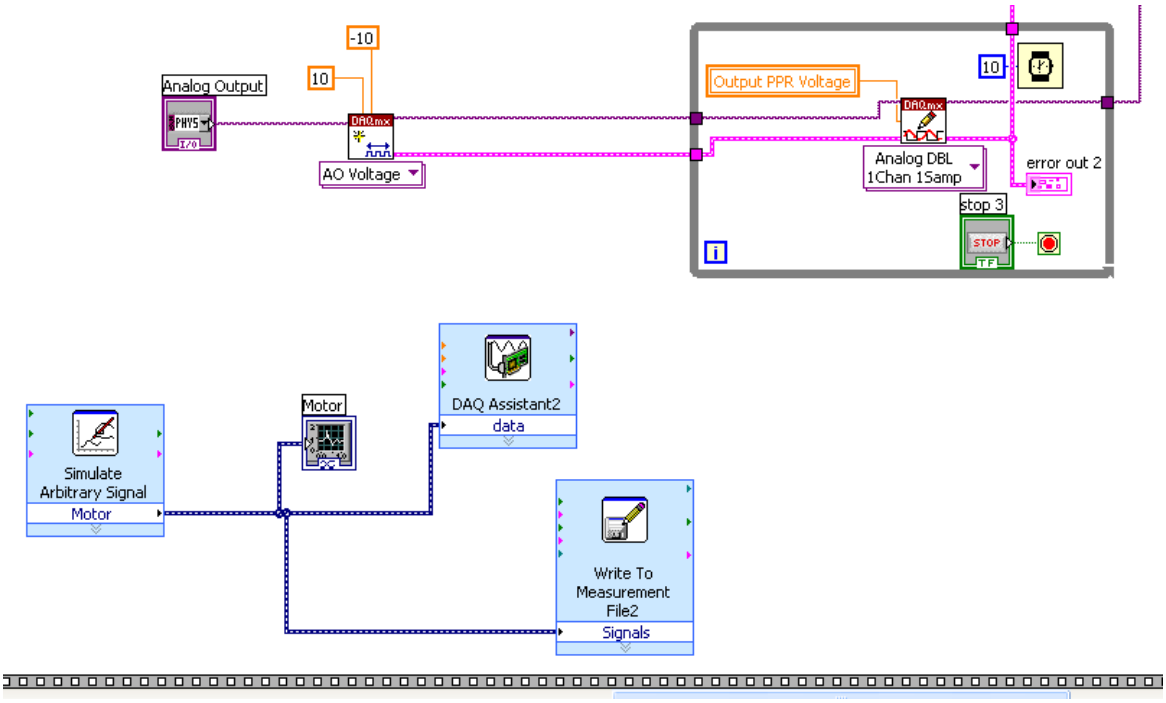

Figure G7: Closed Loop LabView Code Block Diagram Output Signal Commands

Mathscript Code found in Figure G5. Input parameters include load cell voltage (LcellV), motor voltage (MotorV), and time indicator (counter). The output parameter is the voltage sent to the proportional pressure regulator (PPRV).

MathScript Code

```
L=(LcellV-0.0347)/0.0041;
if L<=0
   L=0;
end

F=(82.599*MotorV)-18.119;
Fa=F+abs(F-L);
theta=(counter/100)*((pi/2)/8);

P1=(Fa+16.889+1279.271*theta) / (5.12224+3.24993*theta);
P2=(Fa-390.461+1279.271*theta) / (2.40654+3.24993*theta);
P3=(Fa-390.461+607.3775* theta) / (2.40654+0.59436*theta);
P4=(Fa-1388.071+607.3775*theta) / (0.02244+0.59436*theta);

              if P1<150
                 P=P1;
              elseif P2>=150 & P2< 253
                 P=P2;
              elseif P3>=253 & P3<418.4
                 P=P3;
              elseif P4>=418.4 & P4<550
                 P=P4;
              else P4>=550
                 P=550;
              end

              if theta>=1.57 | Fa<=0 | P<=0
         P=0;
       end
if counter<=5
   Pave=P;
   p1=0; p2=0; p3=0; p4=0;
end
if counter > 5
   Pave=(Psum+P)/5;
end
```

```
p1=p2; p2=p3; p3=p4; p4=Pave;
Psum=p1+p2+p3+p4;

    PPRV=((Pave/100)+0.2041)/0.5993;
```

Appendix H

Additional Model Application Results

The dynamic test system is commanded with the same motor profile for both the open loop and closed loop studies for each human assist percentage. The open loop study also commands the pressure into the pressure regulator. In addition to the LVDT response shown in section 3.3.1, the response from the load cell and the pressure transducer is collected for both the open loop and closed loop studies. The following figures (Figures H1-H18) contain these additional graphical commands and responses for 70%, 80%, and 90% human assist. The figures correspond to the same experimental trial analyzed in the results section 3.0.

Results from five trials of the open loop and closed loop studies are reported in Tables H1 – H12. Tables H1 – H3 and Tables H7 – H9 contain the 95% confidence interval (CI) for the slope. Tables H4 – H6 and Tables H10 – H12 contain root mean square error (RMSE) values.

70% Control Profiles and Additional System Response

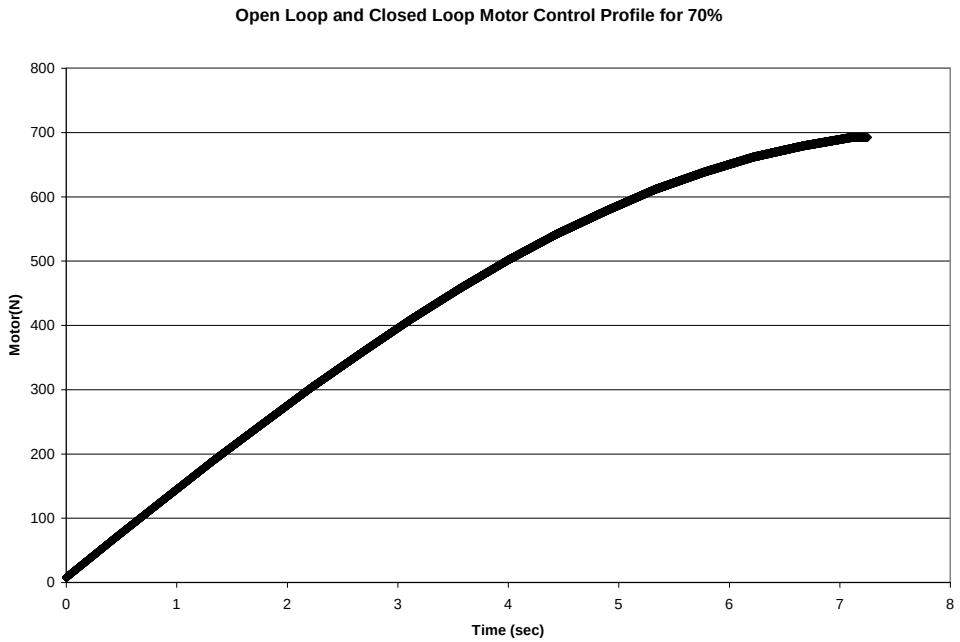

Figure H1: Open Loop and Closed Loop Motor Control Profile at 70% Human Assist

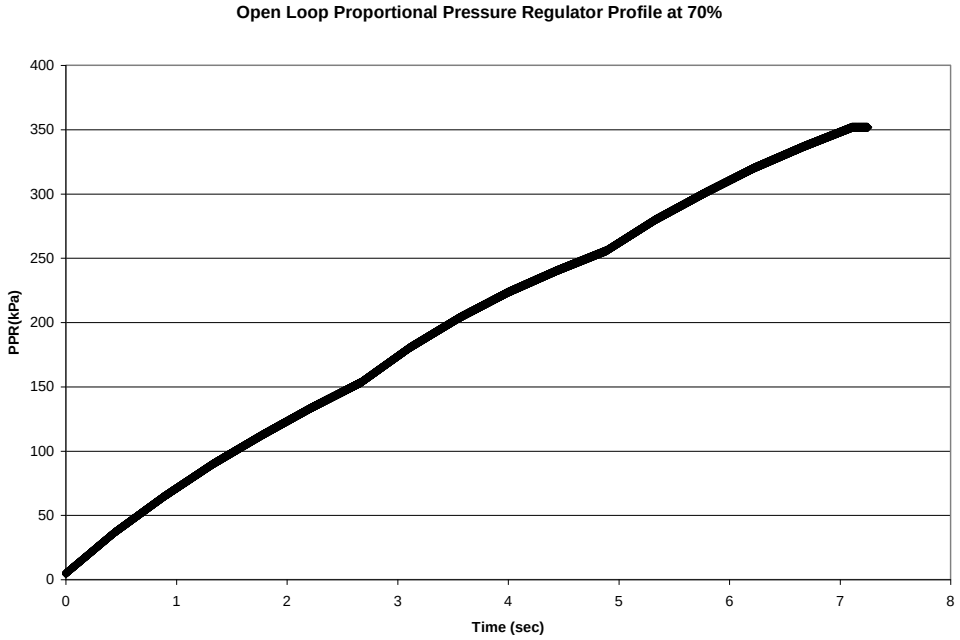

Figure H2: Open Loop Proportional Pressure Regulator Profile at 70% Human Assist

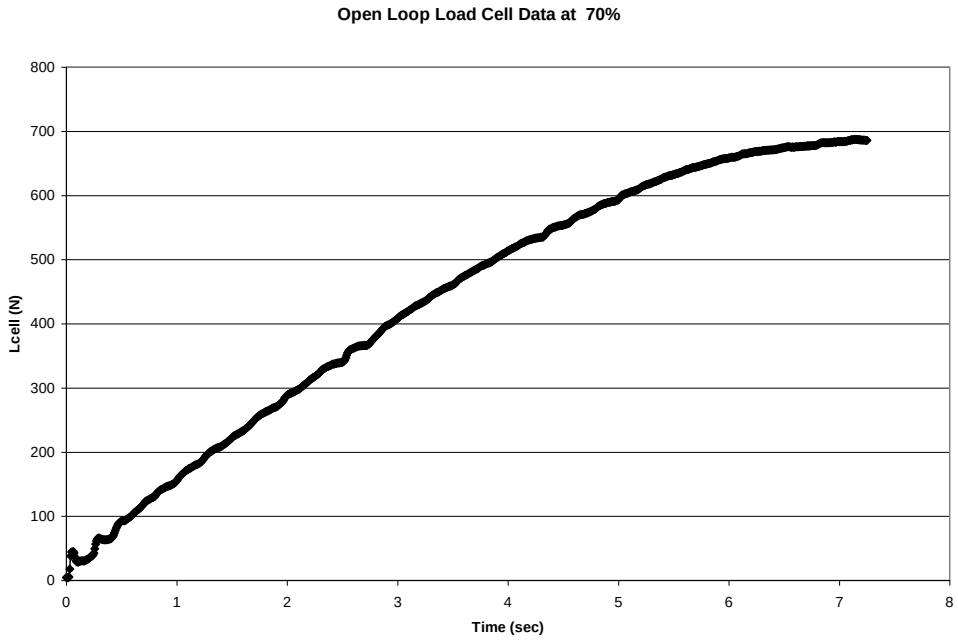

Figure H3: Open Loop Load Cell Data at 70% Human Assist

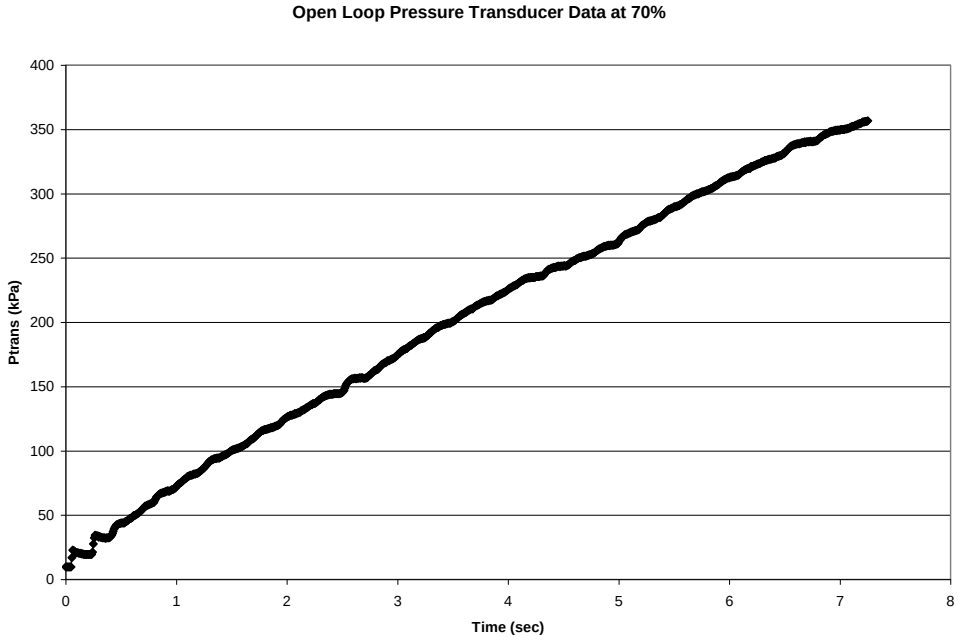

Figure H4: Open Loop Pressure Transducer Data at 70% Human Assist

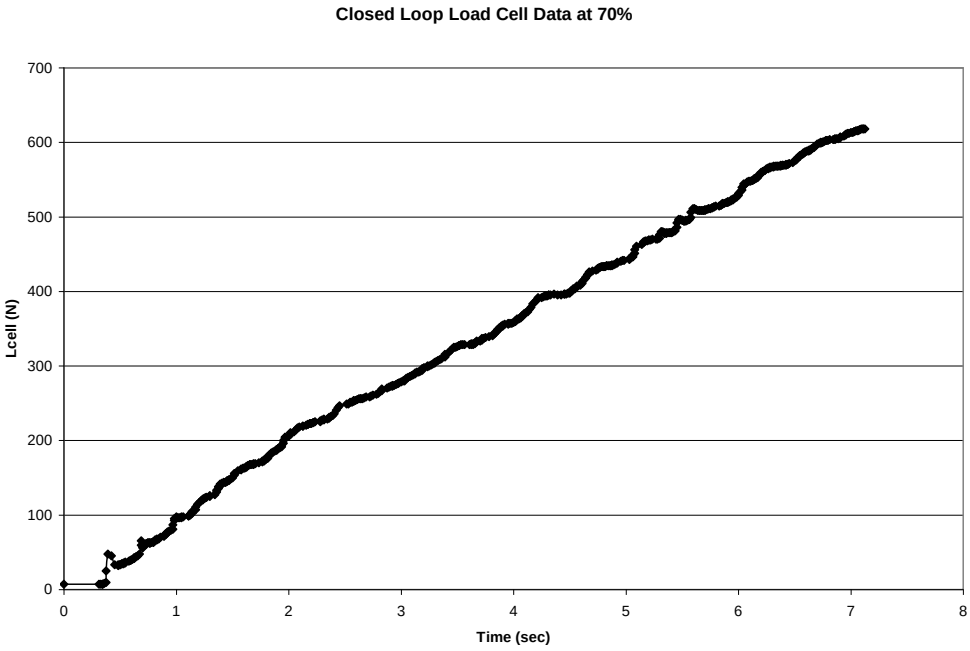

Figure H5: Closed Loop Load Cell Data at 70% Human Assist

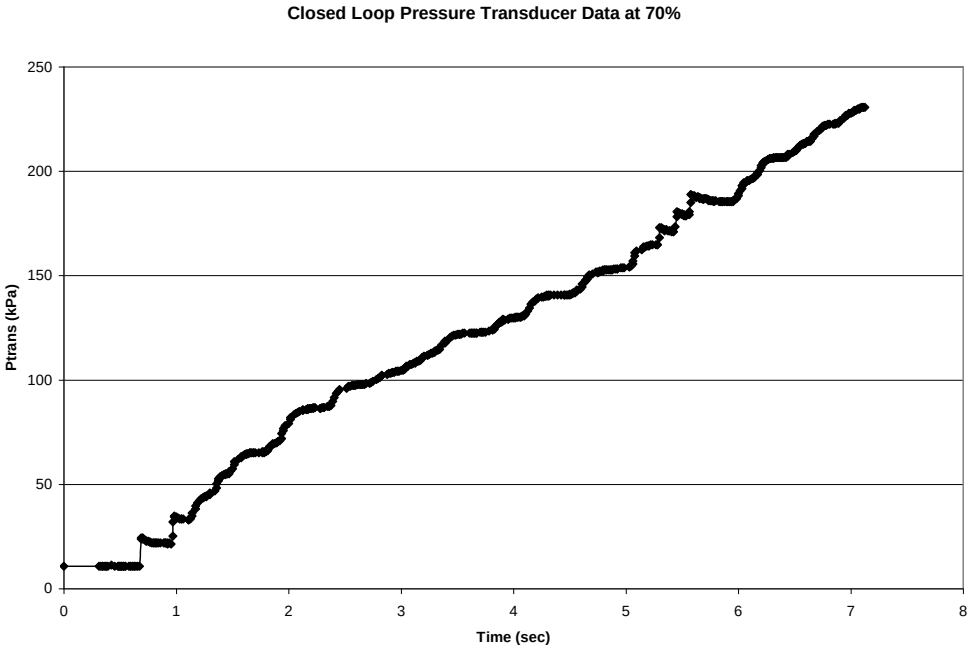

Figure H6: Closed Loop Pressure Transducer Data at 70% Human Assist

80% Control Profiles and Additional System Response

Figure H7: Open Loop and Closed Loop Motor Control Profile at 80% Human Assist

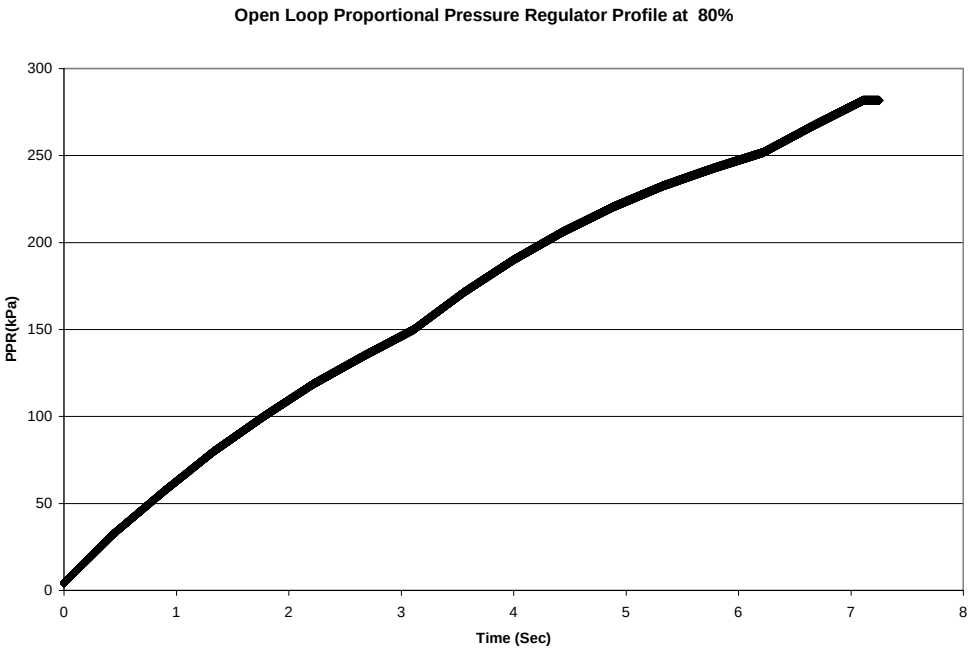

Figure H8: Open Loop Proportional Pressure Regulator Profile at 80%

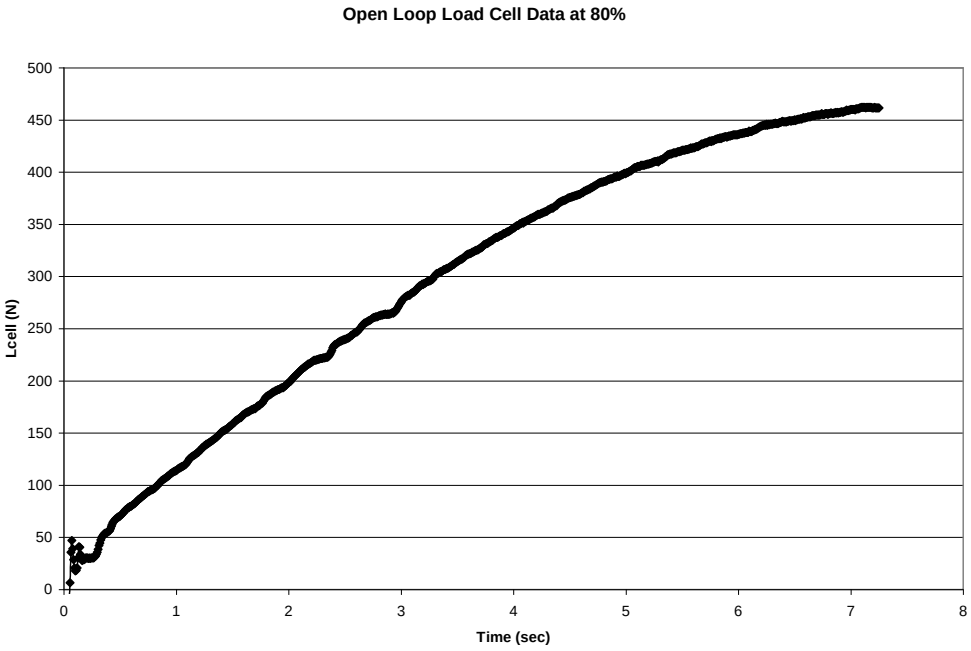

Figure H9: Open Loop Load Cell Data at 80% Human Assist

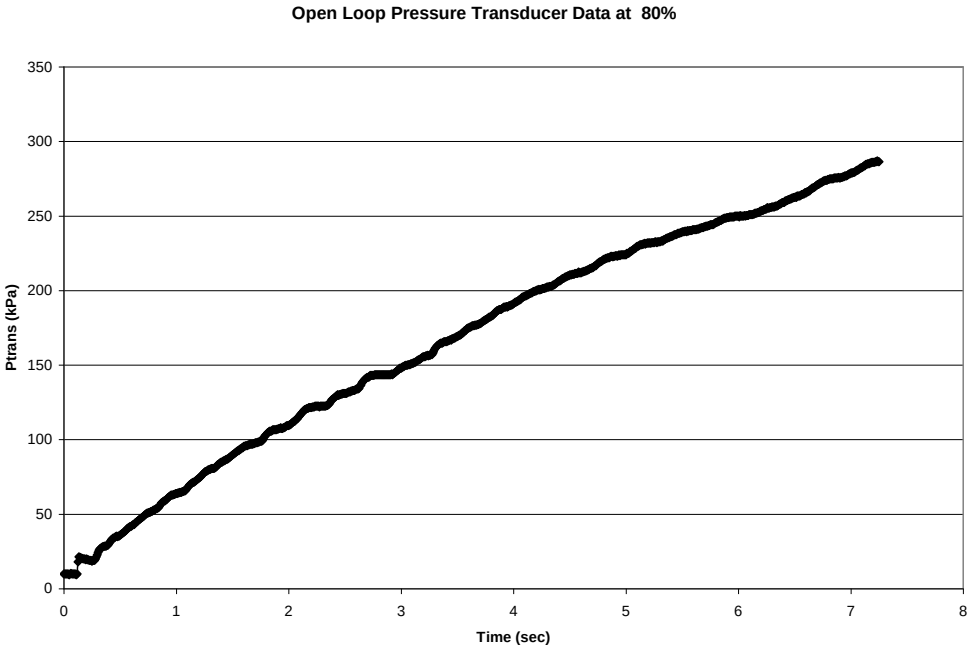

Figure H10: Open Loop Pressure Transducer Data at 80% Human Assist

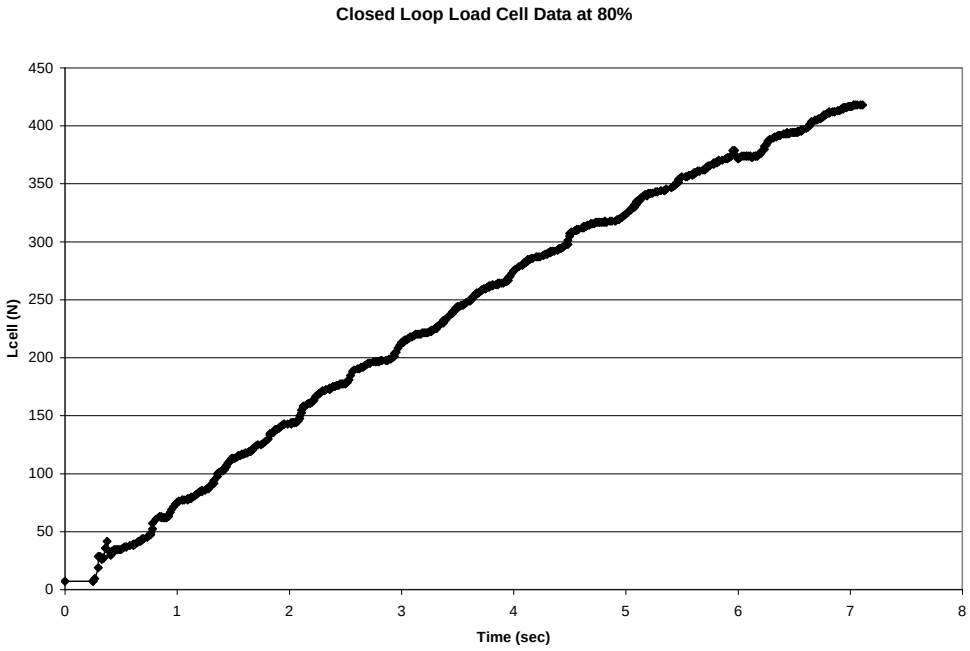

Figure H11: Closed Loop Load Cell Data at 80% Human Assist

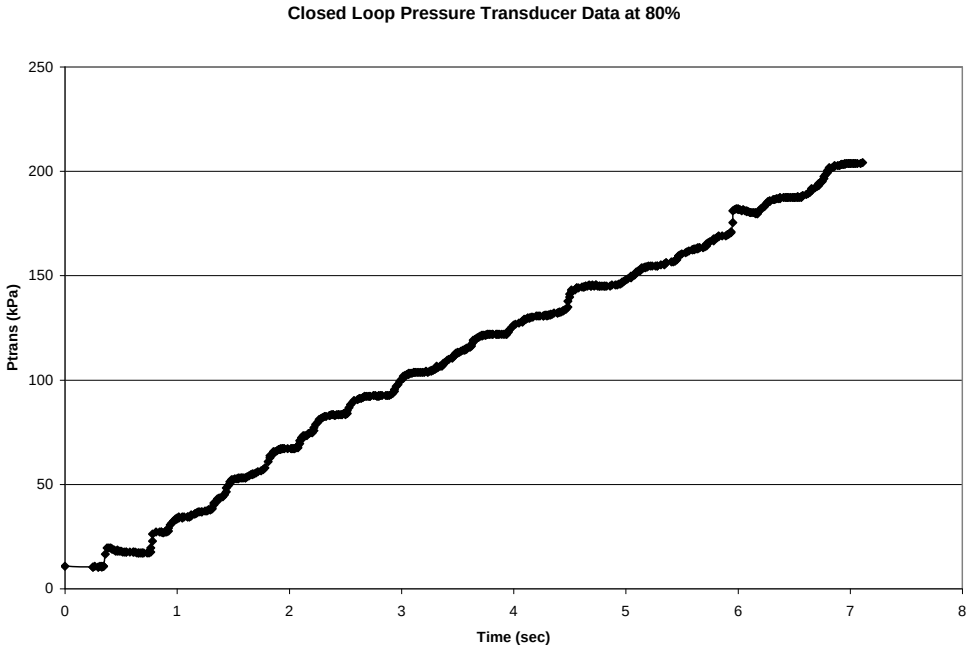

Figure H12: Closed Loop Pressure Transducer Data at 80% Human Assist

90% Control Profiles and Additional System Response

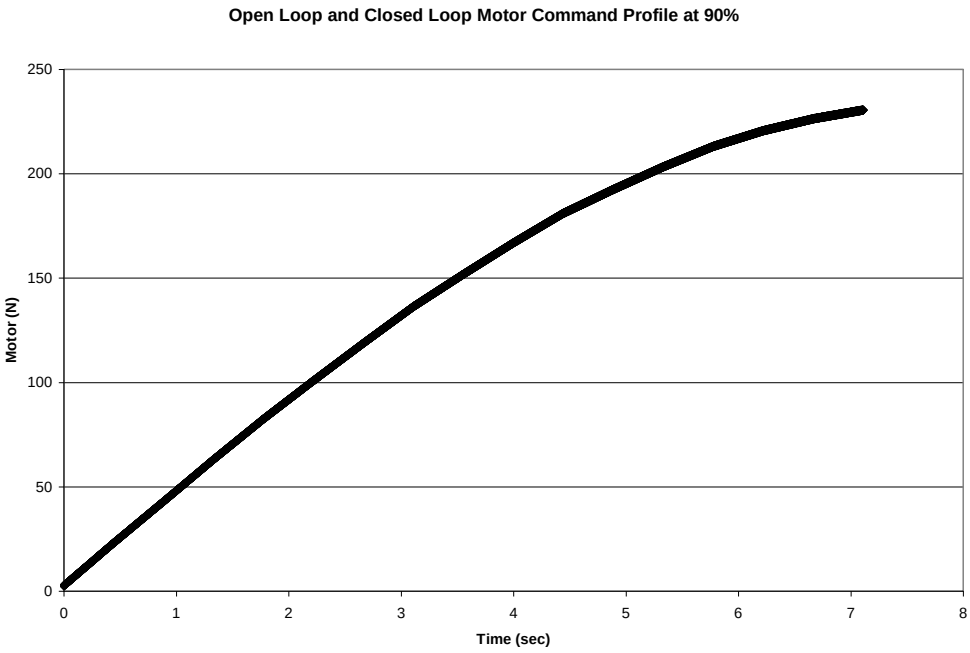

Figure H13: Open Loop and Closed Loop Motor Command Profile at 90% Human Assist

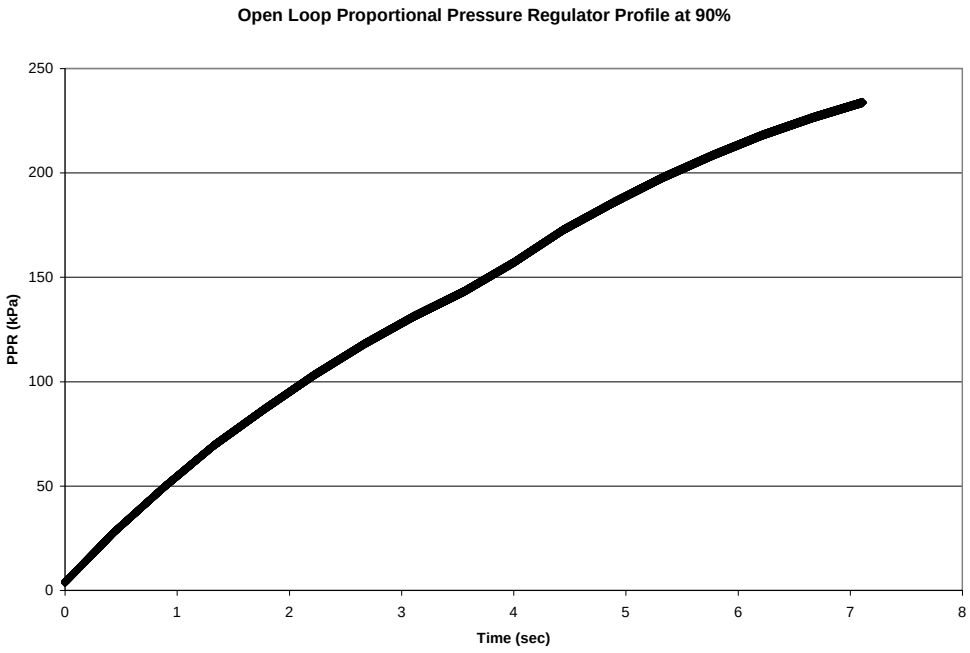

Figure H14: Open Loop Proportional Pressure Regulator Profile at 90% Human Assist

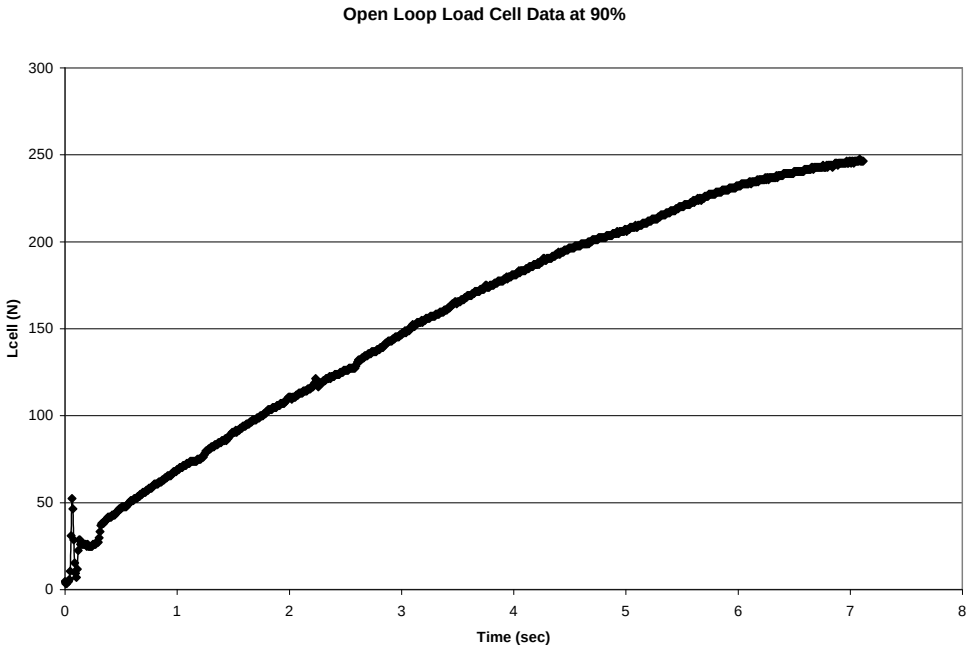

Figure H15: Open Loop Load Cell Data at 90% Human Assist

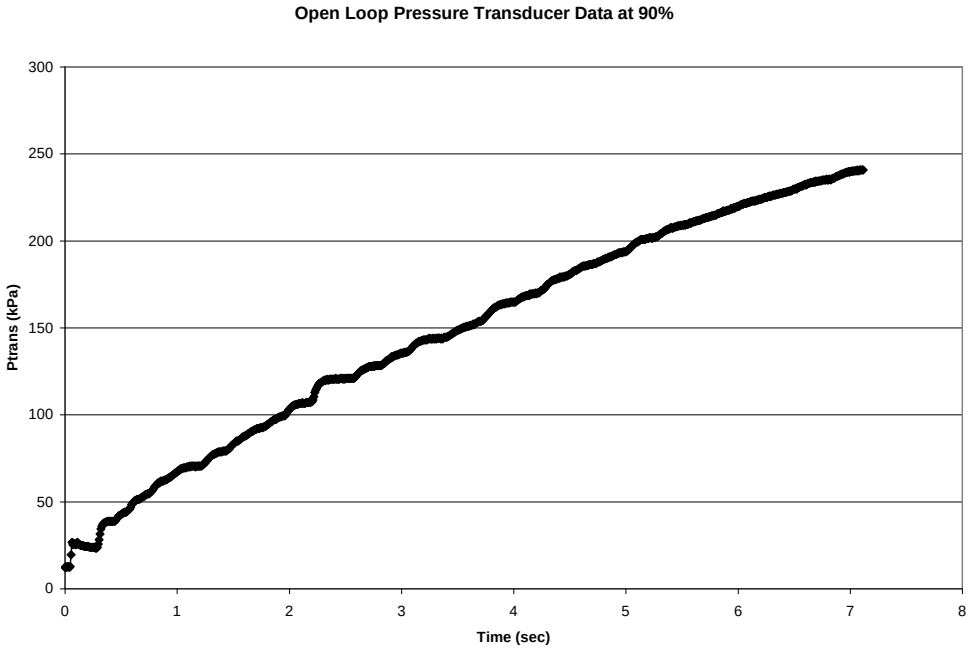

Figure H16: Open Loop Pressure Transducer Data at 90% Human Assist

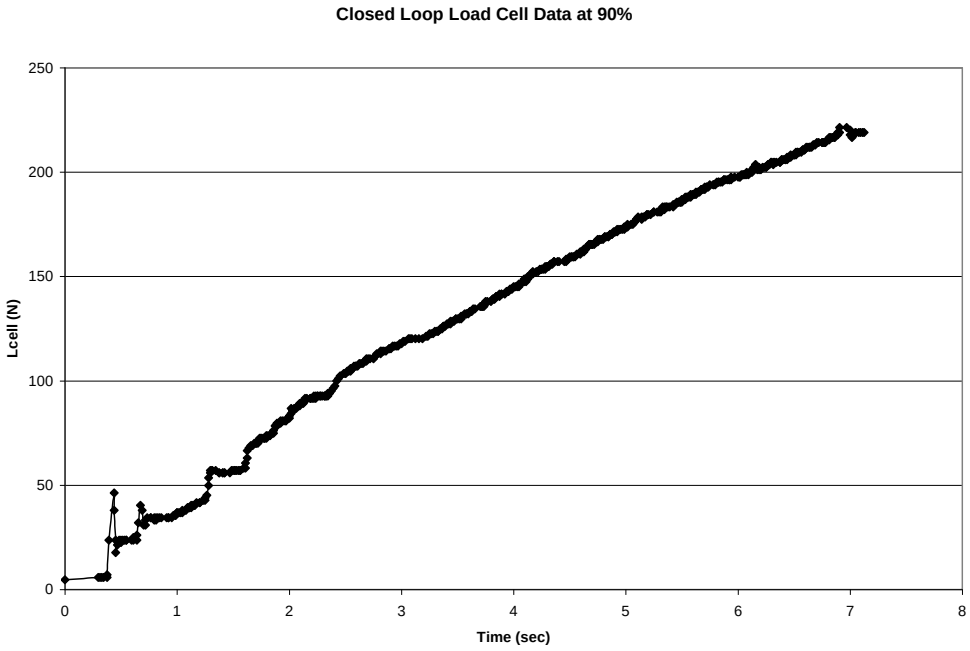

Figure H17: Closed Loop Load Cell Data at 90% Human Assist

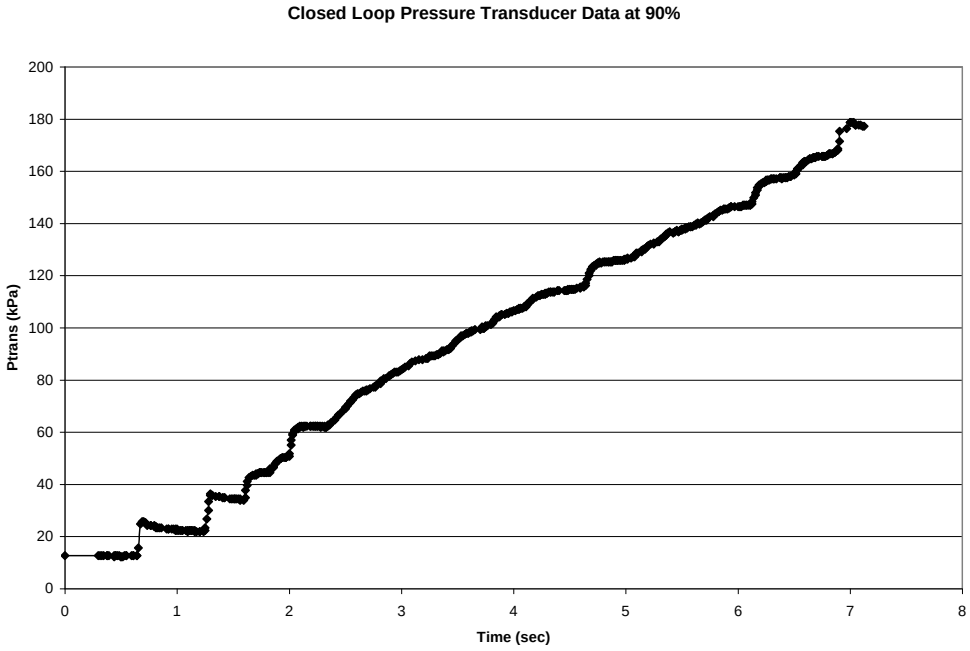

Figure H18: Closed Loop Pressure Transducer Data at 90% Human Assist

Multiple Trial Analysis (Slope and RMSE) for 70% Human Assist

TABLE H1: Open Loop 95% CI for 70% Human Assist

	Lower	Upper
Trial 1	0.7412	0.8057
Trial 2	0.7323	0.7957
Trial 3	0.7273	0.7959
Trial 4	0.7536	0.8203
Trial 5	0.7353	0.8034

TABLE H2: Open Loop 95% CI for 80% Human Assist

	Lower	Upper
Trial 1	0.9704	1.0046
Trial 2	0.9939	1.0263
Trial 3	1.0134	1.046
Trial 4	0.9975	1.034
Trial 5	1.0147	1.0484

TABLE H3: Open Loop 95% CI for 90% Human Assist

	Lower	Upper
Trial 1	1.9428	1.9747
Trial 2	1.9966	2.0333
Trial 3	1.9595	2.0021
Trial 4	2.0067	2.041
Trial 5	2.0115	2.0465

TABLE H4: Open Loop RMSE for 70% Human Assist

Trial 1	2.63975
Trial 2	2.64483
Trial 3	2.78804
Trial 4	2.7828
Trial 5	2.656

TABLE H5: Open Loop RMSE for 80% Human Assist

Trial 1	4.17199
Trial 2	4.09721
Trial 3	4.17892
Trial 4	4.39014
Trial 5	4.24334

TABLE H6: Open Loop RMSE for 90% Human Assist

Trial 1	7.80355
Trial 2	7.89771
Trial 3	8.13156
Trial 4	8.04915
Trial 5	8.01574

TABLE H7: Closed Loop 95% CI for 70% Human Assist

	Lower	Upper
Trial 1	-0.0279	-0.0192
Trial 2	-0.0227	-0.0078
Trial 3	-0.0784	-0.0565
Trial 4	-0.0804	-0.0674
Trial 5	-0.0281	-0.0194

TABLE H8: Closed Loop 95% CI for 80% Human Assist

	Lower	Upper
Trial 1	0.3201	0.3428
Trial 2	0.02024	0.2248
Trial 3	0.2495	0.2768
Trial 4	0.3087	0.3343
Trial 5	0.5388	0.576

TABLE H9: Closed Loop 95% CI for 90% Human Assist

	Lower	Upper
Trial 1	0.8876	0.9132
Trial 2	0.9891	1.0123
Trial 3	0.9658	0.9943
Trial 4	0.9984	1.0408
Trial 5	0.9922	1.0371

TABLE H10: Closed Loop RMSE for 70% Human Assist

Trial 1	0.20305
Trial 2	0.30035
Trial 3	0.27412
Trial 4	0.29613
Trial 5	0.20293

TABLE H11: Closed Loop RMSE for 80% Human Assist

Trial 1	1.15893
Trial 2	1.06012
Trial 3	1.70456
Trial 4	1.37676
Trial 5	1.87599

TABLE H12: Closed Loop RMSE for 90% Human Assist

Trial 1	3.08428
Trial 2	3.6308
Trial 3	3.55047
Trial 4	3.82813
Trial 5	3.97548

REFERENCES

[1] D.W Repperger, K.R. Johnson, and C.A. Phillips, Nonlinear feedback controller design of a pneumatic muscle actuator system, *In: Proc American Control Conference* **3**, 1525-1529 (1999).

[2] B. Hannaford and J. M. Winters, *Actuator properties and movement control: Biological and technological models*, In J. M. Winters & S. Woo (Eds.), pp. 101-120. Multiple Muscle Systems: Biomechanics and Movement Organization. New York: Springer-Verlag, (1990).

[3] C.P. Chou and B. Hannaford, Static and Dynamic Characteristics of McKibben Pneumatic Artificial Muscles, *IEEE International Conference on Robotics and Automation*, 281-286 (1994).

[4] D. G. Caldwell, G.A. Medrano-Cerda, and M.J. Goodwin, Characteristics and adaptive control of pneumatic muscle actuators for a robotic elbow, *Proceedings: 1994 IEEE International Conference on robotics and Automation*, May, 3558-3563 (1994).

[5] D.G. Caldwell, N. Tsagarakis, and G.A. Medrano-Cerda, Bio-mimetic actuators: Polymeric pseudo muscular actuators and pneumatic muscle actuators for biological emulation, *Mechatronics* **10**, 499-530 (2000).

[6] K. Inoue, *Rubbertuators and applications for robots*, pp. 57-63. In: Robotics Research: the 4th International Symposium, edited by R. Bolles and B. Roth. Cambridge, MA: MIT Press (1998).

[7] D.B. Reynolds, D.W. Repperger, C.A. Phillips, and G. Bandry, Modeling the dynamic characteristics of pneumatic muscle, *Annals of Biomedical Engineering*, **31**, 310-317 (2003).

[8] C. Anglin and U. P. Wyss, Arm motion and load analysis of sit-to-stand, stand-to-sit, cane walking and lifting, *Clinical Biomechanics* **15**, 441-448 (2000).

[9] B. Tondu and P. Lopez, The McKibben muscle and its use in actuating robot-arms showing similarities with human arm behavior, *Industrial Robotics* **24**, 432-439 (1997).

[10] D. G. Caldwell, G.A. Medrano-Cerda, and M. Goodwin, Control pneumatic muscle actuators, *IEEE Control System Magazine* **2,** 40-48 (1995).

[11] H.F. Schulte, *The characteristics of the McKibben artificial muscle*, pp. 94-115. In: The Application of External Power in Prosthetics and Orthotics. Washington, DC: Pub. 874 National Academy of Science-National Research Council (1961).

[12] C.P. Chou and B. Hannaford, Measurement and modeling of McKibben pneumatic artificial muscles, *IEEE Transactions on Robotics and Automation* **12**, 90-102 (1996).

[13] G.K. Klute and B. Hannaford, Accounting for elastic energy storage in McKibben artificial muscle actuators, *Journal of Dynamics Systems, Measurement, and Control* **122**, 386-388 (2000).

[14] S. Davis, N. Tsagarakis, J. Canderle, and D.G. Caldwell, Enhanced modeling and performance in braided pneumatic muscle actuators, *International Journal of Robotic Research* **22**, 213-227 (2003).

[15] D.W. Repperger, C.A. Phillips, A. Neidhard-Doll, D.B. Reynolds and J. Berlin, Actuator design using biomimicry methods and a pneumatic muscle system, *Control Engineering Practice* **14**, 999-1009 (2006).

[16] C.A. Phillips, D.W. Repperger, A.T. Neidhard-Doll, and D.B. Reynolds, Biomimetic model of skeletal muscle contraction: I. An energetic visco-elastic model for the skeletal muscle isometric force twitch, *Computers in Biology and Medicine* **34**, 307-322 (2004).

[17] A.T. Neidhard-Doll, C.A. Phillips, D.W. Repperger, and D.B. Reynolds, Biomimetic model of skeletal muscle isometric contraction: II. A phenomenological model of the skeletal muscle excitation-contraction coupling process, *Computers in Biology and Medicine* **34**, 323-344 (2004).

[18] D.W. Repperger, K.R. Johnson, and C.A. Phillips, A VSC position tracking system involving a large scale pneumatic muscle actuator, *Proceedings of the 37th IEEE Conference Decision and Control*, December, 4302-4307 (1998).

[19] S.M. Mason, Simplifying complexity: a review of complexity theory, *Geoforum* **32**, 405-414 (2001).

[20] K.M. Hangos, J. Bokor, and G. Szederkényi, *Analysis and control of nonlinear process systems*, Springer-Verlag London Limited, London (2004).

[21] M.H. Petrick and B. Wigdorowitz, A priori nonlinear model structure selection for system identification, *Control Engineering Practice* **5**(8), 1053-1062 (1997).

[22] F. Casciati, L. Faravelli, and T. Yao, Control of nonlinear structures using the fuzzy control approach, *Nonlinear Dynamics* **11**, 171-187 (1996).

[23] D.J. Wagg, Adaptive control of nonlinear dynamical systems using a model reference approach, *Meccanica* **38**, 227-238 (2003).

[24] P. Zlateva, Variable-structure control of nonlinear systems, *Control Engineering Practice* **4**(7), 1023-1028 (1996).

[25] D. Cai and Y. Dai, A sliding mode controller for manipulator driven by artificial muscle actuator, *Electronics and Communications in Japan, Part 3* **86**(11), 290-297 (2003).

[26] V. Balasubramanian and K.S. Rattan, Feedforward control of a non-linear pneumatic muscle system using fuzzy logic, *In: IEEE International Conference on Fuzzy Systems* **1**, 272-277 (2003).

[27] T.D.C. Thanh and K.K. Ahn, Nonlinear PID control to improve the control performance of 2 axes pneumatic artificial muscle manipulator using neural network, *Mechatronics* **16**, 577-587 (2006).

[28] D.G. Shurr and J.W. Michael, *Prosthetics and Orthotics*, *2nd Edition*, pp. 3. Upper Saddle River, New Jersey: Prentice Hall (2002).

[29] M.M. Lusardi and C.C. Nielsen, *Orthotics and Prosthetics in Rehabilitation 2nd Edition*, pp. 5. St. Louis, Missouri, Saunders (2007).

[30] K.E. Gordon, G.S. Sawicki, D.P. Ferris. Mechanical performance of artificial pneumatic muscles to power an ankle-foot orthosis. *Journal of Biomechanics*, **39**, 1832-1841 (2006).

[31] J.S. Petrofsky, C.A. Phillips, P. Larson, and R. Douglas, Computer synthesized walking: an application of orthosis and functional electrical stimulation (FES), *Journal of Neurological and Orthopedic Surgery* **6**, 219-230 (1985).

[32] J.S. Petrofsky, C.A. Phillips, R. Douglas, and P. Larson, Computer-controlled walking system: The combination of an orthosis with functional electrical stimulation, *Journal of Clinical Engineering* **11**, 121-133 (1986).

[33] C.A. Phillips and J.S. Petrofsky, A total neural prosthesis for spinal cord injury rehabilitation: the cognitive feedback system with an F.E.S.-orthosis, *Journal of Neurological and Orthopedic Medical Surgery* **7**, 225-234 (1986).

[34] C.A. Phillips, Sensory feedback control of upper and lower extremity motor prostheses. *CRC Critical Review of Biomedical Engineering* **16**, 105-140 (1988).

[35] T. Noritsuga and T. Tanaka, Application of rubber artificial muscle manipulator as a rehabilitation robot, *IEEE/ASME Transactions On Mechatronics* **2**, 259-267 (1997).

[36] R. O'Conner, 'Pistonless' actuator speeds paper punch, *Design News* **57**(6), 70 (2001).

[37] B. Wiebusch, Fluidic Muscles flex in three diverse applications, *Design News* **58**(9), 65-66 (2002).

[38] C.A. Phillips, M.J. Gerschutz, D.B. Reynolds, D.W. Repperger, J.L. Serres, and S. Mohler, Dynamic control modeling of an antagonist pneumatic muscle when performing a simulated knee extension task, *Aviation, Space and Environmental Medicine* (In Press).

[39] A.V. Hill, The heat of shortening and the dynamic constants of muscle, *Proc. R. Soc.* Ser. B **126,** 136-195 (1938).

[40] D.W. Repperger, C.A. Phillips, A. Neidhard-Doll, D.B Reynolds, and J. Berlin, Power/energy metrics for controller evaluation of actuators similar to biological systems, *Mechatronics* **15**, 459-469 (2005).

[41] M. A. Hughes, B.S. Myers, and M.L. Scheulsman, The role of strength in rising from a chair in the functionally impaired elderly, *Journal of Biomechanics* **29**, 1509-1513 (1996).

[42] E. Papa and A. Cappozzo, Sit-to-stand motor strategies investigated in able-bodied young and elderly subjects, *Journal of Biomechanics* **33**, 1113-1122 (2000).

[43] I. Rothera, R. Jones, R. Harwood, A. Avery, and J. Waite, Health status and assessed need for a cohort of older people admitted to nursing and residential homes, *Age Ageing* **32**, 303-309 (2003).

[44] C. Mazza, M. Zok, and U.D. Croce, Sequencing sit-to-stand and upright posture for mobility limitation assessment: Determination of the timing of the task phases from force platform data, *Gait & Posture* **21,** 425-431 (2005).

[45] K. M. Kerr, J.A. White, D.A. Barr, and R.A.B. Mollan, Analysis of the sit-to-stand movement cycle in normal subjects, *Clinical Biomechanics* **12**(4), 236-345 (1997).

[46] D.O. Riley, M.L. Schenkman, R.W. Mann, and W.A. Hodge, Mechanics of a constrained chair-rise, *Journal of Biomechanics*, **24**(1), 77-85 (1991).

[47] D.A. Winters, *Biomechanics and motor control of human movement 2nd edition,* pp. 52, 56-57. John Wiley, New York (1990).

[48] N.B. Alexander, A.B. Schultz, and D.N. Warwick, Rising from a chair: effects of age and function ability on performance biomechanics, *Journal of Gerontology: Medical Science* **46,** M91-98 (1991).

[49] W.E. Prentice and M.I. Voight, *Techniques in Musculoskeletal Rehabilitation,* pp. 59-60. McGraw-Hill (Medical Publishing Division), New York (2001).

[50] D.M. Pincivero, V. Grandhi, M.K. Timmons, and A.J. Coelho, Quadriceps femoris electromyogram during concentric, isometric and eccentric phases of fatiguing dynamic knee extensions, *Journal of Biomechanics* **39**, 246-254 (2006).

[51] D. Hendershot, J.S. Petrofsky, C.A. Phillips, and M. Moore, Blood pressure and heart rate responses in paralyzed and nonparalyzed men during isokinetic leg training, *Journal of Neurological and Orthopedic Surgery* **6,** 259-264 (1985).

[52] C. A. Phillips, The medical criteria for active physical therapy: Physician guidelines for patient participation in a program of functional electrical. *Rehabilitation* **66**, 269-286 (1987).

[53] C.A. Phillips, J.S. Petrofsky, D.M. Hendershot, and D. Stafford, Functional electrical exercise: A comprehensive approach for physical conditioning of the spinal cord injured individual, *Orthopaedics* **7**, 1112-1123 (1984).

[54] C.A. Phillips, *Functional electrical rehabilitation: Technological restoration after spinal cord injury*, pp. 224. Springer-Verlag, New York (1991).

[55] C.A. Phillips, Electrical muscle stimulators in combination with a reciprocating gait orthosis for ambulation of paraplegics, *Journal of Biomedical Engineering* **11,** 338-344 (1989).

[56] C.A. Phillips, R.J. Koubek, and D.M. Hendershot, Walking while using a sensory (tactile) feedback system: Potential for use with a function electrical stimulation orthosis, *Journal of Biomedical Engineering* **13**, 91-96 (1991).

[57] B. N. Ezenwa, R.M. Glaser, W. Couch, S.F. Figoni, M.M. Rodgers, Adaptive control of function neuromuscular stimulation-induced knee extension, *Journal of Rehabilitation and Research Development* **28**(4), 1-8 (1991).

[58] C.A. Phillips, *Human factors engineering*, pp. 252-314. John Wiley & Sons, New York (2000).

[59] MATLAB version 6.5, 2002.

[60] I. Mareels and J.W. Polderman, *Adaptive systems: An introduction*, pp. 13-18. Birkhauser, Boston (1996).

[61] B. Zhou, M.L. Accorsi, J.W. Leonard, A new finite element for modeling pneumatic muscle actuators, *Computers and Structures* **82**, 845-856 (2004).

[62] M. Ozkan, K. Inoue, K. Negishi, and T. Yamanaka, Defining a neural network controller structure for a rubbertuator robot, *Neural Networks* **13,** 533-544 (2000).

[63] P. Smagt, F. Groen, and K. Schulten, Analysis and control of a rubbertuator arm, *Biological Cybernetics* **75**, 433-440 (1996).

[64] Shadow Robot Company Ltd. Technical Documents, Retrieved February 14, 2008 from http://www.shadowrobot.com/airmuscles/techspec.shtml

[65] Robotic hand has that human touch, *Machine Design* **77**(20), 26 (2005).

[66] Festo Corporation, Fluidic Muscle DMSP/MAS Technical Documents, Retrieved February 14, 2008 from https://xdki.festo.com/xdki/xDKI.asp

[67] The bionic upper body, *Design News* **61**(9), 18 (2006).